DESIGN AND STUDIES OF SOME CHROMOPHORE FUNCTIONALIZED METAL NANOPARTICLES

THESIS SUBMITTED TO
THE UNIVERSITY OF KERALA
FOR THE DEGREE OF
DOCTOR OF PHILOSOPHY
IN CHEMISTRY
UNDER THE FACULTY OF SCIENCE

By

BINIL ITTY IPE KANDAPPALLIL

PHOTOSCIENCES AND PHOTONICS DIVISION
REGIONAL RESEARCH LABORATORY (CSIR)
TRIVANDRUM – 695 019
KERALA, INDIA

DECEMBER 2003

Dedicated to

My Parents &
        family members

STATEMENT

I hereby declare that the matter embodied in the thesis entitled, *"Design and Studies of Some Chromophore Functionalized Metal Nanoparticles"* are results of investigations carried out by me at the Photosciences and Photonics Division of the Regional Research Laboratory (CSIR), Trivandrum, under the supervision of Dr. K. George Thomas and the same has not been submitted elsewhere for a degree.

In keeping with the general practice of reporting scientific observations, due acknowledgement has been made wherever the work described is based on the findings of other investigators.

Binil Itty Ipe

Photosciences and Photonics Division
REGIONAL RESEARCH LABORATORY
(Council and Scientific and Industrial Research)
TRIVANDRUM-695 019. INDIA

Dr. K. GEORGE THOMAS
Scientist E1

Tel: 91-2471-2515364   Fax: 91-471-2490186
e-mail: georgetk@md3.vsnl.net.in

December 12, 2003

CERTIFICATE

This is to certify that the work embodied in the thesis entitled: *"Design and Studies of Some Chromophore Functionalized Metal Nanoparticles"* has been carried out by Mr. Binil Itty Ipe Kandappallil under my supervision and the same has not been submitted elsewhere for a degree.

K. George Thomas
Thesis Supervisor

ii

ACKNOWLEDGEMENTS

iii

CONTENTS

Chapter 1. ***Chromophore Functionalized Metal Nanoparticles: An Overview***

PREFACE

Nanoscience and nanotechnology are important areas of research at present due to their size and shape dependent properties in the nanoscale regime, which are helpful in the development of new materials and devices. For example, nanomaterials such as nanoparticles, nanorods and nanotubes possess unusual optoelectronic properties and they are potential building blocks for nanoscale devices. Such nanoscale devices will have improved properties as compared to the present day macroscopic devices. Although considerable progress has been made in recent years, several challenges still remain for realizing nanoscale systems. Some of the challenges in the area of nanotechnology include i) tailoring the optoelectronic properties of these nanoscale building blocks, ii) integrating these blocks into larger assemblies and devices of specific properties and functions. The "bottom-up" approach is one of the most efficient and popular methods for tuning the properties of nanomaterials, wherein 'building blocks in nanoscale' are integrated to larger assemblies of interest. It is possible to design photoresponsive nanomaterials by functionalizing nanoparticles with chromophoric molecules. With this objective, attempts have been made in this thesis for the design and study of chromophore functionalized gold nanoparticles. The major focus of this study is to understand the excited state deactivation processes of chromophores when linked to the surface of Au nanoparticles and to investigate the potential application of photoresponsive metal nanoparticles as photoswitchable controlled release systems, nanophosphors and sensors.

The first chapter provides a general introduction to the field of nanotechnology and nanomaterials, with special emphasis on the past attempts to understand the photophysical properties of chromophore functionalized metal nanoparticles. A brief account of the various methods adopted for the synthesis of metal nanoparticles, their characterization techniques and approaches for

controlling the self-assembly is described. The last part of this chapter provides a brief description on the strategies adopted for the design of nanoscale devices.

In the second chapter, a detailed description of the synthesis of gold nanoparticles functionalized with pyrene derivatives (**P1, P2** and **P3**) and the excited state deactivation process of surface bound chromophores are reported. Contrary to the belief that the singlet excited state of chromophores are strongly quenched on metal surfaces, we observe a suppression in quenching of pyrene fluorescence when bound to the surface of gold nanoparticles. Extensive spectroscopic characterization of pyrene functionalized Au nanoparticles were investigated by varying the i) solvent polarity, ii) distance of chromophore from gold core, iii) loading of pyrene on gold surface. The long flexible alkyl chains tethering the pyrene moieties in **P2** and **P3** allow intermolecular excimer formation, at higher loadings. Also, we report the first spectroscopic evidence for photoinduced electron transfer between a gold nanoparticle and a surface-bound fluorophore **P2** in a polar solvent. Singlet lifetime measurements and transient absorption studies confirm that the excited-state of pyrene transfers an electron to Au nanocore and the charge separation is sustained for several microseconds before undergoing recombination.

The third chapter of this thesis describes photoswitchable self-assemblies of amino acid derivatives by anchoring spiropyrans onto the three-dimensional surface of Au nanoparticles. A new photochromic spiropyran derivative possessing thiol group **SP** and the corresponding model compound **SP1** were synthesized and the former derivative was capped on to gold nanoparticles (**Au-SP**). Based on the particle diameter of 1.5-2.0 nm, it was established that approximately 130 molecules of SP were capped on each nanoparticle. Irradiation of **Au-SP** with UV light resulted in the formation of the zwitterionic merocyanine form (**Au-MC**). Light regulated changes in the topographic properties of spiropyran capped Au nanoparticles (i.e., interconversion between the zwitterionic

merocyanine **MC** and neutral forms) were further exploited for the assembly of amino acids (L-tryptophan, L-tyrosin) and amino acid based therapeutic agents such as L-DOPA as a second layer on **Au-MC**. The two point electrostatic interaction between the zwitterionic merocyanine linked gold nanoparticles and the amino acid derivatives results in the formation of highly stable complexes. For example, the half-life ($t_{1/2}$) of **Au-MC::::**tyrosine complex is ~14 h whereas, that of **Au-MC→ Au-SP** is 23 min. The **Au-MC::::**amino acid complex dissociates on irradiation at 520 nm and undergoes thermal ring closure to **Au-SP**, releasing the amino acid derivatives. The complexation/decomplexation cycle could be repeated several times. The **Au-MC::::**amino acid complexes were estimated using steady state and time resolved techniques.

In the fourth chapter, we report the synthesis of gold nanoparticles functionalized with bipyridine ligands and studies on their complexation with transition and inner transition metals in an effort to develop nanosensors and nanophosphors. Synthesis and photophysical studies of a thiol derivative of 2.2'-bipyridyl, **BT** and its three dimensional assembly on gold nanoparticles (**Au-BT**) are reported. Metal ion binding properties of these bipyridine functionalized gold nanoparticles were investigated, in detail. The strong coordination ability of Cu^{II} ions bring **BT**s on adjacent gold nanoparticles, leading to the formation of three dimensional superstructures through metal induced self-assembly of ligands. Superstructures were characterized using TEM studies. A red shifted absorption band at 780 nm was observed as a result of interparticle plasmon coupling. The luminescence of Eu^{III} and Tb^{III} was found to increase many fold upon complexation with bipyridine capped on Au nanoparticle. Based on continuous variation method (Job's), it is concluded that a 1:1 complexation stoichiometry exists between **BT** on the surface of gold nanoparticles and Eu^{III}/Tb^{III}. High stability constant (~10^4 M^{-1}) for the complex formation of **Au-BT** with Eu^{III}/Tb^{III} indicates that such systems may have potential application as nanophosphors. The

luminescence lifetimes of Eu^{III} and Tb^{III} in the presence of **BT** were estimated as 0.4 ms and 0.56 ms, respectively. The lifetimes of the lanthanide complex remain unaffected when functionalized on Au nanoparticles. Allosteric effects of Ca^{II} and Mg^{II} on **Au-BT:Eu^{III}** complex in acetonitrile were also investigated. The dramatic quenching of emission observed in the present case revealed that Ca^{II}/Mg^{II} ions replace Eu^{III} from **Au-BT:Eu^{III}** complex. Such systems can be utilized for the design of nanosensors.

CHAPTER 1

Chromophore Functionalized Metal Nanoparticles: An Overview

1.1. An Introduction to Nanotechnology and Nanomaterials

Nanotechnology, one of the most popular areas of research in this decade, is fundamentally changing the way in which materials and devices are fabricated. Broadly, nanotechnology can be defined as (i) the creation of useful materials, devices and systems through the control of matter in the nanometer length scale; (ii) the exploitation of novel properties and phenomena developed at that scale.[1] Materials of any kind of matter, whose size is greater than that of molecules but too small to exhibit characteristic bulk properties can be classified under nanomaterials. Such materials are in the size regime of few hundreds of nanometers, in at least one of the three dimensions. Roughly, one nanometer (10^{-9} m) can be represented as four fold the diameter of an individual atom or about 1/80,000 of the diameter of a human hair.

The importance of nanomaterials is based on the fact that manipulation of size and shape in the nano regime alters the quantum mechanical properties of matter. Hence it is possible to control fundamental properties like melting temperature, mechanical strength, magnetic properties, charge capacity and even

optical properties without changing the material's chemical composition. For example, depending on size, nanoparticles of gold can behave as conductors, semiconductors or insulators. Extensive reviews[2-4] are available on the size dependent properties of metal nanoparticles. The size and shape dependent optical and electronic properties of metal nanoparticles open numerous possibilities for photochemists and photobiologists, particularly for exploiting their role in light-induced chemical reactions. In the last decade, several methodologies have been reported for the synthesis of metal and semiconductor nanoparticles possessing well-defined size and shape, with high level of monodispersity.[5] A greater challenge in this area involves the hierarchical integration of nanoscale building blocks having defined size and shape into functional assemblies, further to complex and multifunctional systems.

A brief description of the size dependent physical properties of metal nanoparticles is summarized below.

1.2. Size Dependent Properties of Nanoparticles

Although colloidal nanoparticles were used right from mid 17th century for ornamental decoration and staining glasses, it was Michael Faradey in 1857 who perfected the technique for the synthesis of metal colloids and attempted to provide reasons for their brilliant color. He elucidated the mechanism of formation of metal nanoparticles, explained that the "divided metals" formed during reduction is responsible for their fascinating color.[6]

Recent advances in the field of nanoparticles indicate that the metal nanoparticles cannot be simply treated as minute elements of a block of metal as implied by the term "divided metals". The conduction band present in the bulk metal is absent in metal nanoparticles and they appear as discrete states at the band edge as shown in Figure 1.1.
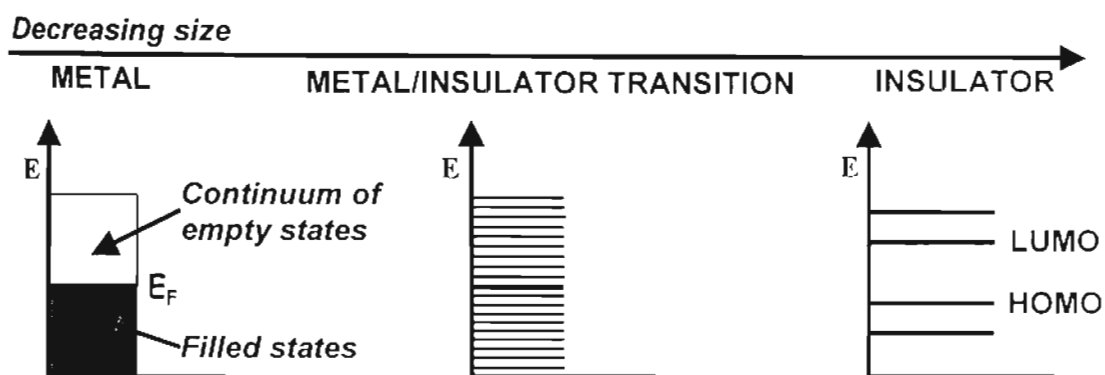
Figure 1.1. Electronic situations with respect to size decrease in metals.

The size as well as shape dependent optoelectronic properties of nanoparticles can be explained by the quantum confinement of electrons (particle in a box approximation), which is responsible for the changes in their properties compared to the bulk. When the size of metal or semiconductor particles become comparable to the wavelength of electrons, the electrons undergo quantum confinement and show properties of zero-dimensional quantum dots.[4] The laws of classical physics fail in explaining zero-dimensional quantum dot properties, and quantum confinement behavior is interpreted in terms of quantum mechanical rules. The electronic situation in metals when transformed from bulk to nano regime is illustrated in Figure 1.1.[7]

Nanoparticles of noble metals such as Ag, Au and Cu possess strong absorption in the visible region often referred to as "surface plasmon absorption". In metals, the conduction electron (-) and ionic core (+) form a plasma state. For nanoparticles, whose size is smaller than the wavelength of light, the confined electrons in them give rise to plasmon excitons, on interaction with electromagnetic radiation. When an external electric field is applied to a metal, electrons move so as

Plasmon absorption
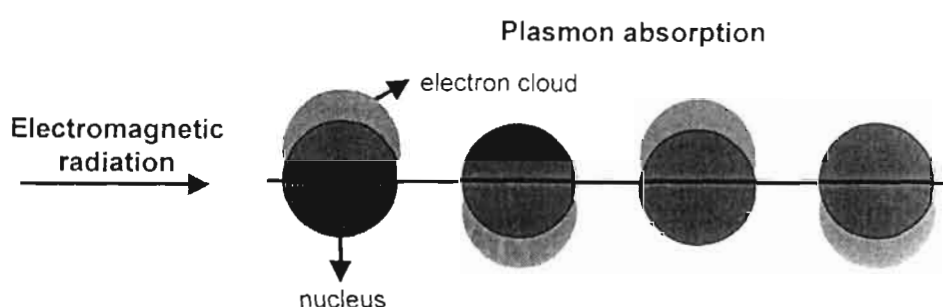
Figure 1.2. The oscillation of electron cloud in the presence of an electromagnetic radiation.

to screen the perturbed charge distribution, further get displaced beyond the neutral state (Figure 1.2). When the electron cloud is displaced with respect to the nuclear framework, a restoring force arises between the electrons and nucleus due to coulombic attraction. As a result, the electron cloud returns to the neutral state and establishes an oscillation. This oscillational frequency depends on various factors like the density of electrons, the effective electron mass, and the shape and size of the charge distribution. The surface plasmon absorption originating from this collective oscillation is termed as plasma oscillation (Figure 1.2).[8] In a recent paper, Rechberger *et al.* have reported the synthesis of arrays of gold nanoparticles on ITO glass plates separated at different distances with respect to each other, and

investigated the interparticle plasmon interactions in the presence of polarized light.[9]

When the polarization direction is parallel to the long axis of the array, a red shifted

plasmon absorption was observed and a blue shifted plasmon absorption for

orthogonal polarization. This is explained by means of a dipolar interaction

mechanism (Figure 1.3) according to which polarization of the electron charge
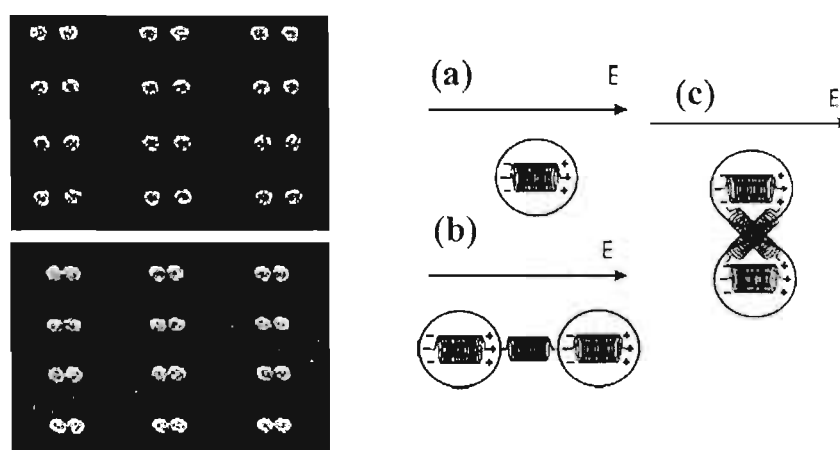
Figure 1.3. Assembly of nanoparticles at different distances with respect to each other and the illustration of the electromagnetic interaction between closely spaced nanoparticles, (a) an isolated particle, (b) a pair of close particles with the polarization of the exciting field parallel to the long particle pair axis and (c) orthogonal to the long particle pair axis.[9]

distribution on metal nanoparticles in the presence of an external electromagnetic

radiation results in additional forces between adjacent particles, that may be either

attractive or repulsive, as shown in Figure 1.3. These attractive/repulsive forces

lead to a change in the resonance frequency resulting in a bathochromic or

hypsochromic shift.

Another size dependent property is the dramatic effect on the surface area

on moving to the nanoscale. The surface to bulk ratio increases markedly with

decrease in size making them suitable for catalysis with enhanced surface area, high edge concentration and unusual electronic properties.[10] For example, a nanoparticle of 10 nm diameter has ~10 % of atoms on the surface compared to 100 % for a particle of 1 nm diameter.[11]

1.3. Synthetic Methodologies of Metal Nanoparticles

The design of nanodevices for electronic, and biomolecular applications require suitably functionalized building blocks of nanoparticles.[12,13] This has encouraged the development of supramolecular,[14] biomolecular[15] and dendrimeric[16] methods for engineering materials at angstrom to nanoscale dimensions. Diverse kinds of such building blocks have been developed by constructing nanoparticle arrays on surfaces. Several methods have been recently reported for the preparation of nanoparticles in aqueous and nonaqueous solvents.[5] Current research in this area is focussed towards the design of metal and semiconductor nanoparticles with high degree of control over the size and shape of nanoparticles.

Naked nanoparticles are unstable in solution and they agglomerate rapidly. Stabilizing agents such as tetraalkylammonium salts, phosphonium salts, thiols are often used as protecting agents and they provide charge as well as solubility properties which keep the nanoparticles suspended, thereby preventing them from aggregation.[17] The solubility of nanoparticles in a particular solvent could be achieved by capping them with suitable stabilizing ligands. For example, gold

nanoparticles functionalized with tetraalkylammonium salts are soluble in non-polar solvents whereas mercaptopropionic acid stabilized gold nanoparticles are water-soluble.[18] Pictorial representations of metallic clusters capped by tetraalkylammonium bromide, alkyl thiol and mercaptopropionic acid are shown in Figure 1.4. Metal nanoparticles possess size dependent optoelectronic properties and hence another focus is on the synthesis of metal nanoparticles of controlled size and assemblage. When organic molecules such as thiols suitably cover nanoparticles, they become self-organized in crystalline arrays of one, two or three dimensions and these structures form the basis of nanoscale devices. Syntheses of nanoparticles of varying size by employing physical, chemical and electrochemical methods have been reported and a brief summary is presented here.

TOAB capped metal nanoparticles　　**Alkylthiol capped metal nanoparticles**　　**Mercaptopropionic acid stabilized metal nanoparticles**
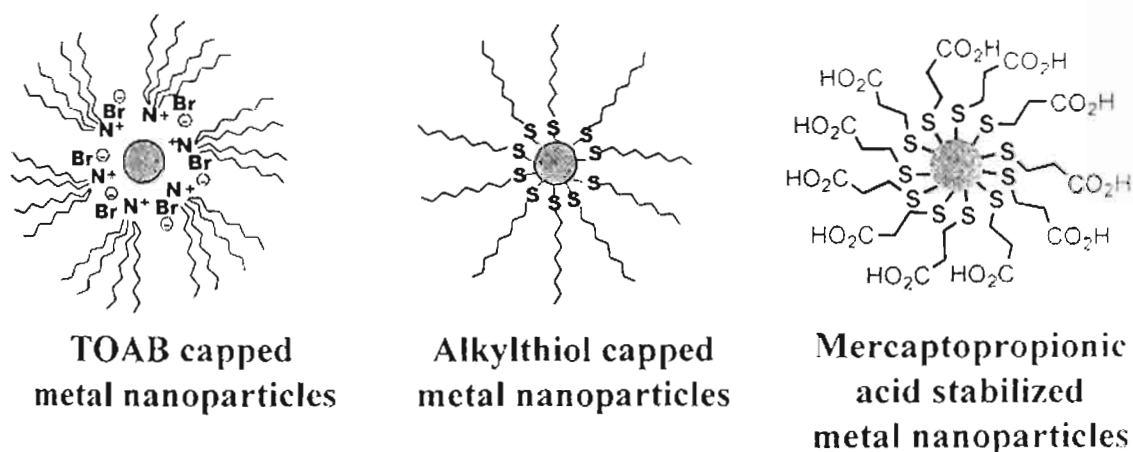
Figure 1.4. Pictorial representations of metallic clusters capped by tetraalkylammonium bromide, alkyl thiol and mercaptopropionic acid.

1.3.1. Reductive synthesis of colloids

The simplest and by far the most commonly employed method for the preparation of nanoparticles in aqueous media is by the reduction of metal salts

(for e.g., H[AuCl$_4$], AgNO$_3$, H$_2$[PdCl$_4$] and H$_2$[PtCl$_6$]) using sodium citrate or sodium borohydride.[18-20] An elegant method of preparing metal nanoparticles functionalized with thiols was reported by Brust *et al.*, adopting extraction of metal ions to an organic solvent, followed by their reduction.[21] Another method adopts the use of alcohols as reducing agents, which allows better control over particle size.[22] Extensive reviews on the synthesis, characterization and reactions of monolayer protected metals are available.[23] Functionalization of metal nanoparticles with organic ligands by means of place-exchange and amide forming coupling reactions giving rise to monolayer-protected gold clusters (MPCs) has been reported by Murray and coworkers.[24]

Metal nanoparticles can also be capped with conductive shell (e.g., bimetallic nanoparticles from silver capped gold particles), semiconductor shell (e.g., shell of CdS on gold nanoparticles) or inert shell (e.g., silica caged gold nanoparticles). Capping can be done *in situ* if the reductive formation of nanoparticles is performed in the presence of the shell forming material or shell can be organized later through a chemical reaction on the surface of the nanoparticles. Synthesis and characterization of such capped and caged metal nanoparticles are well documented.[25]

1.3.2. Electrochemical methods

Electrochemical methods are also employed for the preparation of nanoparticles.[17] The electrochemical set up consists of a sacrificial anode

composed of the bulk metal to be transformed into the corresponding metal clusters. The supporting electrolyte consists of tetraalkylammonium salts, which also serve as stabilizer for metal clusters. The various electrode processes are indicated below.

Anode : $Met_{bulk} \longrightarrow Met^{n+} + ne^-$ (1.1)

Cathode : $Met^{n+} + ne^- + stabilizer \longrightarrow Met_{nano}(stabilizer)$ (1.2)

Overall : $Met_{bulk} + stabilizer \longrightarrow Met_{nano}(stabilizer)$ (1.3)
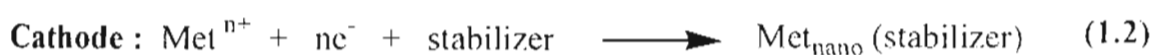
The overall process is the oxidation of the anode, forming metal cations and subsequent reduction of the cations at the cathode to form adatoms (equations 1.1-1.3).[17] These adatoms form nanoclusters (Met_{nano}) protected by ammonium ions. It is found that, on increasing the current density, particle size decreases. Clusters of Pd and Ni are found to be more stable than Cu, Au, Ag nanoclusters, when synthesized electrochemically. Nanoparticles composed of two metals (bimetallic nanoparticles) are of interest in the catalysis of some organic reactions and in fuel cell technology.[23] Electrochemical synthesis of bimetallic clusters of nickel and palladium have also been reported by using two anodes and a cathode.[17]

1.3.3. Photochemical methods

Several reports on photochemical methods for nanoparticle synthesis are available in the literature.[26] More recently, the synthesis of metal nanoparticles of Au, Ag, Pt and Pd using photooxometalates as photocatalysts and stabilizers has

been reported by Troupis and coworkers.[27] These photooxometalates (POMs) are metal-oxygen cluster anions having ability to undergo stepwise, multielectron redox reactions under different conditions. Recently, Sastri and coworkers reported the use of Keggin ions (a type of photooxometalates consisting of $H_3(PW_{12}O_{40})$) as UV-switchable reducing agents in the synthesis of Au core-Ag shell nanoparticles.[28] They have also synthesized gold nanosheets by reduction of chloroaurate ions using anthracene anions, which were generated by exposure to photochemically reduced phototungstate.[29]

Several other methods are reported for the synthesis of metal nanoparticles. These include the synthesis in gas phase[30] or by ablation using high power laser pulses.[31] Metal nanoparticles can also be etched, electrodeposited or synthesized directly on surfaces or by using LB films.[32] The simplest of all these is the reduction method of synthesis summarized in Section 1.3.1, which doesn't require any specialized laboratory equipment.

1.4. Characterization of Nanoparticles

The ease of handling of MPCs (particularly, the excellent solubility in organic solvents) facilitates their structural as well as compositional analysis, which can be categorized as that of the central core (size and shape) and those of the surrounding monolayer. Various methods adopted for characterizing core size and shape as well as MPC monolayers are presented below.

1.4.1. Core size and shape

Recent advances in high-resolution microscopy enable the direct observation of nanoparticles and characterization of their size, shape and surface morphologies.[24] The direct measurement of the core size and shape is possible by means of transmission electron microscopy (TEM). In a recent article, Wang has reviewed the fundamentals of TEM, its applications in structure determination of shape-controlled nanocrystals and their assemblies.[33] TEM allows concomitant observation of the self-ordering and regular core-core spacing found in thin MPC films. In addition to high-resolution lattice imaging, TEM is powerful in identifying and quantifying the chemical and electronic structure of nanomaterials. Similarly, measurement of the core dimension is also possible by means of small angle X-ray scattering (SAXS), laser desorption-ionisation mass spectroscopy (LDI-MS) and X-ray diffraction (XRD) techniques.

The UV-Vis absorption spectrum of a dilute dispersion of colloidal particles can be calculated using Mie theory.[34] Theoretical studies and experimental findings have shown that nanomaterials also possess shape dependent optical properties. The shape of noble metal nanomaterials could be identified by means of UV-Vis absorption spectroscopy, making use of their plasmon resonance absorption. Recently, Noguez and coworkers have theoretically investigated the absorption characteristics of silver nanomaterials as a function of their shape.[35] A few representative examples are shown in Figure 1.5. Gold nanoparticles possess characteristic plasmon absorption around 520 nm. Interestingly in the case of

nanorods of gold, the plasmon absorption is characterized by two bands, one at a shorter wavelength (~520 nm) and the other at a longer wavelength.[36] The electron cloud in nanorods has two modes of vibration; longitudinal (parallel to the length of the nanorod) and transverse (along the short axis). The short wavelength band corresponds to the transverse mode of vibration and the long wavelength band to the longitudinal mode of vibration. El Sayed and coworkers have theoretically shown that the longitudinal absorption of gold nanorods shifts towards longer wavelengths with increasing aspect ratio.[37] Later on, the dependence of longitudinal absorption of nanorods was experimentally demonstrated in a series of nanorods synthesized photochemically, having different aspect ratios.[38]
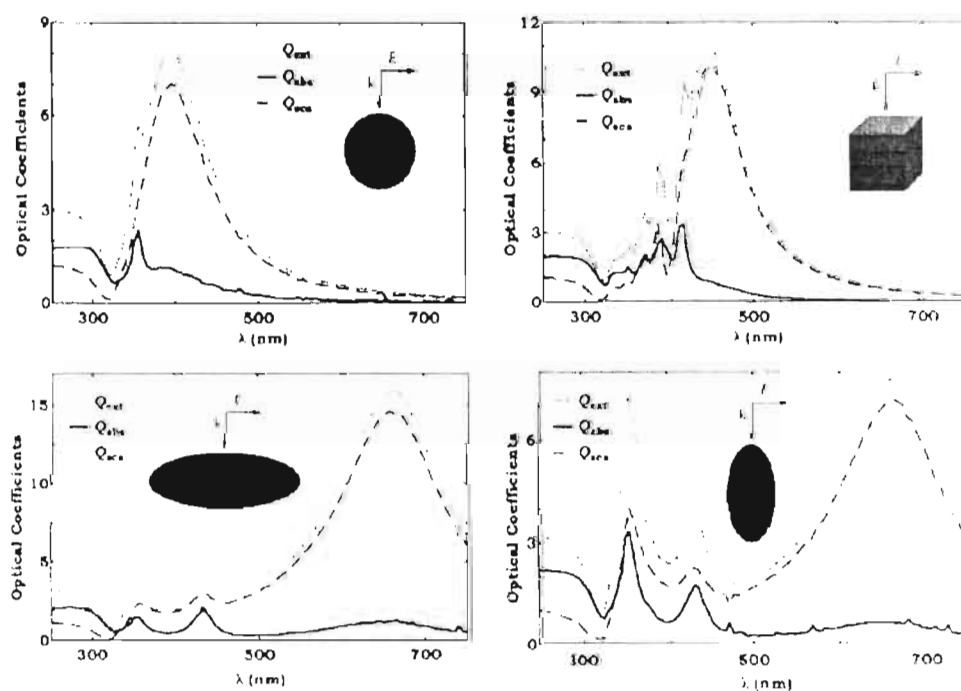
Figure 1.5. Representation of the theoretically calculated variation in optical properties of silver nanoparticles as a function of shape.[35]

1.4.2. MPC monolayers

While scanning tunneling microscopy (STM) and atomic force microscopy (AFM) can be used in conjunction with transmission electron microscopy (TEM) to find the thickness of the monolayer on the surface of metal nanoparticles, NMR spectroscopy is informative about the structure and content of MPC monolayers.[24] ^{1}H and ^{13}C NMR resonances of MPC monolayers of alkanethiols are characteristically broadened relative to those of free alkanethiols; the factors include spin-spin relaxational (T_2) broadening, a distribution in chemical shifts due to differences in Au-SR binding sites, and a gradient in monolayer packing density from near-core to chain terminus with associated dipolar broadening.[24] A typical illustration is shown in Figure 1.6.[24]
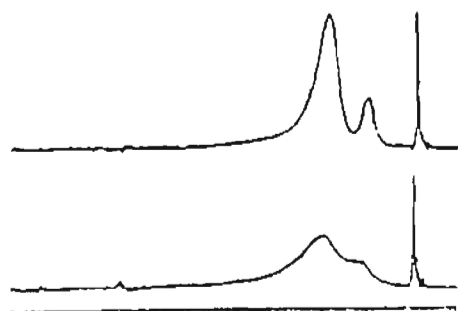
Figure 1.6. Broadening of the ^{1}H NMR resonances of α-methyl protons of dodecanethiol on the surface of gold.[24]

1.5. Supramolecular Self-assembly Using Metal Nanoparticles

The surface functionalization of nanoparticles allows their covalent attachment, self-assembly and organization of surfaces. The functionalization of nanoparticle surfaces has led to the construction of nanoparticle dimers and trimers, controlled aggregates, wires, ordered monolayers and multilayers.[39] The integration

of functional nanoparticles with surface has enabled the organization of nanoscale devices including single electron devices.[39] Chemical principles, in combination with symmetry considerations allow one to design rational strategies necessary for the construction of a variety of nanoscale systems with desirable shape, size and ultimately functions. The self-assembly process driven by noncovalent interactions, have long been exploited by nature, starting with photobiogenesis and the subsequent evolution of living organisms.[39] The power and versatility of this motive have been illustrated by the recent investigation of (i) the noncovalent synthesis of "rosette" aggregates, (ii) two- or three-dimensional self-assemblies of mesoscale objects by Whitesides and coworkers,[40] (iii) preparation of nanoporous molecular sandwitches by Ward *et al.*,[41] and (iv) the synthesis of self organized nanostructures by Stupp and coworkers.[42]

Recently, Wei *et al.* using resorcinarene tetrathiol[43] (Figure 1.7) have reported self-organization of large gold nanoparticle arrays at the air water interface. The hydrophobic interaction between the long alkyl chains has rendered the
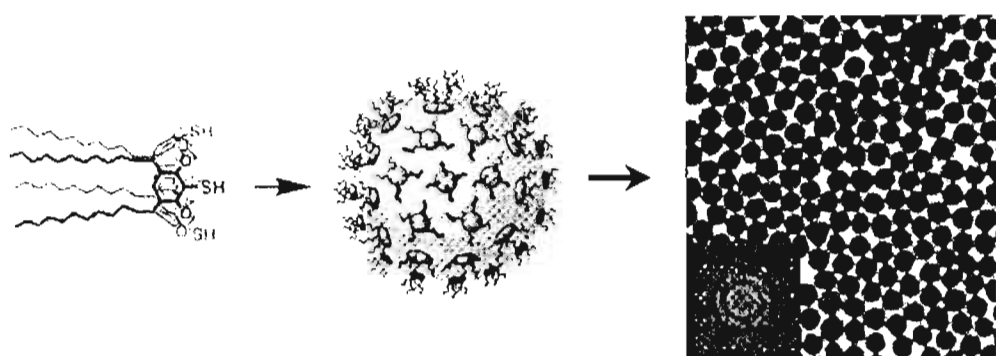
Figure 1.7. Gold nanoparticle functionalized with resorcinarene tetrathiol and electron micrograph of the corresponding self-organized assembly.[43]

encapsulated nanoparticles amphiphilic, hence promoting self-organization at the air-water interface.

By making use of the principles of self-organization, Mirkin *et al.* have reported a highly selective, colorimetric polynucleotide detection method based on mercaptoalkyl oligonucleotide modified gold nanoparticle probe.[44] Introduction of a single stranded target oligonucleotide into a solution containing the appropriate probes resulted in the formation of a polymeric network of nanoparticles with a concomitant red to pinkish/purple color change (Scheme 1.1).
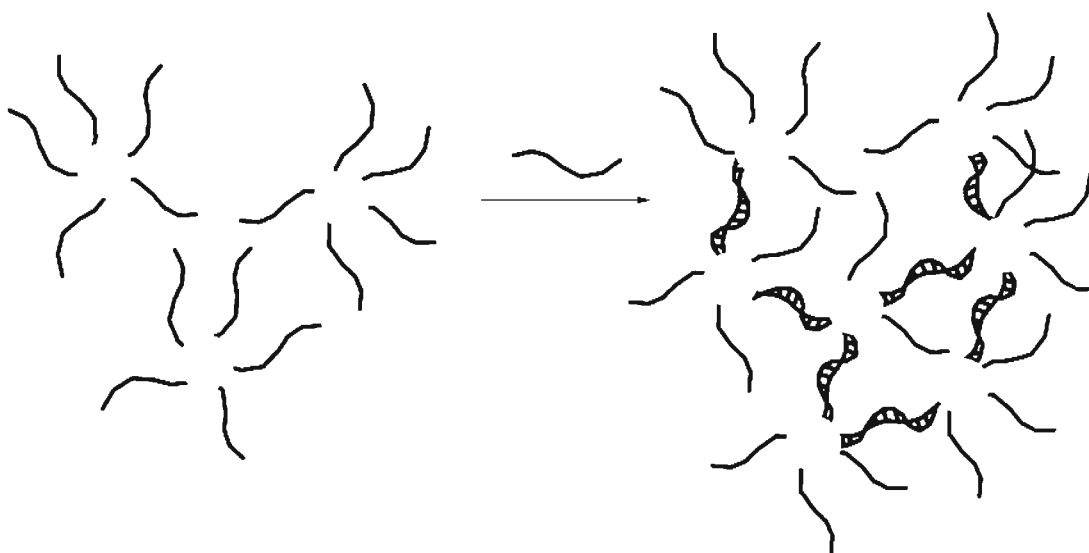
Scheme 1.1. Representation of the concept for the generation of aggregates of nanoparticles using oligonucleotides.[44]

Very recently, Shenhar and Rotello have presented a detailed review on the role of nanoparticles as scaffolds and building blocks for the fabrication of molecular devices such as sensors in the nanometric dimension with complete control of the 3-dimensional structure by the "bottom-up" approach.[45]

1.6. Chromophore Functionalized Metal Nanoparticles

Major challenges in the area of nanotechnology are (i) tailoring the optoelectronic properties of the nanoscale building blocks such as nanoparticles, nanorods, nanotubes and (ii) integrating them into functional assemblies and devices. It is possible to selectively tailor the optical and electrochemical properties of MPCs by capping the metal core with photo/electroactive molecules as shell materials. For example, extending the surface modification method to alkylthiols possessing ω-functionalized chromophore results in the formation of a well-ordered and tightly bound photoresponsive shell of nanometric dimensions, encapsulating the nanoparticle core. A pictorial representation of photoresponsive organic-inorganic nanohybrids is illustrated in Figure 1.8. Such photoresponsive antennae-systems may have potential applications as building blocks in diverse

Spacer   *Photoresponsive molecule*
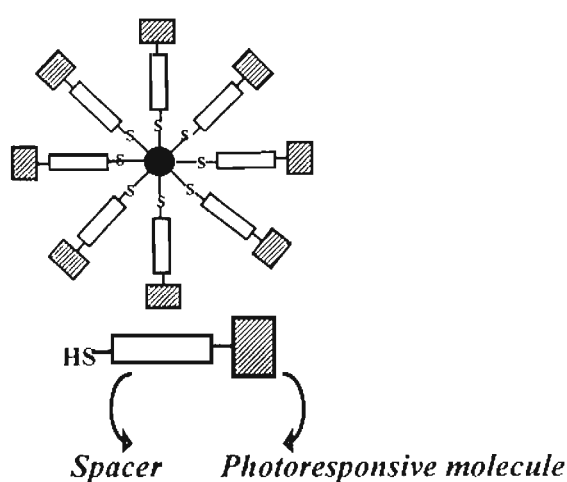
Figure 1.8. Photoresponsive organic-inorganic nanohybrid materials.

optoelectronic devices (sensors, switches, biological probes, light harvesting assemblies) and photonic systems.

Even though material properties of metal nanoparticles functionalized with thiols have been studied extensively, reports on the detailed photophysical and photochemical properties of these monolayer protected clusters (MPCs), modified with photoactive chromophores are rather few. This indirectly reflects the general belief that the metal cores of MPCs strongly quench the excited states of the chromophores when attached on the surface, through an energy transfer mechanism, impeding their photochemical properties and thus limiting their applications in devices. Interestingly, recent studies on the photophysical properties of chromophore linked gold nanoparticles from this laboratory[12] and others[46] have suggested a dramatic suppression in the quenching of singlet-excited state of these chromophores when compared with their 2-D assemblies. Also, these results suggest that the chromophoric molecules when capped on to metal nanoparticles possess unusual photophysical as well as excited state properties (unlike unbound chromophores), which could be exploited for device applications. Synthesis of MPCs bearing different chromophores such as pyrene,[47] porphyrin,[48] quinone,[49] fluorescene,[50] stilbinyl [51] and dansyl[52] chromophores have been reported by various groups. A brief summary on the photochemistry of chromophore functionalized metal nanoparticle is presented below. It may be noted that most of the reports on the synthesis and photophysical properties of chromophore functionalized metal nanoparticles appeared in last few years and the results presented below are not in chronological order, but summarized to understand the evolution of the topic.

1.6.1. Photochemistry of chromophore functionalized metal nanoparticles

Functional groups such as amines, isothiocyanates and thiols bind strongly to the gold surface and can provide a link between the photoactive group and gold surface. One of the earlier attempts to bind functionalized organic molecules on Au nanoparticle was reported by Thomas *et al.* by incorporating a fluorophore namely 1-aminomethylpyrene (Py-CH$_2$NH$_2$)[47] and a model compound ^{15}N labeled benzylamine (C$_6$H$_5$-CH$_2$NH$_2$) on TOAB capped gold nanoparticles.[53] The binding of ^{15}N labeled benzylamine to gold nanoparticles was probed using ^{15}N NMR spectroscopy. Two sets of signals were observed, one from the free molecules and the other from the molecules complexed to Au nanoparticles. In the case of 1-aminomethylpyrene (Py-CH$_2$NH$_2$) a dramatic enhancement of fluorescence (Figure 1.9) was observed on binding to the surface of gold nanparticles.[47] Py-CH$_2$NH$_2$ molecule in THF is weakly fluorescent since the intramolecular
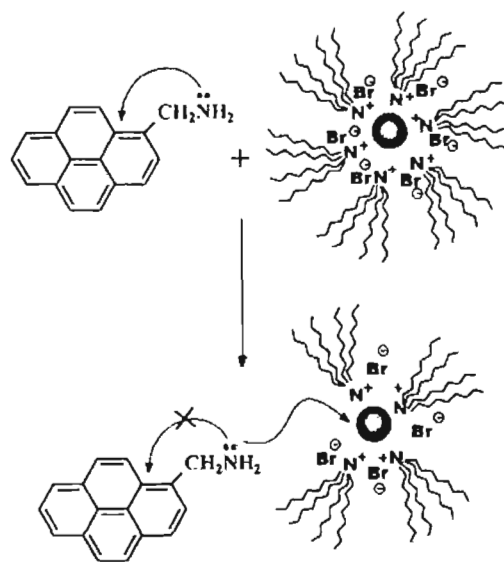
Figure 1.9. Fluorescence enhancement of aminomethylpyrene on the surface of gold.[47]

quenching due to electron transfer dominates the deactivation of the singlet excited state. Once Py-CH$_2$NH$_2$ molecules are attached to the surface of gold. the intramolecular electron transfer from the lone pair of the amine to pyrene is suppressed whereby the fluorescence is retained.

Extending the surface modification method to alkyl thiols possessing ω-functionalized chromophores results in the formation of chromophore functionalized Au-MPCs, which could be isolated from unbound chromophores and purified. Very recently Perry and coworkers reported the synthesis of ultrabright supramolecular beacons based on the self-assembly of two-photon chromophores on silver nanoparticles.[54] In biological imaging. there is a need for fluorescent labels with a large two-photon cross-section (δ) and high quantum efficiency (η) to enable detection at the single label level. In this MPCs. they could pack ~2500 chromophores with a nanoparticle of <10 nm diameter (Figure 1.10). These
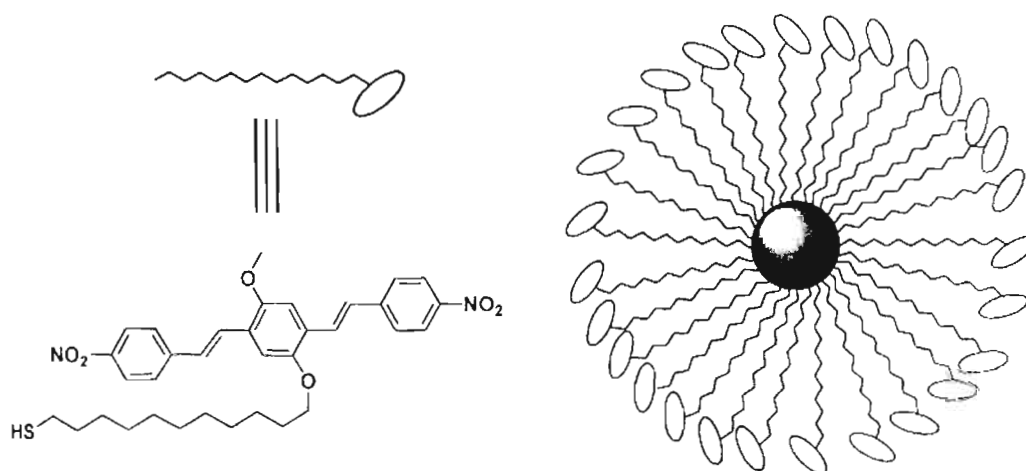
Figure 1.10. Schematic representation of silver nanoparticles coated with densely packed chromophore (structure of chromophore is shown on left).[54]

nanoparticles has one of the highest ever reported two-photon cross section. The high concentration of the chromophore and polyfunctionalizibility can have impact on ultrasensitive detection.

The above mentioned reports indicate that the fluorophore functionalized Au nanoparticle are emissive in nature which is against the belief that the emission of the chromophore is totally quenched on metal surface (for e.g., Au film). There are also several reports during last four years (2000-2003) illustrating photoinduced energy transfer processes from surface-bound chromophores such as dansyl derivative,[52] Ru(bpy)$_3$$^{2+}$,[55] fluorenyl derivative[56] and fullerene-C$_{60}$[57] to gold nanoparticle. Gold MPCs possessing mixed monolayers of alkanethiolate and ω-carboxylalkanethiolate ligands (Figure 1.11) were synthesized by Murray and
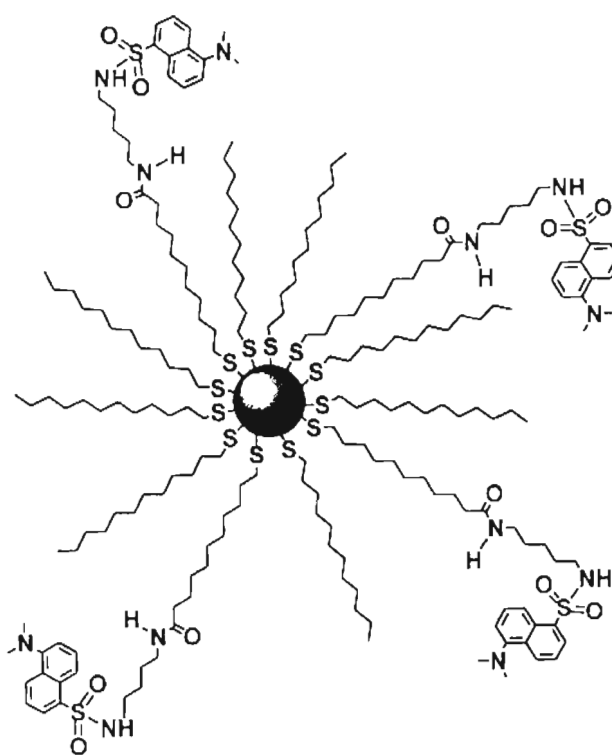
Figure 1.11. Dansyl chromophore functionalized gold nanoparticles.[52]

coworkers and functonalized them with chromophoric groups by reacting with fluorescent dansyl cadaverine molecules.[52] In these systems, distance dependent energy transfer were reported from the excited state dansyl group bound on gold MPCs. The emission intensity for MPC-attached dansyl group varied with (i) the number of dansyl sites per MPC, (ii) with the linker chain length between the gold core and dansyl site and (iii) with chain lengths of alkanethiolates in the surrounding MPC monolayer coating. They also observed that emission intensities of MPC-attached dansyl labels are lower than those for equivalent concentrations of dansyl units and MPCs in unattached form.

In a recent effort, Sudeep *et al.* synthesized fullerene molecules containing thiol functionality and attached them on the surface of gold nanoparticles (Figure 1.12).[57] An effecient energy transfer was observed from the excited state of
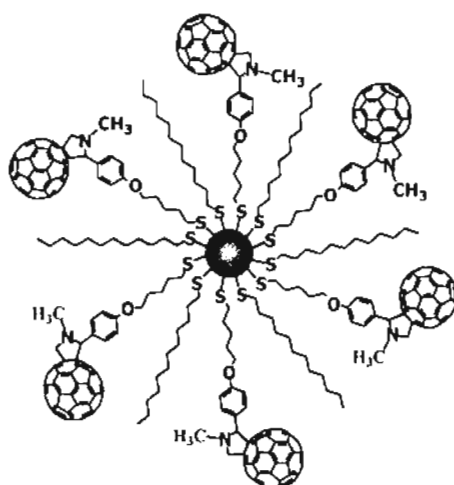
Figure 1.12. Fluorescence quenching of fullerene on gold nanoparticles.[57]

fullerene molecules to the gold nanocore. Large clusters of gold nanoparticles appended with fullerenes were observed under TEM. The cluster formation is

induced by the hydrophobic interaction between fullerene moieties. Here also they observed an efficient suppression of intersystem crossing ($S^1 - T^1$). In another report, light induced energy transfer from fluorene appended on long alkyl chains to gold nanocore was suggested by Fox and coworkers.[56] According to them, a dramatic quenching of the singlet excited state of fluorene was observed when bound to the surface of gold nanoparticles (Figure 1.13).[56] Also, the intersystem crossing (from fluorenyl singlet to the corresponding triplet) was suppressed due to the fast energy transfer. No evidence of electron transfer was observed in the case of fluorene capped Au nanoparticles.
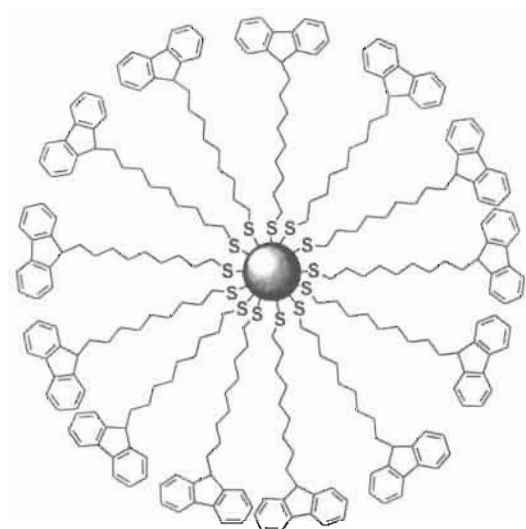
Figure 1.13. Fluorene functionalized gold nanoparticles.[56]

It is known for the past four decades or so that when a fluorophore molecule is bound to bulk metal surfaces, its singlet state lifetime decreases as a result of energy transfer from the excited dye molecules to metal films. Distance-dependent quenching of singlet excited states of chromophores on metal surfaces

was observed by Drexhage and coworkers.[58] In contrast, comparative studies on the photophysical and excited state properties of the chromophores when functionalized on gold nanoparticles (Au-MPCs) were not available till recently. The first systematic comparison of the time-resolved fluorescence of a porphyrin on the surface of Au metal films (Au-SAM) as well as on gold nanoparticles (Figure 1.14) has been reported by Imahori *et al.*[48] In both the cases, the porphyrin exhibited a biexponential decay with a short lived and a long lived component. The long lived species corresponds to the unquenched species exhibiting their intrinsic lifetime. The lifetime of the short lived species in Au-SAMs (0.04 ns) is 35 times smaller than that of the short lived component on Au-MPCs (1.2 ns). These results indicate that the quenching of the singlet excited state of porphyrin by gold clusters *via* an energy transfer is much suppressed relative to energy transfer quenching on Au(111) surface.[48]
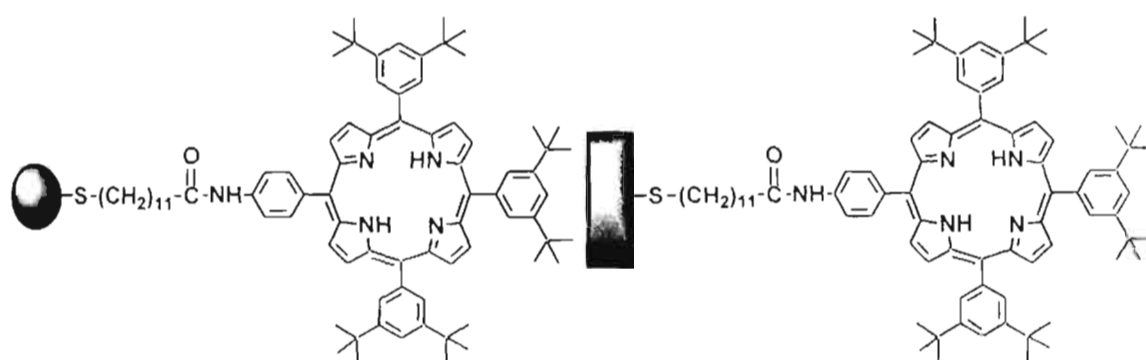
Figure 1.14. Comparative study of porphyrin fluorescence on Au nanoparticles and on gold electrode.[48]

The comparative studies summarized in the above section clearly indicate that the photophysics of chromophores bound on metal surface is significantly affected on transition from bulk metal to isolated nanoparticle. As mentioned in

Section 1.1, depending on size, metal nanoparticles can behave as conductors, semiconductors or insulators. For understanding the effect of this transition behavior of metal nanoparticles more clearly, Dulkeith *et al.*[59] functionalized lissamine molecules on gold nanoparticles of different size and isolated the resonant energy transfer rate from the decay rates of the excited dye molecules (Figure 1.15). The increase in lifetime with decreasing particle size (particle diameter range of 1-30 nm) was indicative of the decreased efficiency of energy transfer in smaller size particles.
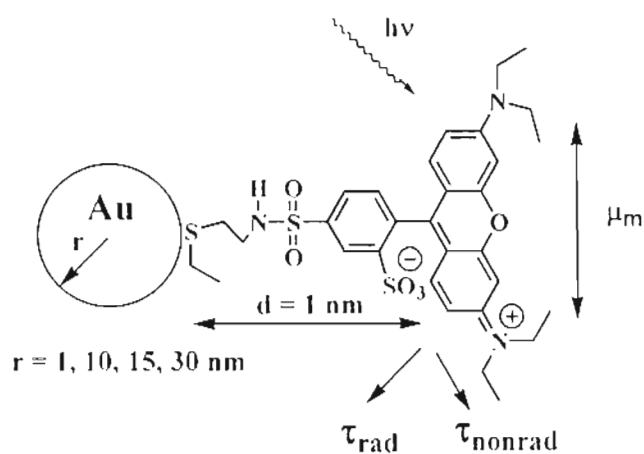
Figure 1.15. Lissamine functionalized gold nanoparticles.[59]

In a more recent study, Heeger and coworkers[60] also investigated the role of energy as well as electron transfer in the quenching of emission of conjugated polymers in the presence of gold nanoparticles of varying size. They suggested that resonance energy transfer dominates when the diameter of Au nanoparticle is >2 nm. In smaller particles, electron transfer dominates although no spectroscopic evidence was presented in the present case for characterizing the electron transfer

products. The charge transport in the nanoscale was extensively reviewed in a recent commentary.[61]

Photoinduced charge separation from J-aggregates of a chromophoric dye on silver nanoparticles was studied by Hranisavljevic *et al.*[62] The dye used was a cyanine derivative, 5,5'-dichloro-3,3'-disulfopropylthiacyanine sodium salt represented in Chart 1.1. They have shown that photoexcitation of the plasmon in Ag nanoparticles coated with J-aggregates leads to exciton dynamics that are much different from that of J-aggregate monolayers on bulk metal surfaces. Specifically, charge-separated states with a lifetime of ~300 ps between the J-aggregate and Ag colloid were formed. The observation is different than that for J-aggregates on the surface of bulk metals, where exciton quenching is observed.
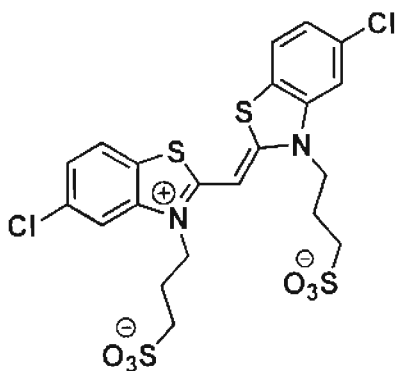
Chart 1.1. Photoinduced charge separation of J-aggregates on silver nanoparticles.[62]

From previous reports on the study of chromophore functionalized metal nanoparticles, it is clear that so far no study has been carried out by varying the concentration of chromophore on the surface of nanoparticles. Moreover several reports are available, indicating the possibility of electron transfer in small metal

nanoparticles, but no spectroscopic characterization is available yet. In the second Chapter of this thesis, we have made a detailed investigation on the excited state properties of pyrene functionalized gold nanoparticles by varying the number of pyrene per nanoparticle and solvent polarity.

1.7. Applications of Functionalized Metal Nanoparticles

Having made substantial advancements in the synthesis, characterization and assembly of metal nanoparticles, efforts are now on, to put these into desired shape, so as to extract functionalized nanomaterials for nanotechnology based devices in near future. With the fundamental finding that particles in the nano-dimensions exhibit fascinating physicochemical properties, there has been a plethora of scientific efforts to exploit their novel properties; potential applications of a few of these as future devices have already been demonstrated.

Dispersions and coatings in the nanodimension with increased surface area could be patterned/ordered at the nanolevel, which could revolutionize industries, dealing with paints, drug delivery, telecommunication, corrosion-protection etc. Colorimetric detection of DNA hybridization has been demonstrated by Mirkin *et al.* using gold colloids coated with DNA strands, which is a milestone in probe technology.[44] These aspects have been illustrated in Section 1.5. The ability of gold surface to bind with specific functional groups has made them suitable for fluorescence patterning.[63] Colloidal gold adsorbs strongly to some proteins, especially antibodies and could be used in sensing.[64,65]

Closely spaced arrays of metal nanoparticles can act as guides for electromagnetic radiations (waveguides) and a newer method for guiding electromagnetic energy, which allows miniaturization of device to sizes below the diffraction limit, has recently been reported by Maier *et al.*[66] (Figure 1.16). These waveguides rely on near-field interactions between closely spaced noble metal nanoparticles that can be efficiently excited at their surface plasmon frequency.[66] Near-field coupling between adjacent particles sets up coupled plasmon modes leading to coherent propagation of energy along these arrays. Such systems may contribute to advances in plasmonics. In a recent paper, a modified
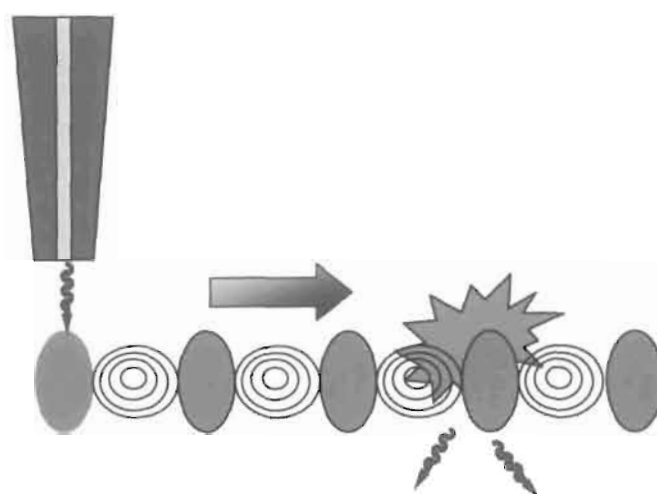
Figure 1.16. Schematic representation of energy transfer by means of near field coupling between closely paced metal nanoparticles.[67]

illumination near field scanning optical microscope (NSOM) was used as a local excitation source of a nanoparticle in these arrays. Transport of excitation energy in closely spaced arrays of metal nanoparticles is studied by imaging the fluorescence of dye-filled latex beads positioned next to the nanoparticle arrays.[67]

A pictorial representation of the energy transfer by near field coupling is shown in Figure 1.16.

In a recent work, Willner and coworkers have reported the assembly of layered 3D-superstructures, consisting of the bis-bipyridinium-Zn(II)-protoporphyrin as photosensitizer-acceptor dyad and gold nanoparticles. A schematic illustration of a photoelectrochemical device[68] fabricated using assembly of Au nanoparticles is shown in Figure 1.17. The superstructures were characterized by interparticle plasmon absorption. The conductivity studies of the array have suggested that these superstructure-modified electrodes could be used as materials for photoelectrochemical cells.
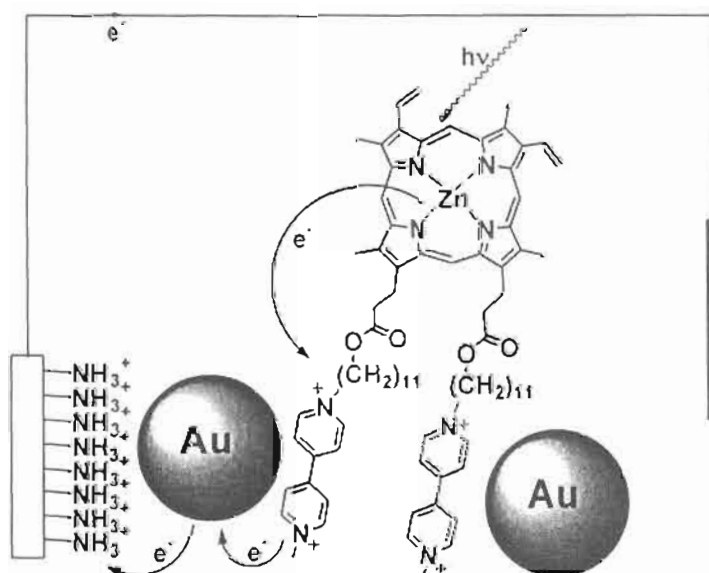
Figure 1.17. Photoelectrochemical device using assembly of gold nanoparticles.[68]

In a major breakthrough, Murray and coworkers have reported the transition from metal-like double-layer capacitive charging to redox-like charging in electrochemical ensemble coulomb staircase experiments with gold

nanoparticles.[69,70] By making use of the quantized capacitance behaviour of gold nanoparticles, Kamat and coworkers[71] have demonstrated the electrochemical modulation of pyrene fluorescence (Figure 1.18) on a nanostructured gold electrode. Spectroelectrochemical experiments were carried out using a thin layer electrochemical cell. As the electrode is biased to negative potentials, an increase in intensity of pyrene emission was observed. The overall shape of the emission band remains the same suggesting that the photoactive molecule contributing to the emission is unperturbed. At potentials more negative than -1.0 V, 90% of the
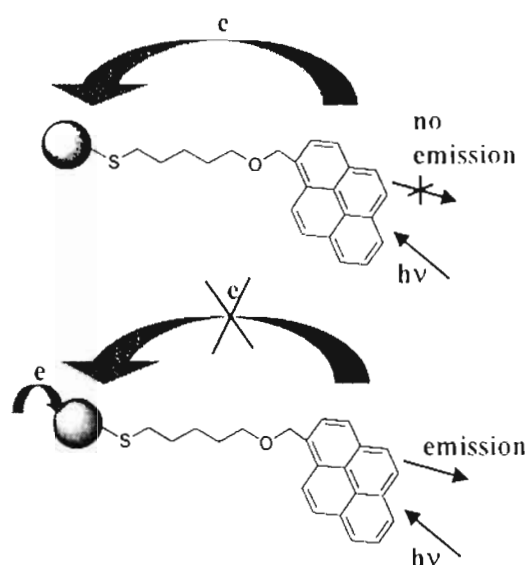
Figure 1.18. Deactivation of excited pyrene molecules on the surface of gold before and after charging the gold nanocore.[71]

quenched emission is restored by charging the gold nanoparticles. The modulation of fluorescence can be explained on the basis of charge transfer interaction between pyrene and gold nanocore at different applied potentials.[71] In the absence of applied potential, the electron transfer interaction between pyrene thiol and gold nanocore

anchored on an ITO plate, results in the quenching of fluorescence of the chromophore and it can be suppressed by applying suitable electrode potentials. The electron transfer from excited pyrene molecules to gold nanocore experiences a barrier when charged with negative electrochemical bias.

Using the principle of energy transfer, attempts are being made to develop biosensors.[72] For example, attachment of oligonucleotide molecules labeled with a thiol group at one end of the gold nanoparticle and a fluorophore at the other end has been used to recognize and detect specific types of DNA sequences and single-base mutations in a homogeneous format.

Second harmonic generation (SHG) properties of fluorescent polymer encapsulated gold nanoparticles (Figure 1.19) have been demonstrated by Campagnola *et al.*[73] The hybrid nanoparticles were prepared from gold particles of 100 nm size, coated with a styrene/methacrylic acid copolymer and were further linked to a naphthyl styryl chromophore *via* a succinimidyl ester linkage.[73]
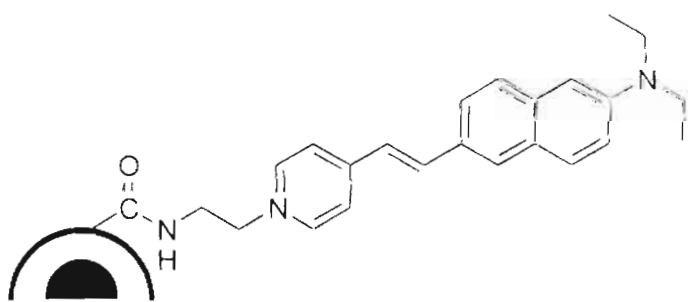
Figure 1.19. Fluorescent polymer encapsulated gold nanoparticles.[73]

Molecular electronics using nanomaterials of size less than 10 nm have been demonstrated by Schiffrin and coworkers by changing the oxidation state of a

bipyridine derivative which is attached to a gold electrode and a gold cluster by a chain of thiol 'clips'.[74] In this system, by using the tip of STM, the current flow through the molecular switch is measured. When bipyridine is in the +2 oxidation state, no current flows while on injection of electrons using STM to bipyridine, there is formation of bipyridine radical cation, resulting in a large current flow (Figure 1.20).
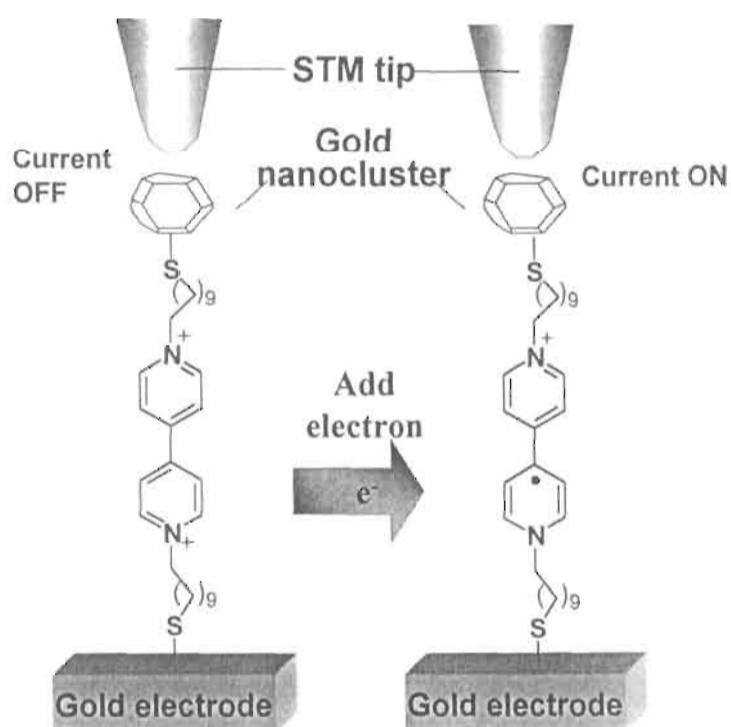
Figure 1.20. The molecular electronic switch using gold clusters and bipyridine.[74]

The results presented here indicate that functionalized nanometrials possess immense potential in miniaturizing future devices and nanotechnology will be central to the next epoch of technological endeavors. Nanotechnology unites chemistry, physics and biology and hence the possibilities are limitless. The design and development of nanoscale materials is not just enough towards

miniaturization. The physical as well as chemical properties of these materials, which are size and shape dependent often exhibit difference from the properties of the bulk material and these differences are not fully explained by current theories. The major challenge is to understand and exploit these unique properties for the development of next generation nanodevices.

1.8. Objectives of the Present Work

As mentioned in section 1.6, it is possible to tune the optoelectronic properties of MPCs by independently manipulating the properties of the organic shell. In this context, we have functionalized gold nanoparticles with photoactive molecules such as (i) polynuclear aromatic hydrocarbon (pyrene), (ii) photochromic molecule such as spiropyran and (iii) bipyridines. Excited state properties of these surface-bound photoactive molecules were examined using steady state and time-resolved techniques. The second chapter of the thesis describes the synthesis of gold nanoparticles functionalized with pyrene chromophore and study of their singlet excited state dynamics on Au surface as a function of i) solvent polarity, ii) distance of chromophore from gold core and iii) loading of pyrene on gold surface.

In the third Chapter we have investigated the photoswitchable self-assembly of amino acid derivatives by anchoring spiropyrans onto the three-dimensional surface of Au nanoparticles. The light-regulated changes in the topographic properties of spiropyran-capped Au nanoparticles (i.e.,

interconversion between the zwitterionic and neutral forms) were exploited for the assembly and release of amino acids such as L-tryptophan, L-tyrosine, L-DOPA and methyl-L-DOPA.

In the fourth Chapter, we report the synthesis of gold nanoparticles functionalized with bipyridine ligands and the study of their complexation studies with transition and inner transition metals in an effort to develop nanosensors and nanophosphors.

1.9. References

(1) *Nanotechnology Research Directions*: Roco, M. C.; Williams, R. S.; Alivisatos, P., Eds.; Kluwer Academic Publishers: Dordrecht, The Netherlands, 2001.

(2) Alivisatos, A. P. *Science* **1996**, *271*, 933.

(3) (a) Shipway, A. N.; Willner, I. *Acc. Chem. Res.* **2001**, *34*, 421; (b) Thomas, K. G.; Kamat, P. V. *Acc. Chem. Res.* **2003**, *36*, asap.

(4) Schmid, G.; Baunile, M.; Geerkens, M.; Heim, I.; Osemann, C.; Sawitonski, T. *Chem. Soc. Rev.* **1999**, 28.

(5) Shipway, A. N.; Katz, E.; Willner, I. *ChemPhysChem* **2000**, *1*, 18.

(6) Faraday, M. *Philos. Trans. R. Soc. London* **1857**, *147*, 145.

(7) Kamat, P. V. *J. Phys. Chem. B* **2002**, *106*, 7729.

(8) Kelly, K. L.; Coronado, E.; Zhao, L. L.; Schatz, G. C. *J. Phys. Chem. B* **2003**, *107*, 668.

(9)   Rechberger, W.; Hohenau, A.; Leitner, A.; Krenn, J. R.; Lamprecht. B.; Aussenegg, F.R. *Opt. Commun.* **2003**, *220*, 137.

(10)   Lewis, D. N. *Chem. Rev.* **1993**, *93*. 2693.

(11)   Rao, C. N. R.; Kulkarni, G . U.; Thomas, P. J.; Edwards, D. P. *Chem. Soc. Rev.* **2000**, *29*. 27.

(12)   Thomas, K. G.; Ipe, B. I.; Sudeep, P. K. *Pure & Appl. Chem.* **2002**. *74*. 1731.

(13)   Shipway, A. N.; Willner. I. *Chem. Commun.* **2001**, 2035.

(14)   Lomalia, D. A.; Naylor, A. M.; Goddard III, W. A. *Angew. Chem.* **1990**, *102*. 119.

(15)   Lehn, J. M. *Angew. Chem.* **1988**, *100*, 91.

(16)   Niemeyer, C. M. *Angew. Chem.* **1997**, *109*. 603.

(17)   Furstner. A. *Active Metals*, VCH. Weinheim, 1996.

(18)   *Colloidal Gold. Principles. Methods, and Applications*, Vol1; Hayat. M. A., Eds.; Academic Press, New York, 1989.

(19)   Ahmadi, T. S.; Wang, Z. L.; Green, T. C.; Henglein, A.; El-Sayed. M. A. *Science* **1996**, *272*. 1924.

(20)   Turkevich, J.; Stevenson, P. C.; Hiller, J. *Discuss. Faraday Soc.* **1951**, *11*. 55.

(21)   Brust, M.; Walker. M.; Bethell. D.; Schiffrin, D. J.; Whyman, R. *J. Chem. Soc., Chem. Commun.* **1994**, 801.

(22) Teranishi, T.; Hosoe, M.; Tanaka, T.; Miyake, M. *J. Phys. Chem.* 1999, *103*, 3818.

(23) (a) Schmid, G.: *Clusters and Colloids*, VCH, Weinheim, 1994; (b) Schmid, G. *Chem. Rev.* 1992, *92*, 1709.

(24) Templeton, A. C.; Wuelfing, W. P.; Murray, R. W. *Acc. Chem. Res.* 2000, *33*, 27.

(25) (a) Roos, C.; Schmidt, M.; Ebenhoch, J.; Baumann, F.; Deubzer, B.; Weis, J. *Adv. Mater.* 1999, *11*, 761; (b) Freeman, R. G.; Hommer, M. B.; Grabar, K. C.; Jackson, M. A.; Natan, M. J. *J. Phys. Chem.* 1996, *12*, 810.

(26) Esumi, K.; Suzuki, A.; Aihara, N.; Usui, K.; Torigoe, K. *Langmuir* 1998, *14*, 3157.

(27) Troupis, A.; Hiskia, A.; Papaconstantinou, E.; *Angew. Chem. Int. Ed.* 2002, *41*, 1911.

(28) Mandal, S.; Selvakannan, P. R.; Pasricha, R.; Sastry, M. *J. Am. Chem. Soc.* 2003, *123*, 1470.

(29) Sanyal, A.; Sastry, M. *Chem. Commun.* 2003, 1236.

(30) Andres, R. P.; Bielefeld, J. D.; Henderson, J. I.; Janes, D. B.; Kolagunta, V. R.; Kubiak, C. P.; Mahoney, W. J.; Osifchin, R. G. *Science* 1996, *273*, 1690.

(31) Nedderson, J.; Chumanov, G.; Cotton, T. M. *Appl. Spectrosc.* 1993, *47*, 1959.

(32) Moriguchi, I.; Shibata, F.; Teraoka, Y.; Kagawa, S. *Chem. Lett.* 1995, 761.

(33) Wang, Z. L. *J. Phys. Chem. B* **2000**, *104*, 1153.

(34) Mie, G. *Ann. Phys.* **1908**, *25*, 377.

(35) Sosa, I.; Noguez, C.; Barrera, R. *J. Phys. Chem. B* **2003**, *107*, 6269.

(36) Yu, Y. Y.; Chang, S. S.; Lee, C. L.; Wang, C. R. C. *J. Phys. Chem. B* **1997**, *101*, 6661.

(37) Link, S.; Mohamed, M. B.; El-Sayed, M. A. *J. Phys. Chem. B* **1999**, *103*, 3073.

(38) Kim, F.; Song, J. H.; Yang, P. *J. Am. Chem. Soc.* **2002**, *124*, 14316.

(39) Stang, P. J.; Olenyuk, B. *Acc. Chem. Res.* **1997**, *30*, 502.

(40) Terfort, A.; Bowden, N.; Whitesides, G. M. *Nature* **1997**, *386*, 162.

(41) Russell, V. A.; Evans, C. C.; Li, W.; Ward, M. D. *Science* **1997**, *276*, 575.

(42) Stupp, S. I.; LeBonheur, V.; Walker, K.; Li, L. S.; Huggins, K. E.; Keser, M.; Amstutz, A. *Science* **1997**, *276*, 384.

(43) Kim, B.; Tripp, L. S.; Wei, A. *J. Am. Chem. Soc.* **2001**, *123*, 7955.

(44) Elghanian, R.; Storhoff, J. J.; Mucic, R. C.; Letsinger, R. L.; Mirkin, C. A. *Science* **1997**, *277*, 1078.

(45) Shenhar, R.; Rotello, V. M. *Acc. Chem. Res.* **2003**, *36*, 549.

(46) Imahori, H.; Fukuzumi, S. *Adv. Mater.* **2001**, *13*, 1197.

(47) Thomas, K. G.; Kamat, P. V. *J. Am. Chem. Soc.* **2000**, *122*, 2655.

(48) Imahori, H.; Norieda, H.; Yamada, H.; Nishimura, Y.; Yamazaki, I.; Sakata, Y.; Fukuzumi, S. *J. Am. Chem. Soc.* **2001**, *123*, 100.

(49) Yamada, M.; Tadera, T.; Kubo, K.; Nishihara, H. *Langmuir* **2001**, *17*, 2363.

(50) Makarova, O. V.; Ostafin, A. E.; Miyoshi, H.; Norris, J. R.; Meisel, D. *J. Phys. Chem. B* **1999**, *103*, 9080.

(51) Hu, J.; Zhang, J.; Liu, F.; Kittredge, K.; Whitesell, J. K.; Fox, M. A. *J. Am. Chem. Soc.* **2001**, *123*, 1470.

(52) Aguila, A.; Murray, R. W. *Langmuir* **2000**, *16*, 5949.

(53) Thomas, K. G.; Zajicek, J.; Kamat, P. V. *Langmuir* **2002**, *18*, 3722.

(54) Stellacci, F.; Bauer, C. A.; Meyer-Friedrichsen, T.; Wenseleers, W.; Marder, S. R.; Perry, J. W. *J. Am. Chem. Soc.* **2003**, *125*, 328.

(55) Huang, T.; Murray, R.W. *Langmuir* **2002**, *18*, 7077.

(56) Gu, T.; Whitesell, J. K.; Fox, M. A. *Chem. Mater.* **2003**, *15*, 1358.

(57) Sudeep, P. K.; Ipe, B. I.; Thomas, K. G.; George, M. V.; Barazzouk, S.; Hotchandani, S.; Kamat, P. V. *Nano. Lett.* **2002**, *2*, 29.

(58) Drexhage, K. H.; Kuhn, H.; Shafer, F. P. *Ber. Bunsen-Ges. Phys. Chem.* **1968**, *72*, 329.

(59) Dulkeith, E.; Morteani, A. C.; Niedereichholz, T.; Klar, T. A.; Feldmann, J.; Levi, S. A.; Veggel, F. C. J. M. van.; Reinhoudt, D. N.; Moller, M.; Gittins, D. I. *Phys. Rev. Let.* **2002**, *89*, 203002.

(60) Fan, C. H.; Wang, S.; Hong, J. W.; Bazan, G. C.; Plaxco, K. W.; Heeger, A. J. *Proc. Natl. Acad. Sci. U.S.A.* **2003**, *100*, 6297.

(61) Adams, D. M.; Brus, L.; Chidsey, C. E. D.; Creager, S.; Creutz, C.; Kagan, C. R.; Kamat, P. V.; Lieberman, M.; Lindsay, S.; Marcus, R. A.; Metzger, R. M.; Michel-Beyerle, M. E.; Miller, J. R.; Newton, M. D.; Rolison, D. R.;

Sankey, O.; Schanze, K. S.; Yardley, J.; Zhu, X.: *J. Phys. Chem. B* **2003**, *107*, 6668.

(62) Hranisavljevic, J.; Dimitrijevic, N. M.; Wurtz, G. A.; Wiederrecht, G. P. *J. Am. Chem. Soc.* **2002**, *124*, 4536.

(63) Peng, X.; Hisao, Y. *Chem. Mater.* **1999**, *11*, 2626.

(64) Ribrioux, S.; Kelymann, G.; Haase, W.; Hietmann, K.; Ostermeier, C.; Michel, H. *J. Histochem. Cytochem.* **1996**, *44*, 207.

(65) Hainfeld, J. F.; Furuya, F. R. *J. Histochem. Cytochem.* **1992**, *40*, 177.

(66) Maier, S. A.; Brongersma, M. L.; Kik, P. G.; Atwater, H. A. *Phy. Rev. B* **2003**, *65*, 193408.

(67) Maier, S. A.; Kik, P. G.; Atwater, H. A.; Meltzer, S.; Hare, E.; Koel, B. E.; Requicha, A. A. G. *Nature materials* **2003**, *2*, 229.

(68) Lahav, M.; Gabriel, T.; Shipway, A. N.; Willner, I. *J. Am. Chem. Soc.* **1999**, *121*, 258.

(69) Chen, S.; Ingram, R. S.; Hostetler, M. J.; Pietron, J. J.; Murray, R. W.; Schaaff, T. G.; Khoury, J. T.; Alvarez, M. M.; Whetten, R. L. *Science* **1998**, *280*, 2098.

(70) Hostetler, M. J.; Green, S. J.; Stokes, J. J.; Murray, R. W. *J. Am. Chem. Soc.* **1996**, *118*, 4212.

(71) Kamat, P. V.; Barazzouk, S.; Hotchandani, S. *Angew. Chem. Int. Ed.* **2002**, *41*, 2764.

(72) Wang, G. L.; Zhang, J.; Murray, R. W. *Anal. Chem.* **2002**, *74*, 4320.

(73) Clark, H. A.; Campagnola, P. J.; Wuksell, J. P.; Lewis, A.; Loew, L. M. *J. Am. Chem. Soc.* **2000**, *122*, 10234.

(74) Gittins, D. I.; Bethell, D.; Schiffrin, D. J.; Nichols, R, J. *Nature* **2000**, *408*. 67.

CHAPTER 2

Synthesis and Photophysical Studies of Pyrene Functionalized Gold Nanoparticles

2.1. Abstract

Nanoparticles of gold (~2 to 3 nm) functionalized with a mixture of dodecanethiol and pyrene alkylthiols (pyrenes tethered with alkyl chains of different lengths; **P1**, **P2**, **P3**) were synthesized and their photophysical properties were investigated in detail. Steady state and time resolved emission studies indicate that the singlet-excited state of pyrene is quenched on the surface of gold nanoparticles. However, the quenching of pyrene fluorescence is far less on gold nanoparticles than on the surface of Au(111) as reported in the literature. While the singlet state of **P1** is quenched as a result of electron transfer processes to gold core, **P2** and **P3** follow a complex deactivation pathway. The long flexible alkyl chains tethering the pyrene moieties in **P2** and **P3** allow intermolecular excimer formation, in addition to electron transfer processes. In this Chapter, we report the first spectroscopic evidence of direct electron transfer between a gold nanoparticle and a surface-bound fluorophore **P2**, induced by pulsed laser irradiation. The suppression of S^1-T^1 intersystem crossing process as well as the formation of pyrene radical cation, determined by transient absorption studies confirm the excited-state interaction between the metal

nanoparticles and the surface-bound fluorophore. The charge separation is sustained for several microseconds before undergoing recombination.

2.2. Introduction

Unique electronic and chemical properties of metal nanoparticles have drawn the attention of chemists, physicists, biologists, and engineers who wish to use them for a new generation of nanodevices.[1-10] Electrochemical studies have established the electron-storing properties of gold nanoparticles and their ability to act as an electric relay on a given nanotemplate structure.[11-14] The molecule-like charging effects of gold nanoparticles, i.e., the ability of storing and shuttling of electrons, is a potential property worth exploring for photoinduced electron transfer applications.

Modification of the gold nanoparticles with fluorophores is important for the development of biological tracers as well as optoelectronic devices.[12,15,16] Gold nanoparticles themselves show limited photoactivity under UV-Visible irradiation, although photoinduced fusion and fragmentation have been observed under laser irradiation.[17-22] It is possible to tailor the optoelectronic properties of metal nanoparticles by independently manipulating the properties of the shell i.e., organizing chromophores of specific properties and functions on metal nanoparticles, yielding photoresponsive organic-inorganic nanohybrid materials.[23,24] This can be achieved by extending the surface modification method to alkyl thiols possessing ω-functionalized chromophore, resulting in well ordered and tightly bound photoresponsive shell of nanometric dimension, encapsulating the nanoparticle core.

Such metal hybrids of organic molecules assembled as two- or three-dimensional architectures provide routes for the design of hybrid materials with novel electrical, optical and photochemical properties. Also, the organization of densely packed photoresponsive shell encapsulating the nanoparticle core offers exciting opportunities for the design of novel photon-based devices for sensing, switching and drug delivery.

Most of the studies on the interaction between fluorophores and metal are limited to bulk gold surfaces modified with self-assembled monolayers. Direct binding of a fluorophore to the bulk metal surface often results in the total quenching of excited states.[25-28] Both energy transfer and electron-transfer processes are considered to be major deactivation pathways for excited fluorophores on metal surface. Indirect evidence for electron transfer between the chromophore and the gold surface has been obtained from photocurrent measurements.[29,30] In contrast, recent studies on the photophysical properties of chromophore-linked gold nanoparticles (Ru(bpy)$_3^{2+}$,[31] fluorenyl,[32] dansyl,[33] pyrenyl,[24] and porphyrin[30] derivatives) have suggested a dramatic suppression in the quenching of the singlet-excited state when these chromophores are densely packed on Au nanoparticle surfaces and the details are presented in Chapter 1. A better understanding of the excited state processes will enable effective utilization of chromophore-functionalized metal nanostructures for light-harvesting and other specialized applications. The possible deactivation pathways of the photoexcited fluorophore bound to a gold nanoparticle include, (i) emission from the chromphores bound on the metal nanoparticles, (ii)

intermolecular interactions, (iii) energy transfer, and (iv) electron transfer. Gaining insight into such processes using spectroscopic techniques is important for tuning the optoelectronic properties of gold-fluorophore nanoassemblies.

For investigating the excited state interactions between chromopohores and gold nanoparticles, we have selected a polyaromatic hydrocarbon based molecule namely pyrene which possesses interesting photophysical properties.[34,35] For example, pyrene forms excimers as well as exciplexes and act as electron donors or acceptors in photoinduced processes. These aspects are well documented and several pyrene based photochemical devices such as molecular sensors, switches, transducers, light harvesting systems have been proposed.[30,36] In this Chapter, we report the preparation of dodecanethiol stabilized Au nanoparticles, possessing pyrene molecules **P1, P2, P3** (Chart 2.1) tethered by alkyl groups of different chain lengths and the details of the light induced processes in these chromophore functionalized MPC's. The relative ratio of pyrene derivative and dodecanethiol were varied (15%, 30%, 60%) on the surface of gold nanoparticles in order to investigate the influence of chromophore concentration on the photophysical behavior of these nanoparticles. Gold nanoparticles functionalized with **P1, P2** and **P3** are hereafter referred as **Au-P1, Au-P2** and **Au-P3**, respectively.
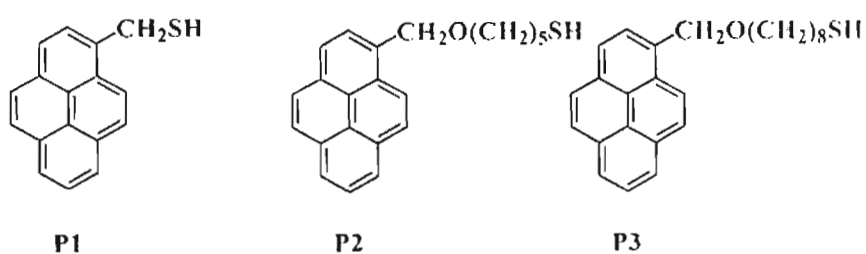
P1   **P2**   **P3**

Chart 2.1

2.3. Results and Discussion

2.3.1. Synthesis and characterization

Synthesis of **P1, P2, P3** was carried out as per Scheme 2.1: bromides (2.3a and **2.3b**) were prepared by following a nucleophilic substitution reaction of 1-pyrenemethanol with the corresponding α,ω-dibromoalkanes using sodium hydride as base. The conversion of bromides (**2.2, 2.3a** and **2.3b**) to thiols (**P1, P2** and **P3**) was carried out using the method reported by Fox and coworkers.[37] by reacting with a mixture of tetrabutylammonium fluoride and hexamethyldisilathiane. The details of the synthetic procedure and spectral characterization of these pyrene derivatives are given in the Experimental Section 2.5.
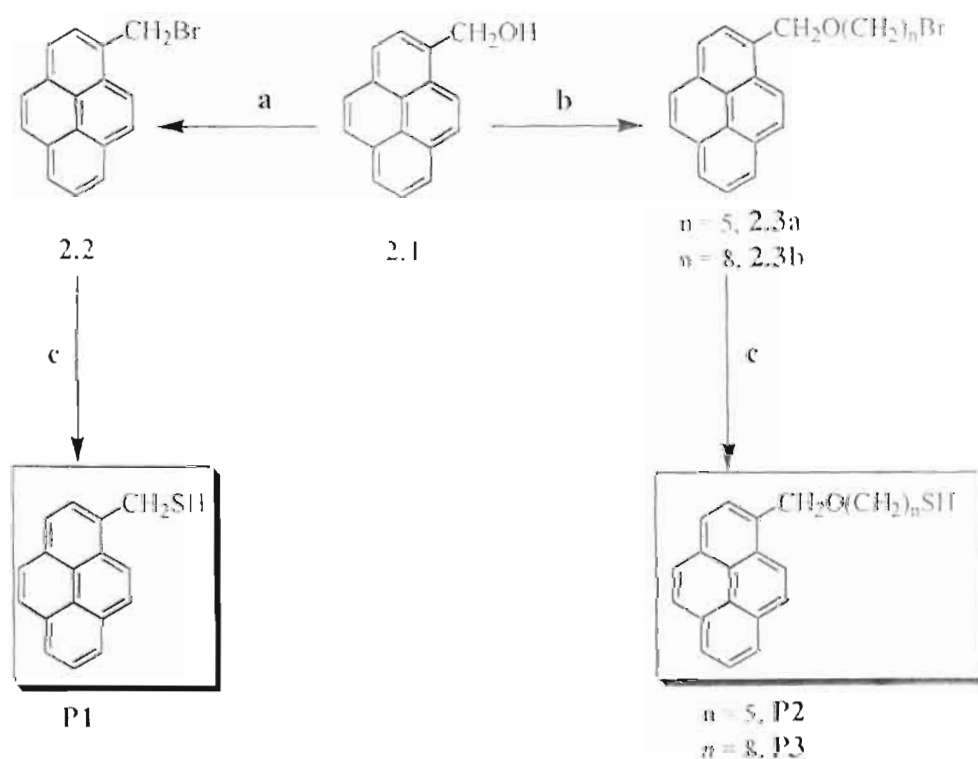
Scheme 2.1. (a) PBr₃, CHCl₃; (b) Br(CH₂)ₙBr, NaH, THF, reflux; (c) hexamethyldisilathiane, tetrabutylammonium fluoride, THF, -10 °C.

Synthesis of gold nanoparticles functionalized with **P1**, **P2**, **P3** was carried out by a modified procedure involving the biphasic synthesis reported by Brust *et al.*[38] The details of the synthesis and characterization of pyrene derivatives as well as pyrene functionalized gold nanoparticles are given in the Experimental Section. The coverage of the photoresponsive molecule was varied by co-binding with alkyl thiols and thiol derivatives of photoresponsive molecules (see Scheme 2.2).
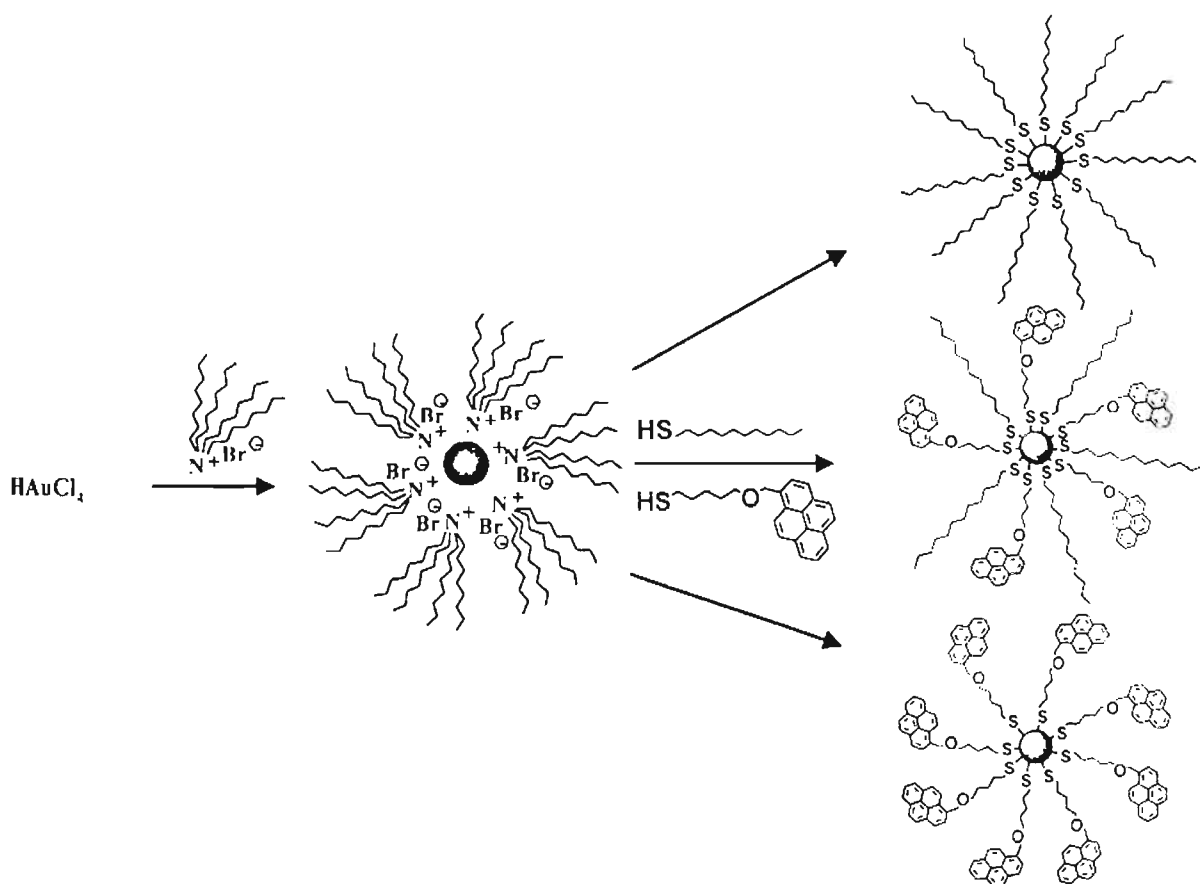
Scheme 2.2 Synthesis of gold nanoparticles with different loadings of pyrene

in different proportions (15%, 30%, 60%) which enabled us to fix the desired number of photoactive molecules around the metal nanoparticles. Also, co-binding with dodecanethiol ensured the uniform dispersion of pyrene moieties on gold

surfaces without inducing any ground state aggregation. The schematic representation of the functionalization of gold nanoparticles with pyrene derivatives and dodecanethiol in different molar ratios is presented in Scheme 2.2. Removal of any unbound fluorophores from the suspension was ensured by repeated precipitation using ethanol and details are presented in the experimental section (Section 2.5).

2.3.2. ^{1}H NMR spectroscopic characterization of gold nanoparticles

The surface functionalization of gold nanoparticles with pyrenyl ligands was investigated by means of one-dimensional ^{1}H NMR spectroscopy. Figure 2.1
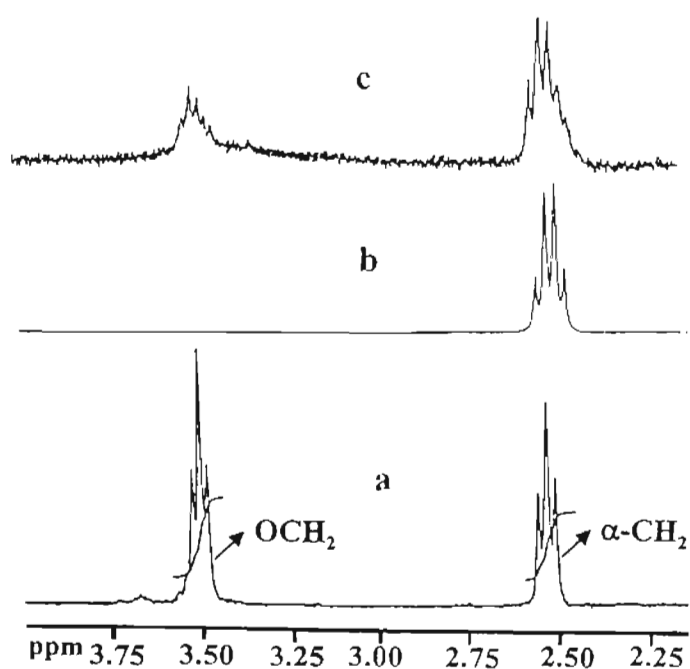
Figure 2.1. ^{1}H NMR spectra of a) **P2**, b) dodecanethiol, c) a mixture of **P2** and dodecanethiol (40:60) on the surface of gold clusters.

shows a representative example where the ^{1}H NMR signals of **P2** and **Au-P2** are compared. A significant broadening of the NMR signals (for example. α-

methylene protons) was observed for **P2** on the surface of gold nanoparticles. One of the factors contributing to the peak broadening is the dipolar spin relaxation of **P2** on the densely packed regions near to the thiolate/gold interface, when compared to free thiolates.[4] Another factor which contributes to the broadening is the differences in the binding sites for **P2** molecules on Au nanoparticles. It may be noted that the surfaces of gold nanoparticles are not uniform. The heterogeneity arising due to the non-uniform distribution of thiolate ligands during synthesis, thus leads to the broadening of resonance peaks. In summary, the broadening of NMR signals confirms the attachment of the thiolates on metal nanoparticle surfaces.

2.3.3. TEM studies of pyrene functionalized gold nanoparticles

The size of Au nanoparticles was determined by means of TEM experiments. The TEM and HRTEM images of Au nanoparticles functionalized with P2 are shown in Figure 2.2. It is observed that the average size of gold nanoparticles synthesized is ~2 nm. The size of the ligand is one of the factors which influences the size of nanoparticles during its formation. It is reported that arenethiolate stabilized gold nanoparticles possesses larger size than alkylthiolate stabilized gold nanoparticles.[39] In the present case, the average size of gold nanoparticles functionalized with **P2** is similar to that of alkylthiol protected clusters (MPCs). Although pyrenyl groups are bulky, they are well separated from the gold core by means of the alkyl chain and hence may not influence the size of the particles.
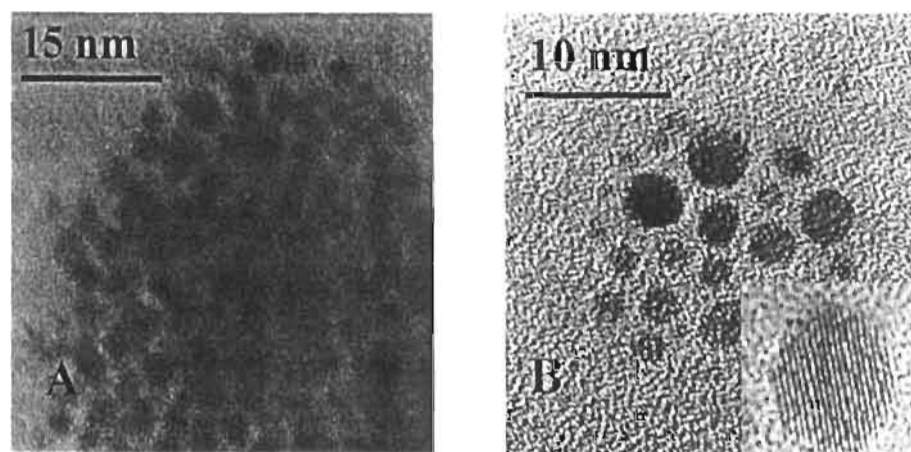
Figure 2.2. TEM (a) and HRTEM (b) images of gold nanoparticles functionalized with **P2**.

2.3.4. Absorption studies

Details of the synthetic procedure for preparing pyrene functionalized Au nanoparticles (**Au-P1, Au-P2, Au-P3**) are presented in the Experimental Section. In the preparation of these functionalized nanoparticles, not all ligands may react with gold nanoparticles and the concentrations of these unreacted ligands were evaluated from the absorption spectra of the filtrates. The concentration of the pyrene alkylthiols per Au nanoparticle was estimated, assuming that the reacted chromophores are evenly distributed on each nanoparticle. It was earlier estimated that a nanoparticle of gold having 2 nm size possesses approximately 314 atoms.[40] Based on the assumption that Au nanoparticles are spherical in shape, the number of pyrene molecules functionalized on the surface of gold were estimated as ~30, 45 and 55 for 15%, 30% and 60% loadings, respectively in the case of **Au-P2**.

Monolayer protected gold nanoparticles possess a characteristic surface plasmon absorption band, centered around 520 nm, arising from the interaction of external

electromagnetic radiation with the highly polarizable Au $5d^{10}$ electrons of gold nanoparticles.[41,42] The absorption spectra of pyrene capped gold nanoparticles normalized at 520 nm with different loadings of **P1, P2, P3** are presented in Figure 2.3.
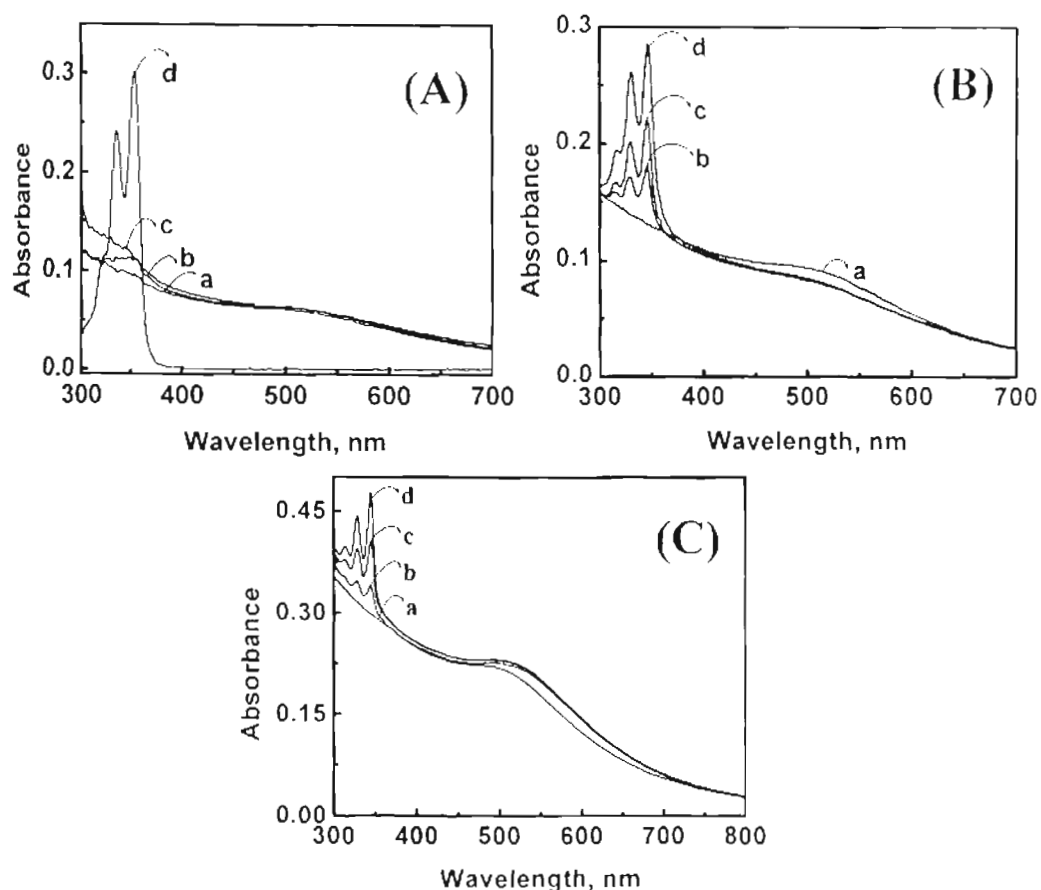
Figure 2.3. Absorption spectra of Au nanoparticles functionalized with different loadings of pyrene thiols (A): (a) 15%, (b) 30%, (c) 60% of **P1**.(d) **P1**; (B): (a) 0%, (b) 15%, (c) 30%, (d) 60% of **P2**; (C): (a) 0%, (b) 15%, (c) 30%, (d) 60% of **P3**, in toluene.

In the present case, the absorption spectrum of **Au-P1, Au-P2** and **Au-P3** possesses two sets of bands; an absorption band in the UV region, characteristic of functionalized pyrene molecules and a broad band in the visible region (~520 nm), attributed to the surface plasmon absorption of gold nanoparticles. A significant

dampening and broadening of surface plasmon absorption was noticed for all the three compounds. Dampening of surface plasmon band is characteristic of smaller gold nanoparticles (< 5 nm), capped with organic molecules such as thiols.[11,13]

A comparison of the absorption characteristics of **P1** and **Au-P1**, possessing different loadings of **P1** are presented in Figure 2.3A. The structured absorption bands of pyrene molecule are found to be significantly perturbed in the case of **P1** (pyrene methylthiol), when functionalized on to the surface of gold nanoparticle (traces 'a' to 'e'), indicating a strong ground state interaction. The absorption characteristics of **P2** and **P3** functionalized gold nanoparticles holding different concentrations of pyrene chromophores are presented in Figures 2.3B and 2.3C. Interestingly, the absorption spectra of **P2** and **P3** capped gold nanoparticles are almost the additive spectra of dodecanethiol capped gold and pyrenethiols of respective loadings, in each case. The absorption in the 300-350 nm region show three distinct absorption bands (313, 328, and 345 nm), corresponding to the absorption of pyrene. The structured absorption bands of pyrene remain more or less unperturbed (trace 'b-d'), indicating the absence of any ground state interaction.

The flexible methylene spacers in **P2** and **P3** are long enough to prevent the through bond electronic interaction of pyrene to gold nanocore in **Au-P2** and **Au-P3**. Also, the possibility of different conformers directly interacting with gold is very less due to the densely packed alkyl chains on Au nanoparticles. The interdigitation of a bulky polynuclear aromatic hydrocarbon like pyrene through these alkyl chains is still minimized by hydrophobic repulsive interactions with the alkyl chain moieties. On the

other hand pyrenyl moiety on **Au-P1** is very close to the metal surface and the possibility of electronic perturbation is very high. In an earlier communication by Thomas and Kamat.[24] a similar ground state interaction was observed between 1-pyrenemethylamine and TOAB (Tetraoctylammonium bromide) stabilized gold.

2.3.5. Steady state emission studies

Pyrene has a characteristic structured emission between 375 to 390 nm corresponding to the singlet excited state of the monomer form of pyrene, whereas a broad emission is observed between 450-550 nm, in certain cases, as a result of intermolecular excimer formation.[44] The latter emission is observed when the concentration of pyrene is high enough to form excited state dimers or in constrained/heterogenious media wherein the mobility of the polynuclear aromatic hydrocarbon molecules is minimized. It is well established that the optimum condition for excimer formation in pyrene is a parallel, sandwich type arrangement with an interplanar separation of 353 pm.[44]

The emission spectra of different loadings of **Au-P1**, **Au-P2** and **Au-P3** are presented in Figure 2.4. In all the three cases, the structured emission, characteristic of the monomer emission of pyrene was observed between 375 to 390 nm. Interestingly, the excimer formation of pyrene alkylthiolates functionalized on gold nanoparticles was strongly dependent on the loading of the chromophores and the length of the spacer groups. At a lower loading of 15%. excimer formation was not observed in all the three cases. This may be due to the

restricted interaction between pyrene moieties on a single nanoparticle, resulting from the interdigitation with long dodecanethiol ligands.

Eximer formation was also investigated by varying the linker properties (Figure 2.4). In the case of **Au-P1**, where pyrene is linked to Au nanoparticle by a
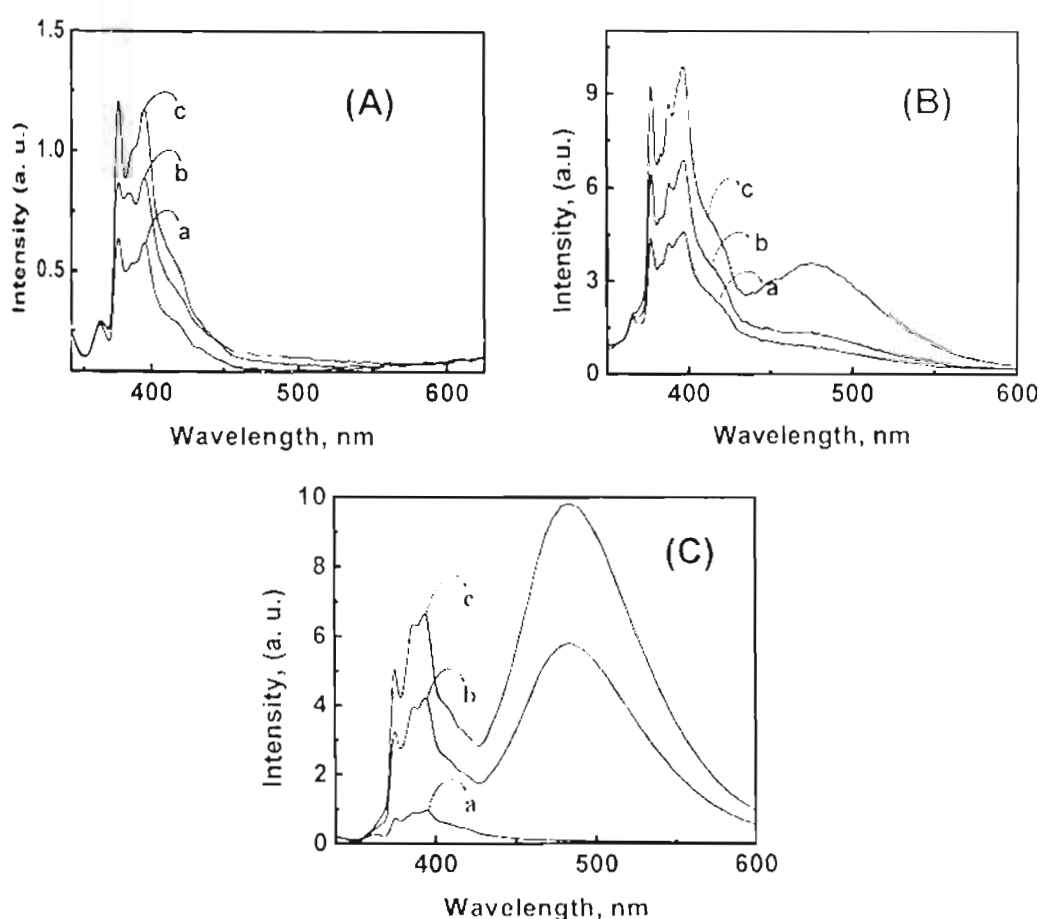
Figure 2.4. Emission spectra of Au nanoparticle functionalized with different loadings of pyrene thiols (A): (a) 15%, (b) 30%, (c) 60% of **P1**; (B): (a) 15%, (b) 30%, (c) 60% of **P2**; (C): (a) 15%, (b) 30%, (c) 60% of **P3**, in toluene. (excitation wavelength 328 nm, Au concentrations were kept constant by optically matching the solutions at 520 nm).

methylene group, no excimer emission was observed even at a high loading of 60% pyrene. In constrast, the excimer emission centered around 480 nm

become prominent for **Au-P2** and **Au-P3** systems at higher loadings (Figures 2.4B and 2.4C). It may be noted that **Au-P2** and **Au-P3** nanoassemblies possess five and eight methylene spacer groups between Au nanoparticle and pyrene chromophore. The situation is slightly different for **Au-P3** system: it shows prominent excimer emission even at low loadings of pyrene (30%), and interestingly the excimer emission is more intense than the normal fluorescence at 60% loading. The flexible alkyl chain tethering pyrene in Au-P3 is sufficiently long enough to protrude outside the dodecanthiol layer allowing free interaction between pyrene molecules, at higher loadings. On the other hand, pyrene chromophores in **Au-P1** are linked to Au nanoparticle by a single methylene group and the interplanar distance between the pyrene molecules is larger due to the restrictions imposed by the curvature of gold surface. In the case of **Au-P1**, no excimer emission was observed even at 60% loadings, may be because the pyrene chromophores are deeply embedded inside dodecanethiol.

The possibility of formation of excimer resulting from an interparticle interaction is ruled out. In the present case, excimer emission is dependent on the loading of the chromophore. Any possibility for interparticle interactions may lead to the excimer emission, irrespective of the loading of pyrene chromophore. The spectral shapes of the plasmon absorption of gold nanoparticle at different loadings of pyrene alkylthiol (**P1**, **P2**, and **P3**; Figure 2.3) were more or less the same, ruling out the possibility of the formation of

excimer emission through interparticle interactions. Also, such interparticle interactions would give rise to an interparticle plasmon coupling. This type of coupling can shift the plasmon absorption of gold nanoparticles to the red region and such shifts in plasmon absorption are not observed in present case.

From the steady state experiments, it is not possible to evaluate the quantum yield of fluorescence once the pyrene chromophores are attached on the surface of gold due to the overlap with plasmon absorption. Gold nanoparticles have a broad absorption in the spectral region of 300-350 nm and hence some of the excitation energy will be absorbed by gold in **Au-P1, Au-P2** and **Au-P3** systems. Due to these reasons, the fate of the singlet excited state of pyrene functionalized on Au nanoparticle cannot be elucidated comprehensively without time resolved fluorescence studies.

2.3.6. Time resolved fluorescence studies

As mentioned earlier, the possible deactivation pathways of the photoexcited fluorophore bound to a gold nanoparticle are through (i) radiative decay from the singlet excited state of the chromphores, (ii) excited state complex formation resulting from intermolecular interactions such as excimer emission, (iii) energy transfer and (iv) electron transfer processes. The possible deactivation pathways of the photoexcited fluorophore bound to Au nanoparticle were investigated from the singlet lifetimes by varying the (i) length of the alkyl chain, (ii) loading of the chromophores on Au nanoparticle

and (iii) solvent polarity. Fluorescence lifetimes were measured from the fluorescence decay of **P1**, **P2**, **P3** and the corresponding pyrene alkylthiol capped on gold nanoparticles using a picosecond single photon counting system and the details are presented in the Experimental Section. In all these experiments, the solutions were thoroughly degassed using argon. The samples were excited at 360 nm and the emission collected at 390 nm to evaluate the decay of the singlet-excited state of the monomer while the excimer emission (consists of the growth component and decay component) was monitored at 500 nm. The decay components of **P1**, **P2** and **P3** in toluene at 390 nm (see for example trace 'a' in Figure 2.5A for **P2**) and the growth and decay components at 500 nm are presented in Table 2.1.

The decay of pyrene when it is attached to another molecular component is often multiexponential:[45,46] for example, bi-/triexponential decay is reported for pyrenyl dendrimers and their precursors.[47] In the present case the unbound pyrene alkylthiols, **P1**, **P2** and **P3**, follow biexponential decay, both at 390 nm and 500 nm. One of the components of the biexponential decay at 390 nm has a decay time of ~8 ns and is assigned to the inherent lifetime of pyrene alkylthiol. From the steady state emission it is clear that the singlet excited state deactivation of pyrene alkylthiol results in normal emission and excimer formation. The short lived species is assigned to the quenched pyrene alkylthiol molecules, resulting from the interaction with another ground state pyrene alkylthiol molecule leading to the formation of excited state dimers.
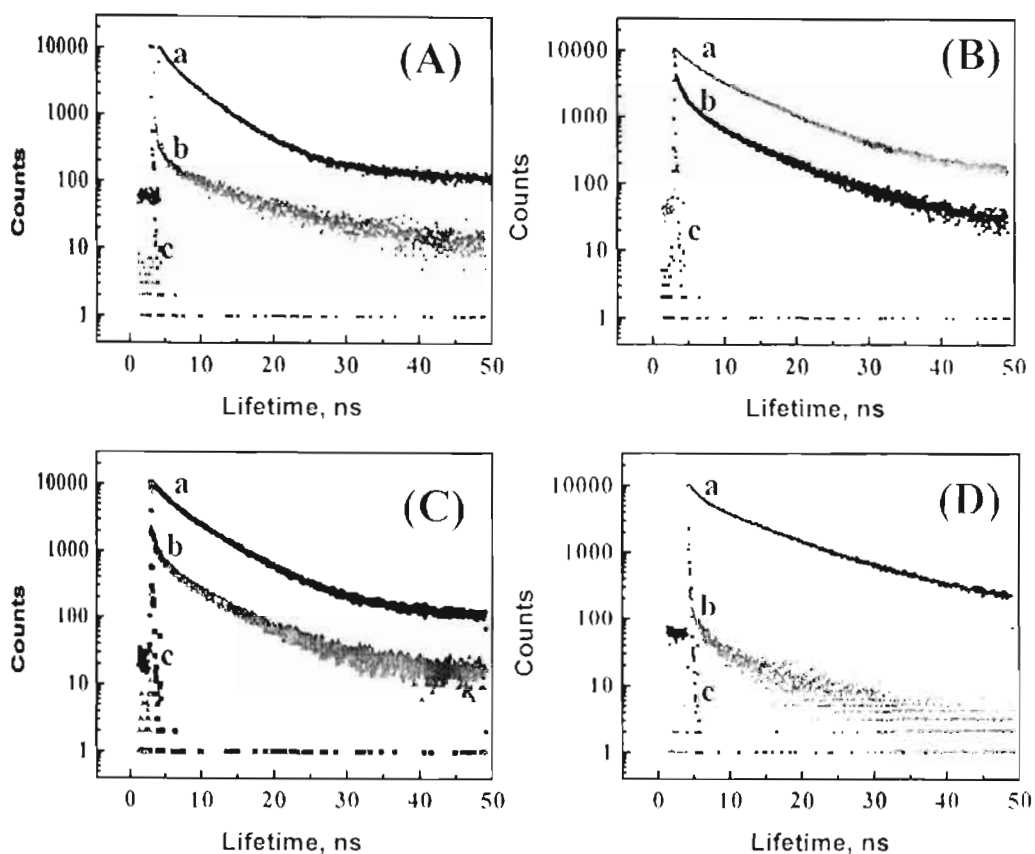
Figure 2.5. Comparison of fluorescence decay profiles; **A** in toluene of a) **P2**, b) **Au-P2**, **B** in tetrahydrofuran of a) **P2**, b) **Au-P2**; **C** in dichloromethane of a) **P2**, b)**Au-P2**; **D** in acetonitrile of a) **P2**, b)**Au-P2**; trace 'c' is the lamp profile in all plots and all **Au-P2** samples has 60 % loading of **P2**. Emission was monitored at 390 nm.

The band at 500 nm corresponds to the excimer emission, based on steady state emission studies, and intermolecular interactions were investigated in detail. The excimer decay of pyrene alkylthiols has a rise-time of ~2 ns and a long-lived decay component (note that the rise-time and decay of excimer were fitted together). The rise time at 500 nm is attributed to the formation of excimer in a dynamic process resulting from the interchromophoric interaction between a ground state and excited state pyrene molecule. This is supported by the fact that the decay kinetics of the short lived

component (~2 ns) at 390 nm matches well with the rise-time of the excimer. The long

lived component at 500 nm corresponds to the intrinsic decay time of pyrene excimer.

Table 2.1. Fluorescence lifetimes[a-c] and fractional contributions[d] of pyrene alkylthiols (**P1**, **P2** and **P3**) in toluene.

System	Fluorescence lifetimes					
	Decay at 390 nm		χ^2	Growth at 500 nm	Decay at 500 nm	χ^2
	τ_1, ns (χ_1%)	τ_2, ns (χ_2%)		τ_2, ns (χ_2%)	τ_1, ns (χ_1%)	
P1	8.6 (81 %)	1.8	1.10	1.8	8.5	1.10
P2	7.9 (65 %)	2.5	1.10	2.5	28.1	1.10
P3	7.6 (71 %)	2.5	1.05	2.5	11.5	1.06

a) τ_1 and τ_2; b) error limit ± 5%; c) excited at 360 nm; d) χ_1 and χ_2.

The singlet lifetimes of pyrene alkylthiols (**P1**, **P2** and **P2**) were investigated

in solvents of varying polarity (see traces 'a' in Figures 2.5 A to D for **P2**) and the

results are summarized in Table 2.2. In all solvent systems investigated, the decay

of the unbound pyrene alkylthiols follows a biexponential decay, with long-lived

(τ_1, 6.3 - 9.6 ns) and short-lived (τ_2, 1.4 - 2.0 ns) components. Lifetimes of the

long-lived (τ_1) and short-lived (τ_2) species and their fractional contributions

remain more or less unaffected ruling out the possibility of an electron transfer

process in polar solvents (note that a slight variaton in fractional contributions was observed in THF).

The decay characteristics of pyrene derivatives namely **P1**, **P2** and **P3** when bound to the surface of gold nanoparticles, were further investigated in a nonpolar solvent such as toluene and are presented in Table 2.3 (see trace 'b' in Figure 2.5 A for **Au-P2**). Lifetimes of the long-lived (τ_1) and short-lived (τ_2) component and their relative distribution remains more or less unaffected for **Au-P3**, in toluene. These results rule out the possibility of any quenching process (electron or energy transfer) in nonpolar solvents (toluene) when **P3** is bound to Au nanoparticles.

Table 2.2. Fluorescence lifetimes[a] and fractional contributions[b] of **P2** by varying the solvent polarity.

Solvent	Fluorescence lifetimes (P2)					
	Decay at 390 nm			Decay at 500 nm	Growth at 500 nm	
	τ_1, ns (χ_1%)	τ_2, ns (χ_2%)	χ^2	τ_1, ns	τ_2, ns	χ^2
Toluene	7.9 (65 %)	2.0 (35 %)	1.10	28.1	2.5	1.10
Dichloromethane	6.3 (58 %)	1.7 (42 %)	1.00	68.0	1.7	1.09
THF	9.6 (74 %)	1.9 (26 %)	0.99	42.0	1.1	1.10
Acetonitrile	8.9 (64 %)	1.4 (36 %)	1.30	27.0	2.7	1.09

a) τ_1 and τ_2; b) error limit ± 5%; c) excited at 360 nm; d) χ_1 and χ_2.

The excimer characteristics (growth and decay at 500 nm: Table 2.3) of pyrene alkylthiols bound to the surface of Au nanoparticle (traces 'b' in Figures 2.5 A – Figures 2.5 D for **Au-P2** represents the decay at 390 nm in different solvents) were similar to those of unbound pyrene alkylthiols (Table 2.1). The excimer decay of **Au-P2** and **Au-P3** has a rise-time resulting from the formation of excimer and a long-lived decay component attributed to the decay of the excimer. Interestingly, an additional fast component with extremely short lifetime (τ_3) was observed when **P1** and **P2** are attached on gold nanoparticles ($\tau_3 = 27$ ps for **Au-P1**, $\tau_3 = 48$ ps for **Au-P2**)

Table 2.3. Fluorescence lifetimes[a-c] and fractional contributions[d] of pyrene derivatives (60 %) on the surface of gold in toluene.

System	Fluorescence Lifetimes							
	At 390 nm				At 500 nm			
	τ_1, ns (χ_1%)	τ_2, ns (χ_2%)	τ_3, ns (χ_3%)	χ^2	τ_1, ns (χ_1%)	τ_2, ns (χ_2%)	τ_3, ns (χ_3%)	χ^2
Au-P1	14.8 (60 %)	3.6 (25 %)	0.027 (15 %)	1.2	-	-	-	-
Au-P2	7.96 (80 %)	1.30 (10 %)	0.048 (10 %)	1.1	9.60	1.50	0.100	1.3
Au-P3	9.02 (90 %)	1.88 (10 %)	-	1.0	8.78	1.50	-	1.2

a) τ_1, τ_2 and τ_3; b) error limit ± 5%; c) excited at 360 nm; d) χ_1, χ_2 and χ_3.

In the case of **Au-P1** and **Au-P2**, pyrene is linked to Au nanoparticle by short methylene groups, and the short linker groups allow effective interaction with Au

nanoparticles resulting in the deactivation of the photoexcited fluorophore (via either energy or electron transfer) even in nonpolar solvents such as toluene.

In polar solvents, photoinduced electron transfer process is thermodynamically more favorable and we have investigated the effect of polarity on the relative amplitude of various decay components (see traces 'b' in Figures 2.5A – 2.5D). The fluorescence decay profiles of **P2** and **Au-P2** in solvents of varying polarity are presented in Figure 2.5. It is observed that the relative abundance of the short lived species (τ_3) increases significantly with increase in solvent polarity (Table 2.4), which is attributed to the light induced electron transfer from pyrene chromophore to the gold nanocore.

Table 2.4. Comparison of fluorescence decay times[a-c] and fractional contributions[d] of **Au-P2** as a function of solvent polarity.

Solvent	Fluorescence Lifetimes of **Au-P2** in different solvents			
	τ_1, ns (χ_1%)	τ_2, ns (χ_2%)	τ_3, ns (χ_2%)	χ^2
Toluene	8.1(64)	1.3(22)	0.048(14)	1.3
Dichloromethane	10(23)	1.1(5)	0.016(72)	1.08
Acetone	e	-	f	-
Acetonitrile	e	-	f	-

a) τ_1, τ_2 and τ_3; b) error limit ± 5%; c) excited at 360 nm; d) χ_1, χ_2 and χ_2; e) long lived component is absent; f) the short lived species is the major component and it is difficult to measure the lifetime since it is close to the instrument response time.

One of the possibilities for a fast decay of the singlet excited state of pyrene in a polar solvent may be through a self-quenching process, i.e., through

intramolecular interactions between pyrene chromophores bound on Au nanoparticles. A self quenching process would mean that the relative amplitude of the quenched species should increase with the concentration of pyrene on nanoparticles. It can be observed that the lifetimes as well as the relative amplitude of all the three components are independent of the concentration of pyrene (Table 2.5) and the self-quenching pathway through interaction of adjacent pyrene is ruled out. These results clearly indicate that the quenching of the singlet excited state of pyrene bound on gold is not due to self-quenching processes but as a result of electron transfer from the singlet-excited state of pyrene to gold nanoparticles.

Table 2.5. Comparison of fluorescence decay times[a-c] and fractional contributions[d] of **Au-P2** as a function of **P2** loading.

Lifetimes of different **P2** loaded gold nanoparticles in THF				
Percentage of **P2**	τ_1,ns(%)	τ_2,ns(%)	τ_3,ns(%)	χ^2
15	9.6(28)	1.2(4)	0.013(68)	1.10
30	8.7(28)	0.64(3)	0.022(69)	1.13
70	10(23)	1.1(5)	0.016(72)	1.08

a) τ_1 and τ_2; b) error limit $\pm$ 5%; c) excited at 360 nm; d) χ_1 and χ_2.

Thus, the main deactivation channels of the singlet excited state of pyrene linked on Au nanoparticles are (a) normal fluorescence, (b) intermolecular excimer formation and (c) the competitive electron transfer to the gold nanocore. The first two processes are favourable in nonpolar solvents whereas the latter one dominates in polar solvents.

2.3.7. Laser flash photolysis studies

Since metals in the nanoparticle dimension are more electronegative than the bulk material, the excited state of fluorophores bound to metal surfaces can also participate in an electron-transfer process. We further probed the fate of pyrene quenching using transient absorption spectroscopy.

Figure 2.6 shows the transient absorption spectra of P2 and Au-P2 in degassed and air-saturated THF solutions. The difference absorption spectrum recorded following 337 nm laser pulse excitation of P2 in degassed THF solutions exhibits a maximum around 425 nm (trace 'a'). This absorption band is characteristic
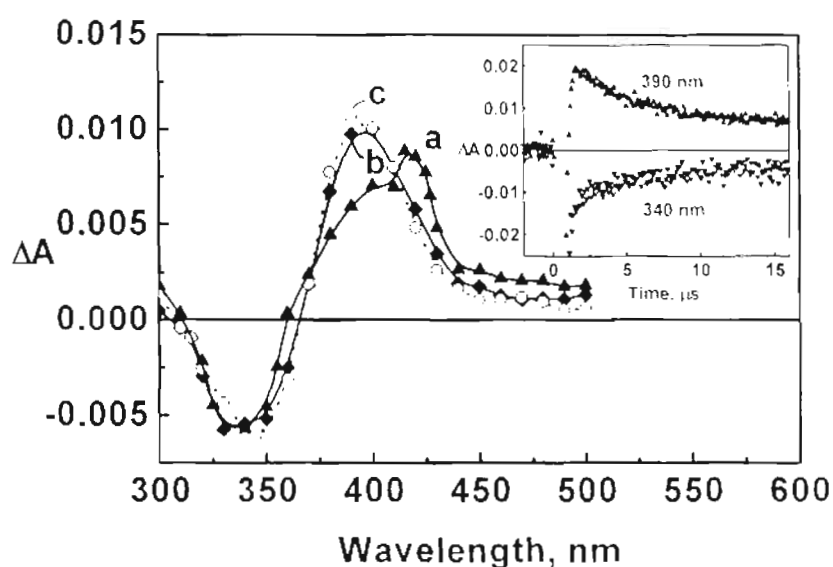
Figure 2.6 (a) Transient absorption spectra of (a) degassed THF solution of P2, (b) degassed THF solution of Au-P2, and (c) oxygenated THF solution of Au-P2. All spectra were recorded 2 μs after 337 nm laser pulse excitation. Inset shows the absorption decay profiles recorded at 390 and 340 nm.

of triplet-triplet absorption of pyrene and is readily quenched in oxygenated solutions. On the other hand, the transient absorption spectrum recorded following

337 nm laser pulse excitation of **Au-P2** shows the formation of a transient with absorption maximum at 400 nm (trace 'b'). Time-resolved spectra recorded at different times confirm the presence of a single transient, which decays with a lifetime of 4.5 µs. The presence of O_2 in the solution has no effect on the formation or decay of the transient (trace 'c' in Figure 2.6). Thus, the properties of the transient observed with **Au-P2** are distinctly different from those recorded with **P2** solution.

The pyrene cation radical has been shown to absorb strongly in the 400-450 nm regions. Evidence in the literature suggests strong dependence of the absorption maximum of pyrene radical cation on the medium and substituent.[48] Pyrene cation radical formed in polynorbornene end-labeled with pyrene has been shown to exhibit absorption maximum at 400 nm. In the present case, we attribute the 400 nm absorption band to the formation of an oxidation product, *viz.,* a radical cation formed by the interaction of excited pyrene with the gold nanocore (reaction 2.1). The absence of triplet-excited state in trace 'b' (Figure 2.6) confirms the role of metal nanocore in suppressing the intersystem crossing and/or total quenching of the triplet excited state in the **Au-P2** system. The decay of the transient absorption at 390 nm and recovery of bleaching at 340 nm (see absorption-time profiles in the inset of Figure 2.6) show a similar first-order kinetics with lifetimes of 4.7 and 4.4 µs, respectively. The similarities between these two processes suggest that the decay of the pyrene cation radical correspond

to the recovery of parent fluorophore *via* a back electron-transfer process (reaction 2.2).

$$Au\text{-}P2 \longrightarrow Au(e)\text{-}P2^{+\cdot} \tag{2.1}$$

$$Au(e)\text{-}P2^{+\cdot} \longrightarrow Au\text{-}P2 \tag{2.2}$$

2.4. Conclusions

Pyrene chromophores linked to gold nanoparticles using methylene groups of varying chain length were prepared and their photophysical properties were investigated in detail. The absorption properties of **P1** (pyrene alkylthiols which possess short chain linkers) are perturbed on the surface of gold while ground state interactions are absent in pyrene tethered through long alkyl chains (**P2** and **P3**). Low loadings of pyrene on gold nanoparticles showed structured emission bands in nonpolar solvents, characteristic of the normal fluorescence, while at higher loadings an additional excimer emission band was observed. The flexible linker provides a topographical control on the various interactions in the three-dimensional monolayers of pyrene on metal nanoparticles, leading to the formation of excited state complexes such as excimers at higher loadings. The suppression in the quenching of the singlet-excited state, observed in these systems could be further extended for the development of photocatalysts as well as chemical and biological sensors. Time-resolved fluorescence studies indicate that in polar solvents, photoinduced electron transfer process, from pyrene to Au

core, is more favoured which was also proved by laser flash photolysis experiments. A cartoonic representation of the various photophysical processes in pyrene functionalized gold nanoparticles is represented in Scheme 2.3. The charge seperation sustained for 4.5 μs before recombination, indicating the feasibility of employing them as light-harvesting assemblies.
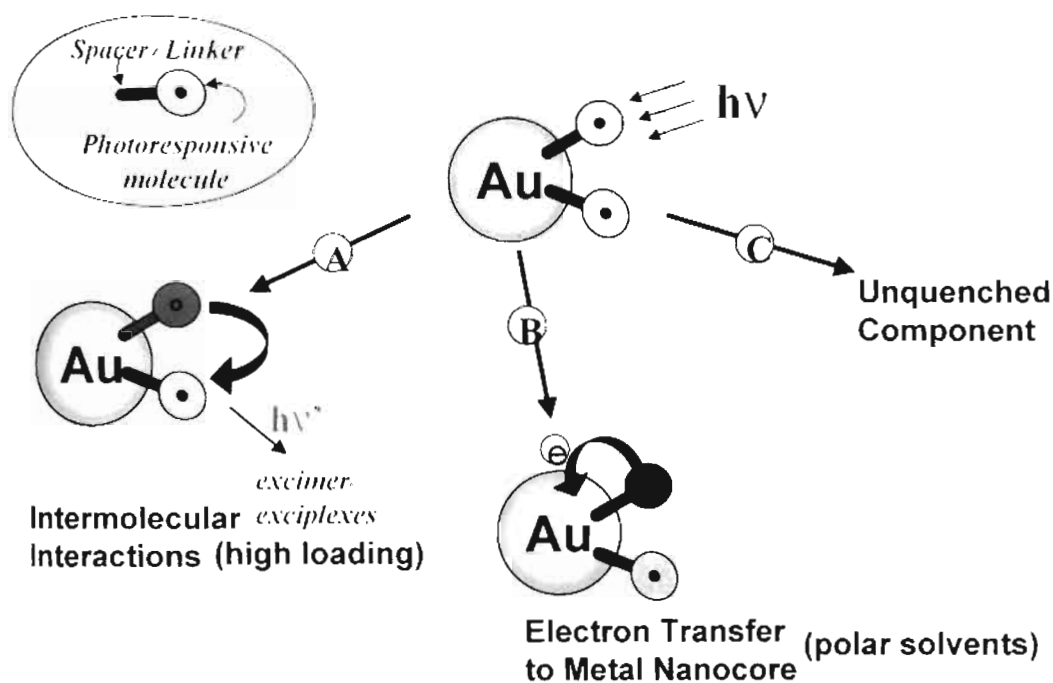
Scheme 2.3. Cartoonic representation of various photophysical processes in pyrene functionalized gold nanoparticles.

2.5. Experimental Section

2.5.1. Materials and instrumental techniques

Solvents and reagents used were purified and dried by standard methods. All starting materials and reagents were purchased from Sigma-Aldrich and were used as such. Photophysical studies were carried out using spectroscopic grade solvents. All melting points were determined with a Mel-Temp-II melting point apparatus and are uncorrected. ^{1}H and ^{13}C NMR spectra were measured on a 300 MHz Bruker Advance DPX spectrometer. IR spectra were recorded on a Nicolet Impact 400D infrared spectrophotometer. Emission spectra were recorded on a SPECTRACQ spectrofluorimeter and corrected using the program supplied by the manufacturer. The electronic absorption spectra were recorded on a Shimadzu Model UV-3101 PC UV-Vis-NIR scanning spectrophotometer. For TEM studies, a drop of colloidal gold solution was placed in a carbon coated Cu grid and the solvent was allowed to evaporate. Specimens were examined on a Hitachi H600 transmission electron microscope.

Fluorescence lifetimes were measured using a Tsunami Spectra Physics single photon counting system. Ti Sapphire laser, having a fundamental wavelength of 934 nm, was used as the excitation source. The average output power is 680 mW with a pump power of 4.5W. The pulsewidth of the laser is ~ 2 ps. The flexible harmonic generator (FHG) gives the second harmonic (467 nm) output from the Tsunami laser system. The fluorescence was detected using two-stage microchannel plate photomultiplier (MCP-PMT R38094). The fluorescence

decay measurements were further analyzed using the IBH software library, which includes an iterative shift of the fitted function as part of χ^2 goodness of the fit criterion.

2.5.2. Synthesis of 1-(1-pyrenyl)-1-bromomethane, 2.2

To a solution of 1-pyrenemethanol (250 mg, 1.07 mmol) in dry dichloromethane (20 mL) kept in an ice-bath, PBr$_3$ was added dropwise while stirring. The reaction mixture was stirred for 12 h and then neutralized with sodium bicarbonate solution. The organic layer was extracted with dichloromethane and concentrated to give 2.2 (317 mg, 1.07 mmol) in nearly quantitative yield, mp 136-137 °C. : IR (KBr) v_{max}; 2952, 1920, 1649, 1593, 1434, 1177, 1181, 1065 cm^{-1}; ^{1}H NMR (300 MHz, CDCl$_3$) δ 5.25 (2H, s, ArCH$_2$) 8.00-8.39 (9H, m, aromatic)ppm; ^{13}C NMR (75 MHz, CDCl$_3$) δ 32.15, 122.78, 124.81, 125.59, 126.23, 127.29, 127.66, 127.99, 128.20 ppm.

2.5.3. Synthesis of 1-(1-pyrenyl)-1-methylthiol, P1

To a stirred solution of 2.2 (200 mg, 0.64 mmol) in distilled THF (10 mL), kept at -10 °C, was added hexamethyldisilathiane (137.6 mg, 0.96 mmol) and 1mL (1 mmol) of terabutylammonium fluoride from a 1 M stock solution in THF containing 5 % water. The reaction mixture was stirred for 12 h and then diluted with dichloromethane. The organic layer was washed with saturated ammonium chloride solution and the solvent was removed under reduced pressure. The

product was precipitated by adding hexane to give 98 mg (60 %) of **P1**, mp 164
°C. IR (KBr) v_{max}: 2941, 2868, 1142, 850, 724 cm^{-1}; ^{1}H NMR (300 MHz, CDCl$_3$)
δ 4.2 (2H, s, ArCH$_2$SH) 7.96-8.39 (9H, m, aromatic)ppm; ^{13}C NMR (75 MHz,
CDCl$_3$) δ 26.89, 122.78, 124.81, 125.59, 126.23, 127.29, 127.66, 127.99, 128.20
ppm; Exact mass calculated 248.0660, (M+) found 248.0579 (EI high-resolution
mass spectroscopy).

2.5.4. Synthesis of 1-(1-pyrenyl)-2-oxo-7-bromoheptane, 2.3a

To a suspension of sodium hydride (200 mg, 0.8 mmol) in dry THF (10 mL)
was added 1-pyrenemethanol (200 mg, 0.8 mmol) and 1, 5-dibromopentane (1 g, 4
mmol) in dry THF (25 mL) dropwise over a period of 30 min. The reaction
mixture was refluxed for 20 h. On cooling, the reaction mixture was quenched
with cold water and the organic layer was extracted with dichloromethane. The
solvent was removed under reduced pressure and the product was recrystallized
from a mixture (1:5) of ethyl acetate and hexane, to give 185 mg (85 %) of **2.3a**,
mp 81 °C; IR (KBr) v_{max}: 2950, 1920, 1647, 1593, 1434, 1181, 1065 cm^{-1}; ^{1}H
NMR (300 MHz, CDCl$_3$) δ 1.5-1.8 (6H, m, alkyl) 3.3-3.8 (2 H, t, CH$_2$Br) 3.5-3.6
(2H, t, OCH$_2$) 5.2 (2H, s, ArCH$_2$) 7.9-8.3 (9H, m, aromatic)ppm; ^{13}C NMR (75
MHz, CDCl$_3$) δ 24.96, 28.96, 32.52, 33.72, 70.07, 71.57, 76.56, 123.44, 124.46,
125.18, 125.90, 126.90, 127.36, 127.64, 129.32, 130.80, 131.23, 131.59 ppm;
Exact mass calculated 381.0854, (M+) found 381.0860 (FAB high-resolution
mass spectroscopy).

2.5.5. Synthesis of 1-(1-pyrenyl)-2-oxo-heptanethiol, P2

To a stirred solution of **2.3a** (500 mg, 1.31 mmol) in distilled THF (10 mL), kept at -10 °C, was added hexamethyldisilathiane (280 mg, 1.57 mmol) and 1.5 mL (1.5 mmol) of terabutylammonium fluoride from a 1 M stock solution in THF containing 5 % water. The reaction mixture was stirred for 12 h and then diluted with dichloromethane. The organic layer was washed with saturated ammonium chloride solution and the solvent was removed under reduced pressure. The product was precipitated by adding hexane to give 400 mg (82 %) of **P2**. mp 88 °C. IR (KBr) v_{max}: 2941, 2868, 1142, 850, 724 cm^{-1}: ^{1}H NMR (300 MHz, CDCl$_3$) δ 1.44-1.67 (6H, m, alkyl) 2.56-2.61 (2H, t, CH$_2$S) 3.55-3.59 (2H, t, OCH$_2$) 5.18 (2H, s, ArCH$_2$) 7.96-8.35 (9H, m, aromatic)ppm; ^{13}C NMR (75 MHz, CDCl$_3$) δ 24.96, 28.96, 32.52, 33.72, 70.07, 71.57, 123.44, 124.46, 125.18, 125.90, 126.90, 127.36, 127.64, 129.32, 130.80, 131.23, 131.59 ppm; Exact mass calculated 334.1391, (M$^+$) found 334.1385 (FAB high-resolution mass spectroscopy).

2.5.6. Synthesis of 1-(1-pyrenyl)-2-oxo-10-bromodecane, 2.3b

To a suspension of sodium hydride (516 mg, 21.5 mmol) in dry THF (10 ml) was added 1-pyrenemethanol (500 mg, 2.15 mmol) and 1, 8-dibromopentane (3 g, 10.75 mmol) in dry THF (25 mL) dropwise over a period of 30 min. The reaction mixture was refluxed for 20 h. On cooling, the reaction mixture was quenched with cold water and the organic layer was extracted with dichloromethane. The solvent was removed under reduced pressure and the product was recrystallized

from a mixture (1:5) of ethyl acetate and hexane, to give 636 mg (70 %) of **2.3b**,

mp 45 °C: IR (KBr) ν$_{max}$: 2951, 1923, 1645, 1591, 1434, 1180, 1065 cm^{-1}; ^{1}H

NMR (300 MHz, CDCl$_3$) δ 0.89-1.25 (12H, m, alkyl) 3.31-3.35 (2 H, t, CH$_2$Br)

3.57-3.61 (2H, t, OCH$_2$) 5.20 (2H, s, ArCH$_2$) 7.97-8.39 (9H, m, aromatic)ppm;   C

NMR (75 MHz, CDCl$_3$) δ 24.96, 28.96, 33.72, 70.07, 71.57, 76.56, 123.44,

124.46, 125.18, 125.90, 126.90, 127.36, 127.64, 129.32, 130.80, 131.23, 131.59

ppm.

2.5.7. Synthesis of 1-(1-pyrenyl)-2-oxo-decanethiol, P3

To a stirred solution of **2.3b** (200 mg, 0.47 mmol) in distilled THF (10 ml),

kept at -10 °C, was added hexamethyldisilathiane (102 mg, 0.56 mmol) and 0.6

ml (0.6 mmol) of terabutylammonium fluoride from a 1 M stock solution in THF

containing 5 % water. The reaction mixture was stirred for 12 h and then diluted

with dichloromethane. The organic layer was washed with saturated ammonium

chloride solution and the solvent was removed under reduced pressure. The

product was precipitated by adding hexane to give 105 mg (60 %) of **P3**, mp 60

°C. IR (KBr) ν$_{max}$: 2941, 2868, 1142, 850, 724 cm^{-1}; ^{1}H NMR (300 MHz, CDCl$_3$)

δ 1.00-1.29 (12H, m, alkyl) 2.58-2.63 (2H, t, CH$_2$S) 3.58-3.62 (2H, t, OCH$_2$) 5.20

(2H, s, ArCH$_2$) 7.97-8.40 (9H, m, aromatic)ppm; ^{13}C NMR (75 MHz, CDCl$_3$) δ

24.96, 28.96, 32.52, 33.72, 70.07, 71.57, 123.44, 124.46, 125.18, 125.90, 126.90,

127.36, 127.64, 129.32, 130.80, 131.23, 131.59 ppm; Exact mass calculated

376.1861, (M+) found 376.1900 (EI high-resolution mass spectroscopy).

2.5.8. Synthesis of gold nanoparticles (Au-P1, Au-P2, Au-P3)

Gold nanoparticles functionalized with **P1, P2, P3** were synthesized by coadsorbing **P1, P2, P3** and dodecanethiol in different molar ratios (15%, 30%, 60%).

In a typical preparation of dodecanethiol/**P1** functionalized gold nanoparticles (60 % loading of **P1**), an aqueous solution of hydrogentetrachloroaurate(III)hydrate (50 μmol in 2 mL) was stirred with tetraoctylammonium bromide (250 μmol in 5 mL toluene) for 5 min. until all the aurate ions were transferred into the toluene layer. To this, a solution of dodecanethiol and **P1**, in the molar ratio 40:60 (metal to thiol molar ratio was kept as 1:1), was added in 2 mL of THF. After stirring for 2 to 3 min. sodium borohydride (2.5 mmol in 2 mL water) was added and stirred for 3 h. The hybrid nanoparticles formed were purified by repeated precipitation and filtration using ethanol(100 mL). The brown powder obtained was redispersed in toluene.

2.6. References

(1) Kreibig, U.; Vollmer, M. *Optical Properties of Metal Clusters*; Springer: Berlin, 1995.

(2) Mulvaney, P. Spectroscopy of Metal Colloids. Some Comparisons with Semiconductor Colloids. In *Semiconductor Nanoclusters-Physical, Chemical and Catalytic Aspects*; Kamat, P. V., Meisel, D., Eds.; Elsevier Science: Amsterdam, 1997; p 99.

(3) Goia, D. V.; Matijevic, E. *New J. Chem.* **1998**, *22*, 1203.

(4)   Templeton, A. C.; Wuelfing, W. P.; Murray, R. W. *Acc. Chem. Res.* **2000**, *33*, 27.

(5)   Link, S.; El-Sayed, M. A. *J. Phys. Chem. B* **1999**, *103*, 8410.

(6)   Zhao, X. M.; Xia, Y. N.; Whitesides, G. M. *J. Mater. Chem.* **1997**, *7*, 1069.

(7)   Badia, A.; Lennox, R. B.; Reven, L. *Acc. Chem. Res.* **2000**, *33*, 475.

(8)   Whetten, R. L.; Shafigullin, M. N.; Khoury, J. T.; Schaaff, T. G.; Vezmar, L.; Alvarez, M. M.; Wilkinson, A.; *Acc. Chem. Res.* **1999**, *32*, 397.

(9)   Hodak, J.; Henglein, A.; Hartland, G. V. *J. Phys. Chem. B* **2000**, *104*, 9954.

(10)   Haynes, C. L.; Van Duyne, R. P. *J. Phys. Chem. B* **2001**, *105*, 5599.

(11)   Baum, T.; Brust, M.; Bethell, D.; Schiffrin, D. J. *Langmuir* **1999**, *15*, 866.

(12)   Chen, S.; Ingram, R. S.; Hostetler, M. J.; Pietron, J. J.; Murray, R. W.; Schaaff, T. G.; Khoury, J. T.; Alvarez, M. M.; Whetten, R. L. *Science* **1998**, *280*, 2098.

(13)   Chen, S.; Murray, R. W. *J. Phys. Chem. B* **1999**, *103*, 9996.

(14)   Fishelson, N.; Shkrob, I.; Lev, O.; Gun, J.; Modestov, A. D. *Langmuir* **2001**, *17*, 403.

(15)   Hickman, J. J.; Ofer, D.; Laibinis, P. E.; Whitesides, G. M.; Wrighton, M. S. *Science* **1991**, *252*, 688.

(16)   Elghanian, R.; Storhoff, J. J.; Mucic, R. C.; Letsinger, R. L.; Mirkin, C. A. *Science* **1997**, *277*, 1078.

(17)   Kamat, P. V.; Flumiani, M.; Hartland, G. *J. Phys. Chem. B* **1998**, *102*, 3123.

(18) Kurita, H.; Takami, A.; Koda, S. *Appl. Phys. Lett.* **1998**, *72*, 789.

(19) Fujiwara, H.; Yanagida, S.; Kamat, P. V. *J. Phys. Chem. B* **1999**, *103*, 2589.

(20) Link, S.; Burda, C.; Mohamed, M. B.; Nikoobakht, B.; El-Sayed. M. A. *J. Phys. Chem. A* **1999**, *103*, 1165.

(21) Takami, A.; Kurita, H.; Koda, S. *J. Phys. Chem. B* **1999**, *103*, 1226.

(22) Ah, C. S.; Soo Han, H. S.; Kim, K.; Jang, D. J. *J. Phys. Chem. B* **2000**, *104*, 8153.

(23) Shipway, A. N.; Katz, E.; Willner, I. *ChemPhysChem* **2000**, *1*, 18.

(24) Thomas K.G.; Kamat, P. V. *J. Am. Chem. Soc.* **2000**, *122*, 2655.

(25) Avouris, P.; Persson, B. N. J. *J. Phys. Chem.* **1984**, *88*, 837.

(26) Saito, K. *J. Phys. Chem. B* **1999**, *103*, 6579.

(27) Pagnot, T.; Barchiesi, D.; Tribillon, G. *Appl. Phys. Lett.* **1999**, *75*, 4207.

(28) Makarova, O. V.; Ostafin, A. E.; Miyoshi, H.; Norris, J. R.; Meisel, D. *J. Phys. Chem. B* **1999**, *103*, 9080.

(29) Enger, O.; Nuesch, F.; Fibbioli, M.; Echegoyen, L.; Pretsch, E.; Diederich, F. *J. Mater. Chem.* **2000**, *10*, 2231.

(30) Imahori, H.; Norieda, H.; Yamada, H.; Nishimura, Y.; Yamazaki, I.; Sakata, Y.; Fukuzumi, S. *J. Am. Chem. Soc.* **2001**, *123*, 100.

(31) Huang, T.; Murray, R.W. *Langmuir* **2002**, *18*, 7077.

(32) Gu, T.; Whitesell, J. K.; Fox, M. A. *Chem. Mater.* **2003**, *15*, 1358.

(33) Aguila, A.; Murray, R. W. *Langmuir* **2000**, *16*, 5949.

(34) Foster, T. *Angew. Chem., Int. Ed. Engl.* **1969**, *8*, 333.

(35) Bouas-Laurent, H.; Castellan, A.; Desvergne, J.-P.; Lapouyade, R. *Chem. Soc. Rev.* **2001**, *30*, 248.

(36) deSilva, A. P.; Gunaratna, H. Q. N.; Gunnlaugsson, T.; Huxley, A. J. M.; McCoy, C. P.; Rademacher, J. T.; Rice, T. E. *Chem. Rev.* **1997**. *97*, 1515; Weinig, H.-G.; Krauss, R.; Seydack, M.; Bendig, J.; Koert, U. *Chem. Eur J.* **2001**, *7*, 2075.

(37) Hu, J.; Fox, M. A. *J. Org. Chem.* **1999**, *64*, 4959.

(38) Brust, M.; Walker, M.; Bethell, D.; Schffrin, D. J.; Whyman, R. *J. Chem. Soc., Chem. Commun.* **1994**, 801.

(39) Chen, S.; Murray, R. W. *Langmuir* **1999**, *15*, 682.

(40) Hostetler, M. J.; Wingate, J. E.; Zhong, C.-J.; Harris, J. E.; Vachet, R. W.; Clark, M. R.; Londono, J. D.; Green, S. J.; Stokes, J. J.; Wignall, G. D.; Glish, G. L.; Porter, M. D.; Evans, N. D.; Murray, R. W. *Langmuir* **1998**. *14*, 17.

(41) Alvarez, M. M.; Khoury, J. T.; Schaaff, T. G.; Shafigullin, M. M.; Vezmar, I.; Whetten, R. L. *J. Phys. Chem. B* **1997**, *101*, 3706.

(42) Bohern, C. F.; Huffman, D. R. *Absorption and Scattering of Light by Small Particles*; Wiley: New York. 1983.

(43) Henglein, A. *Langmuir* **1998**, *14*, 6738.

(44) Bricks, J. B. *Photophysics of Aromatic Molecules*, Wiley. London, 1970.

(45) Frank, R. S.; Merkle, G.; Gauthier, M. *Macromolecules* **1997**. *30*, 5397.

(46)   (a) Lakowiwicz, J. R. *Principles of fluorescence spectroscopy*, 2nd ed.;
       Kluwer Academic/Plenum Publishers: New York. 1999. (b) Vethamuthu.
       M. S.; Almgren, M.; Mukthar. F.: Bahadur, P. *Langmuir* **1992**. *8*. 2396. (c)
       Hoshimoto, S.; Thomas. K. J. *J. Colloid Interface Sci.* **1984**, *102*. 152. (d)
       Yamazaki. I.; Winnik. M. A.; Tazuke, S. *J. Phys. Chem.* **1987**. *91*. 4213.

(47)   Cardona, C. M.; Wilkes, T.; Ong, W.; Kaifer, A. E.; McCarley, T. D.:
       Pandey, S.; Baker. G. A.; Kane, M. N.; Baker, S. N.; Bright, F. V. *J. Phys.
       Chem. B* **2002**, *106*. 8649.

(48)   Possum. R. D.; Fox. M. A. *J. Phys. Chem. B* **1997**, *101*. 6384.

CHAPTER 3

Synthesis and Photophysical Studies of Spiropyran Functionalized Gold Nanoparticles: Towards Controlled Release Systems

3.1. Abstract

A new photochromic spiropyran derivative possessing a thiol group **SP** and the corresponding model compound **SP1** were synthesized. The former derivative was capped on gold nanoparticles (**Au-SP**) by adopting a biphasic extraction-reduction procedure and the nanoparticles were purified by repeated precipitation and centrifugation. Based on the particle diameter of 1.5-2.0 nm, it was established that approximately 130 molecules of **SP** were capped on each nanoparticle. Irradiation of **Au-SP** with UV light resulted in the formation of the zwitterionic merocyanine form (**Au-MC**). Light regulated changes in the topographic properties of spiropyran capped Au nanoparticles (i.e., interconversion between the zwitterionic merocyanine **MC** and neutral forms) were further exploited for the assembly and release of amino acids (L-tryptophan, L-tyrosin) and amino acid based therapeutic agents such as L-DOPA. Adopting this concept, gold nanoparticle based photoswitchable double shell structures, consisting of zwitterionic merocyanine as the first layer and a self-assembled amino acid derivative as the outer shell, were synthesized. The two point electrostatic

interaction between the zwitterionic merocyanine linked gold nanoparticles and amino acid derivatives resulted in the formation of highly stable complexes. For example, the half life ($t_{1/2}$) of **Au-MC::::tyrosine** complex is ~14 h, whereas that of **Au-MC→ Au-SP** is 23 min. The **Au-MC::::amino** acid complex dissociates on photoirradiation at 520 nm and undergoes thermal ring closure to **Au-SP**, releasing the amino acid derivatives. The complexation/decomplexation cycle could be repeated several times. The **Au-MC::::amino** acid complexes were quantitatively characterized using steady state and time resolved techniques and the details regarding the concentration of amino acid complexed as second layer and the rate constants for the thermal dissociation/ring closure of different amino acid derivatives are presented.

3.2. Introduction

Design of nanostructured molecular architecture through "bottom-up-approach" offers wide range of possibilities for the construction of newer types of hybrid organic-inorganic systems.[1-9] Tunable size and shape dependent optoelectronic properties of metal and semiconductor nanoparticles make them versatile building blocks for such systems.[10-12] Chemical linkage of biologically relevant molecules such as proteins, peptides, carbohydrates, lipids and DNA on to metal nanoparticles have led to the development of novel probes for biochemical investigation, with better sensitivity and greater penetration through tissues.[13,14] Furthermore, nanoparticle arrays and superstructures on surfaces are promising in

sensory applications and possess several advantages over single monolayer arrays.[15] Gold nanoparticles functionalized with biomolecules of specific properties and function are being used extensively in medical research and diagnostics.[16] For example, ultrasensitive biosensors incorporating gold nanoparticles and silver enhancement technique, has improved human IgG quantification, by two orders of magnitude.[17] Here the immunoassay is first amplified by gold nanoparticles and further magnified by silver staining.

There have been successful attempts to fabricate molecular devices using nanoparticle scaffolds and these aspects were reviewed recently.[18] Monolayer as well as mixed-monolayer protected clusters (MMPCs) can serve as scaffolds for molecular-level control of properties and as building blocks for macroscopic assemblies. A monotopic receptor for flavin, utilizing the diamidopyridine (DAP)-flavin three-point hydrogen bonding (Chart 3.1A), have been reported as an
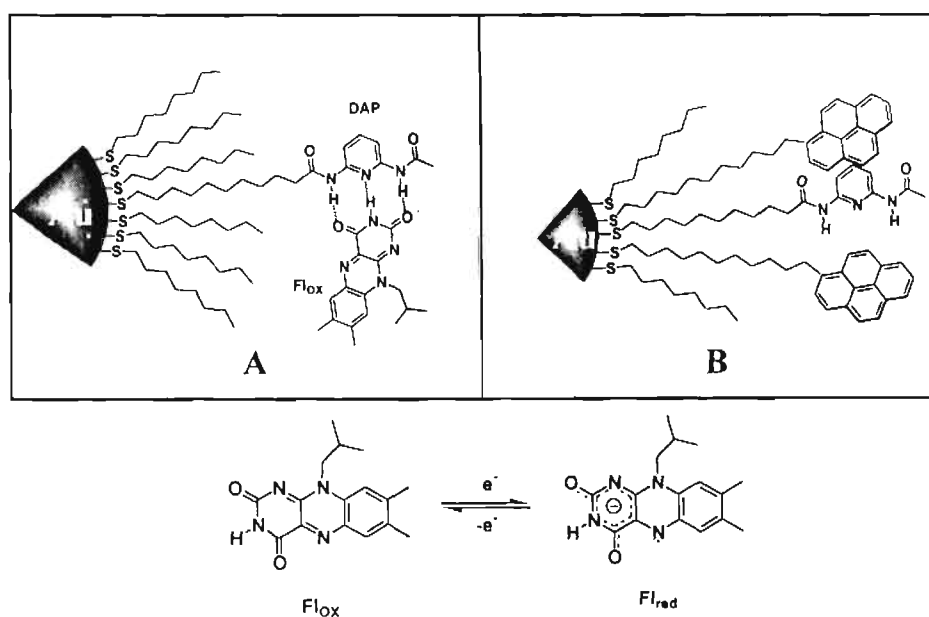
Chart 3.1. Nanoparticle scaffolds for molecular devices.[19,20]

electrochemical device.[19] The electron deficient Fl_{ox} can be selectively recognized by DAP units through hydrogen bonding and the reduced form (Fl_{red}) is inactive. In an attempt to increase the specificity, multivalent recognition sites were fabricated on MMPCs (Chart 3.1B) and the favorable π-stacking with the electron rich pyrene units assist the recognition.[20]

Nanoparticle scaffolds could be used as a unique tool for the creation of catalysts, sensors and devices. They have immense potential for the development of solution-based sensors for small molecules, molecular shuttles for specific drug-delivery, highly efficient catalysts, stimuli-responsive surfaces, scaffolds for layer-by-layer construction etc.

Switchable self-assembly is more important because of the high degree of control and specificity. Switching of self-assembly can be mediated electrochemically, photochemically, thermally etc, of which photochemical pathway is the most powerful one. Photochemical self-assembly could be mediated by incorporating photochromic molecules in the system. 'Photochromism' can be defined as the reversible transformation of a single chemical species induced in one or both directions by UV, Vis or IR radiation between two states having distinguishable absorption spectral properties. Photochromism can be based on different phenomena like "E-Z" isomerization, electrocyclization reactions, cycloadditions, tautomerism, dissociation processes etc. Spiropyrans, spiroxazines and fulgides are examples of photochromic molecules. Of these spiropyrans and related compounds are the most popular

because of their varied and numerous applications in different fields of science and technology. The discrete photoisomeric states of spiropyran exhibit distinctly different physical properties.[21] In the absence of light, majority of spiropyran molecules exist in the 'closed' spiro form (colorless and nonpolar)[21a] which when excited with UV light undergo photoisomerization to the 'open' merocyanine form (highly polar and zwitterionic),[21b] absorbing in the visible region. The ring closure to the spiropyran form can occur either thermally or by exposure to visible radiation. The closed spiro form is non-fluorescent while the open merocyanine form is fluorescent. Several novel applications have been considered based on the light mediated changes in their physical properties, for e.g., light induced polarity changes in spiropyrans have been used for (i) investigating photoswitchable binding interaction on electrode surfaces,[22] (ii) photomodulation of molecular conformation[23] and photoviscosity effects,[24] (iii) wettability studies and photocapillary effects,[25] (iv) chemical separation of molecules,[26a] ions[26b] and transport of amino acids across membranes.[26c] Photocontrolled transport of tryptophan across lipid membranes has been demonstrated by Sunamoto *et al.*[26c] using spiropyran embedded in liposomal bilayers of egg phosphatidylcholine. Here the electrostatic interaction between the zwitterionic merocyanine form of spiropyran and the zwitterionic form of amino acids was utilized for the transport of amino acids across membranes. More recently, variation in the optical properties of spiropyrans has been exploited for demonstrating three-stage molecular switching.[27]

The main objective of the present study was to design a core-shell structure composed of gold core and a shell of photoswitchable chromophores, which can self-assemble biologically important molecules. Light mediated release of these self-assembled molecules could provide newer possibilities for the design of drug delivery systems with controlled release abilities. With this view, a photoswitchable antenna system was synthesized by anchoring 3-dimensional arrays of photochromic spiropyrans, in the periphery of Au nanoparticle core (Au-SP in Chart 3.2). In this chapter, light regulated changes in the topographic properties of spiropyran capped Au nanoparticles (i.e., interconversion between the zwitterionic and neutral forms) were investigated and further exploited for assembling a layer of amino acid derivatives such as L-tryptophan, L-tyrosin and L-DOPA (L-DOPA is effective for the treatment of Parkinson's disease and hypertension) around the core-shell structure. The spiropyran SP1 (Chart 3.2) was used as a model compound to quantify the properties of Au-SP.
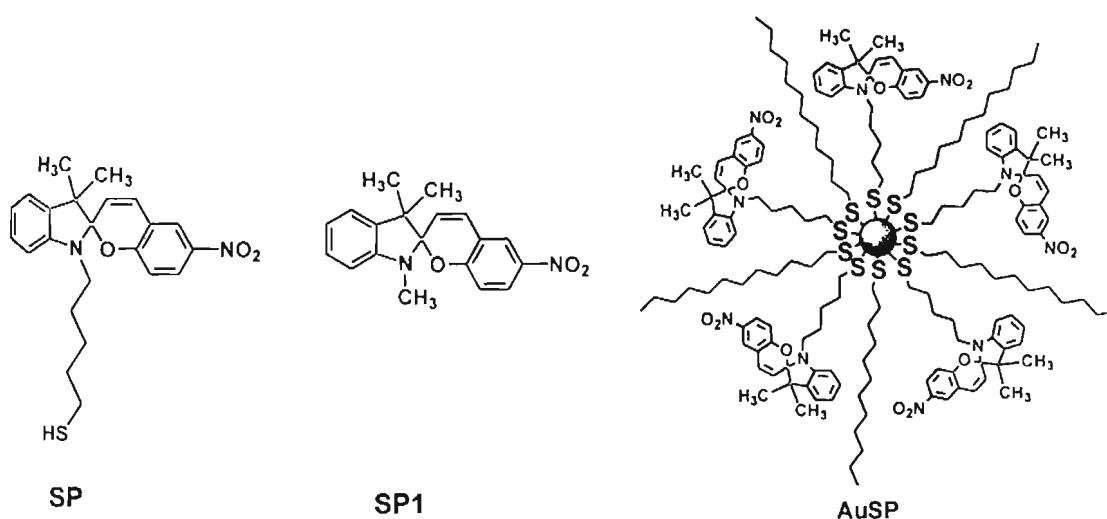

Chart 3.2

3.3. Results and Discussion

3.3.1. Synthesis and characterization

The thiol functionalized spiropyran **SP** was synthesized through pathways shown in Scheme 3.1. adopting modified procedures.[28] Fischer's base **3.1** was first converted to a monobromo derivative, which on treatment with base yielded the methylene derivative **3.2**. Condensation of compound **3.2** with 2-hydroxy-5-nitrobenzaldehyde yielded the bromo-functionalized spiropyran **3.3**, which was further converted to the thiol derivative **SP** by reacting with hexamethyldisilathiane and tetrabutylammonium fluoride. The preparation of the model compound **SP1** involved the treatment of Fischer's base (**3.1**) with
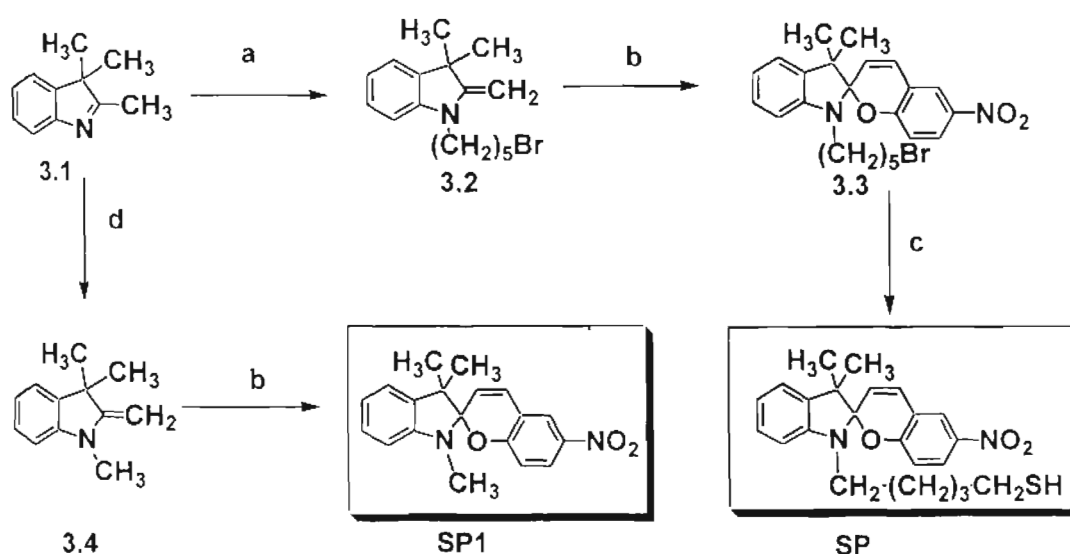
Scheme 3.1. a) $Br(CH_2)_5Br$, 80 ^0C, 12 h, CH_3CN, NaOH. b) 5-nitro-2-hydroxybenzaldehyde, ethanol, 75 ^0C, 8 h. c) hexamethyldisilathiane, tetrabutylammonium fluoride, THF, -10 ^0C to RT, 24 h. d) CH_3I, rt, 2 h, CH_3CN, NaOH.

iodomethane and the resultant quarternary salt was converted to the corresponding methylene derivative using sodium hydroxide. On condensation of the methylene

derivative with 2-hydroxy-5-nitrobenzaldehyde yielded **SP1**. Details on the synthesis, purification and characterization of **SP**, **SP1** and the intermediates are given under the Experimental Section (Section 3.5).

Gold nanoparticles capped with spiropyran (**Au-SP**) were synthesized by reducing hydrogentetrachloroaurate(III)trihydrate in the presence of tetraoctylammonium bromide, adopting a two-phase extraction procedure.[29] The nanoparticles formed were purified by repeated precipitation and centrifugation for three times. Typically, gold nanoparticles functionalized with spiropyran were dispersed in toluene, precipitated by adding methanol and redispersed in a mixture (1:5) of toluene and methanol, which was further, centrifuged for 40 minutes (6000 rpm). Details on the synthesis and purification of spiropyran functionalized gold nanoparticles are provided under the experimental section (Section 3.5). Co-binding with dodecanethiol during the surface modification ensured better stability for these nanoparticles.

3.3.2. TEM studies of spiropyran functionalized gold nanoparticles

The transmission electron micrograph of **Au-SP** nanoparticles, presented in Figure 3.1 indicates an average diameter of ~1.5 nm. The gold nanoparticles are assumed to be spherical and based on the particle size (diameter of 1.5-2.0 nm), approximately ca. 130 molecules of **SP** are capped on each nanoparticle. From the size of the nanoparticle, the number of gold nanoparticles was calculated. For estimating the number of **SP** on each nanoparticle, it is assumed that the **SP**

molecules are evenly distributed over each nanoparticle. The loss of SP while synthesizing nanoparticles was accounted from the optical density of the filtrate.
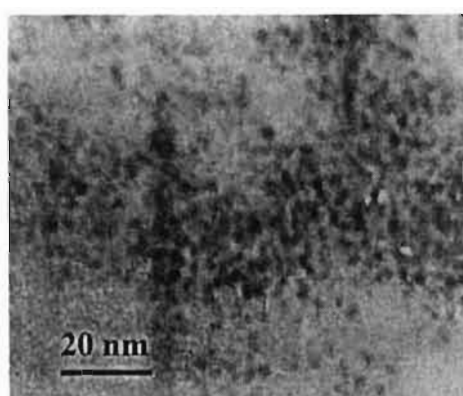

Figure 3.1. TEM image of gold nanoparticles functionalized with SP.

3.3.3. Absorption studies

The photochemical ring opening of SP as well as the thermal/photochemical ring closure of the merocyanine form is similar to that of other reported spiropyran systems. Absorption spectra of spiropyran capped gold
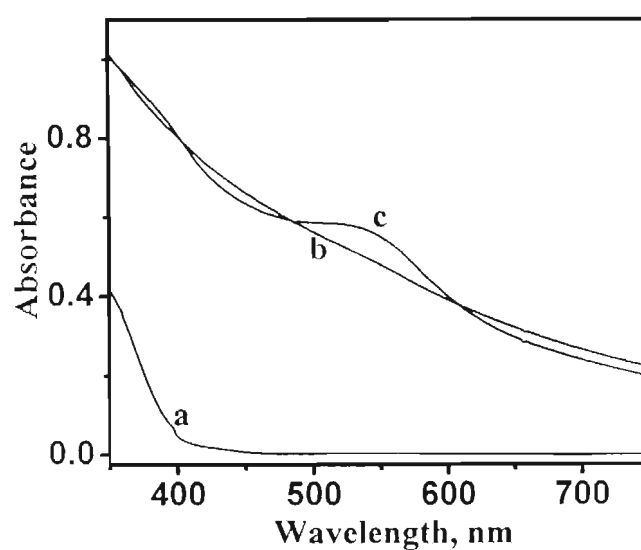

Figure 3.2 Absorption spectra of (a) **SP**, (b) **Au-SP**, (c) **Au-MC**.

nanoparticles **Au-SP** (trace 'b') and **SP** (trace 'a') in methanol are presented in Figure 3.2. The broad absorption observed in the visible region for **Au-SP** is attributed to the surface plasmon absorption of gold nanoparticles. In the present case, a significant dampening and broadening of the surface plasmon absorption was noticed and is characteristic of smaller gold nanoparticles (<5 nm), capped with organic molecules.[30]
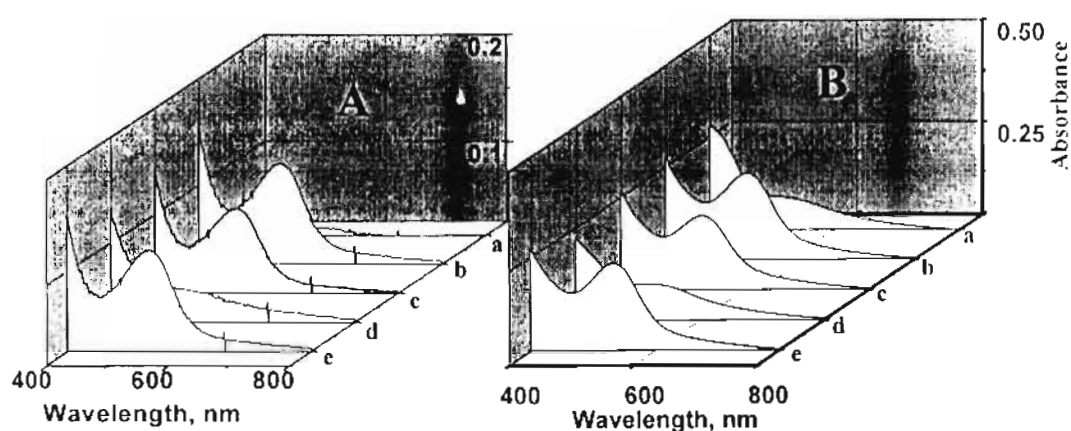
Irradiation of **Au-SP** in methanol, with 360 nm band pass filter, resulted in the formation of an absorption band around 500 nm (trace 'c' in Figure 3.2), which corresponds to the formation of the zwitterionic merocyanine form (**Au-MC**) as represented in Scheme 3.2a. The ability of zwitterionic merocyanines to bind with charged molecules[26c] was further exploited for organizing a second layer of molecules around the core-shell structures. Photoswitching of **Au-SP** to **Au-MC**
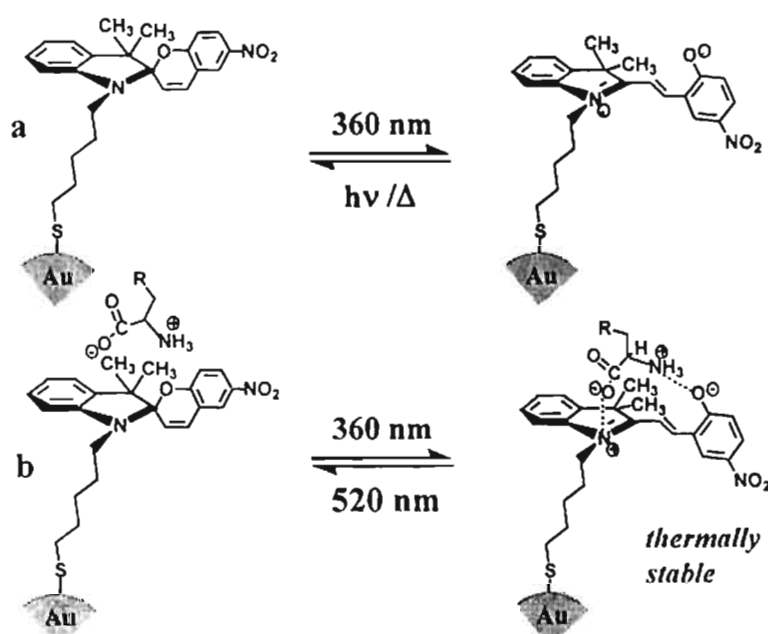
Scheme 3.2. Schematic representations of the photochemical ring opening and closing of **Au-SP** a) in the absence of amino acid derivatives and b) in the presence of amino acid derivatives.

and the thermal ring closure reaction were investigated in the presence of various amino acid derivatives (L-DOPA, L-tryptophan, L-tyrosine, DL-DOPA) by means of absorption spectroscopy. Interestingly, stabilization of the merocyanine form was observed in the presence of the above mentioned amino acid derivatives, blocking the thermal ring closure.

The absorption spectral changes for **Au-SP** and **Au-MC** systems on addition of different concentrations of L-DOPA and L-tryptophan are presented in Figure 3.3. The absorption spectral properties of **Au-SP** remains unaffected on addition of saturated solutions of different amino acid derivatives (e.g., trace 'a' in Figures 3.3A and 3.3B), ruling out the possibility of any ground state interaction. Formation of a visible absorption band (trace 'b' in Figures 3.3 A and B) was observed on irradiation with a 360 nm band pass filter. In contrast to the quick

Figure 3.3. (A) Absorption spectra of (a) a methanolic solution of **Au-SP** containing L-DOPA (42 mM), (b) immediately after irradiation with UV light (360 nm band pass filter), (c) after 2 h, (d) further irradiation with visible light (520 nm band pass filter) and (e) subsequent irradiation with UV light (360 nm band pass filter); (B) traces (a-e) represent similar absorption changes of **Au-SP** in the presence of L-tryptophan.

thermal ring closure of **Au-MC** in the absence of amino acids, an initial decrease in the intensity of the visible absorption band was observed in the present case and then the absorbance persisted, indicating the stabilization of zwitterionic merocyanine form on the surface of Au nanoparticles (trace 'c' in Figures 3.3A and B). The two point electrostatic interaction between the zwitterionic merocyanine form on gold nanoparticles and amino acid derivatives may result in the formation a stable complex[26c] (for e.g., **Au-MC::::tryptophan complex**), which in turn prevents the thermal ring closure of **Au-MC** (Scheme 3.2b). Irradiation of **Au-MC::::amino** acid complex, with 520 nm band pass filter, results in the disappearance of the absorption band in the visible region (trace 'd' in Figures 3.3A and B). These results indicate that the **Au-MC::::amino** acid complex dissociates on photoirradiation at 520 nm and undergoes thermal ring closure to **Au-SP**, releasing the amino acid derivatives. The complexation/dissociation cycles could be repeated many times in the presence of all amino acids under investigation. A decrease in the absorbance was observed with time (traces 'b' and 'c' in Figures 3.3A and B) indicating that only a part of the merocyanine capped on Au nanoparticle is complexed with amino acid derivatives. This may be due to the non-availability of free volume inside the shell, for complexation[31] and the concentration of amino acid complexed as second layer on Au nanocore was estimated using fluorescence spectroscopic studies (Section 3.3.4).

3.3.3.1. Kinetics of thermal ring closure of MC to SP and Au-MC to Au-SP

The kinetics of thermal ring closure of **MC** to **SP** and **Au-MC** to **Au-SP** were estimated using UV-visible absorption spectroscopic studies. Under dark conditions, the rate of switching from **MC** to **SP** is given by equation **3.1**.[27b]

$$-d[MC]/dt = k_1[MC] \qquad\qquad 3.1$$

$$[MC] = [MC]_0\, e^{-k_1 t} \qquad\qquad 3.2$$

where t is time, **[MC]** is the concentration of **MC** at time 't', k_1 is the rate constant, and **[MC]**$_0$ represents the initial concentration of **MC**. The concentration of **MC** ([MC]) is related to absorbance (A), measured at a particular wavelength by equation **3.3**

$$[MC] = (A_t - A_\infty)/\Delta\varepsilon d \qquad\qquad 3.3$$

where $\Delta\varepsilon$ is the difference between molar extinction coefficient of **MC** and that of **SP** at a particular wavelength, 'd' is the path length and A_∞ represents the absorbance at infinite time at the same wavelength. Combining equations **3.2** and **3.3** we get

$$A = (A_0 - A_\infty)\, e^{-k_1 t} + A_\infty \qquad\qquad 3.4$$

From the linear plot of 'A' versus 't' (equation 3.4), first order rate constants for thermal ring closure (k_1) of **MC** to **SP** and **Au-MC** to **Au-SP** were estimated. In the present case, **MC** was generated by irradiating a solution of **SP** for 5 min at 360 nm on an Oriel optical bench using a band pass filter. The absorbance of **MC**

in acetonitrile at different time intervals was recorded (Figure 3.4). The ring closure of **MC** to **SP** was followed in the dark at 25 °C, monitoring the decay of the absorption band at 560 nm (Figure 3.5). The inset of Figure 3.5 shows the plot of $\ln(A_\alpha - A_0)/(A_\alpha - A_t)$ against time for the elucidation of rate constant by using equation **3.4**.
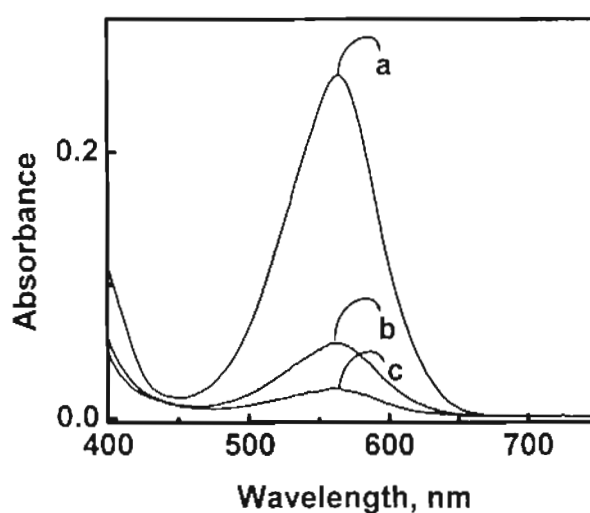
Figure 3.4. The absorption spectra of **SP** collected at different time intervals after irradiating with UV light.
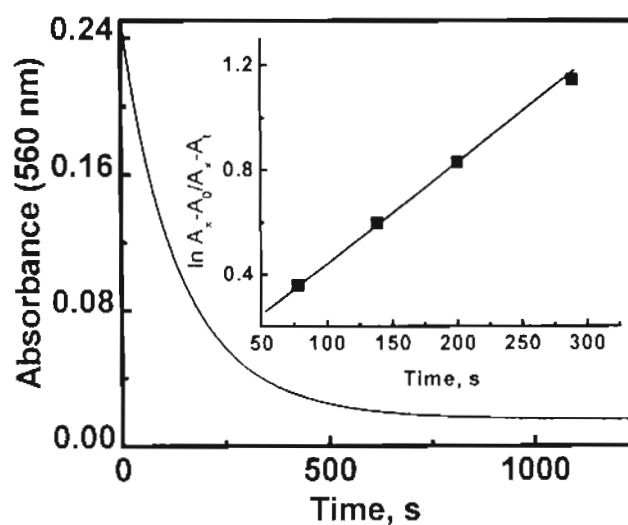

Figure 3.5. Decay of the transient absorption of a solution of **SP** in acetonitrile at 560 nm, following irradiation with UV light. Inset shows the plot of $\ln(A_\alpha - A_0)/(A_\alpha - A_t)$ against time for elucidating the rate constant using equation 3.4.

Similar experiments were carried out **Au-MC** and their stability was compared with that of the free **MC**. The rate constants for thermal isomerization of **MC** to **SP** and **Au-MC** to **Au-SP** were estimated as 7.2 x 10^{-3} s^{-1} and 4.2 x 10^{-3} s^{-1}, respectively. The higher thermal stability observed for **Au-MC**, compared to **MC** may be attributed to the packing of the zwitterionic species in the monolayer protected clusters.

3.3.4. Steady state emission studies

Recent investigations on the fluorescence properties of spiropyran based systems indicate that (i) the closed spiro-form has no strong emission while the zwitterionic merocyanine form emits around 650 nm[21a] and (ii) multiexponential decay of the merocyanine, observed in the time resolved fluorescence is attributed to different isomeric species.[32] The emission spectrum of **Au-MC** is shown in Figure 3.6.
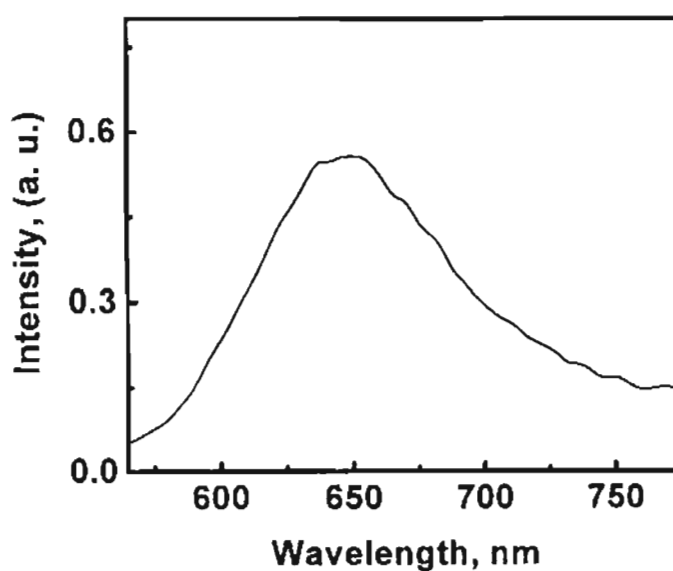
Figure 3.6. Emission spectrum of **Au-MC** (excitation wavelength 520 nm).

In the present case it is difficult to estimate the exact fluorescence quantum yield due to the overlap of the merocyanine absorption with that of the plasmon band of gold nanoparticles. A solution of **Au-SP** was irradiated using a 360 nm band pass filter, continuously for 3 min, in the presence and absence of different amino acids. The lamp was turned off and the emission intensity at 640 nm was recorded at intervals of 10 min for all the samples (Figure 3.7).
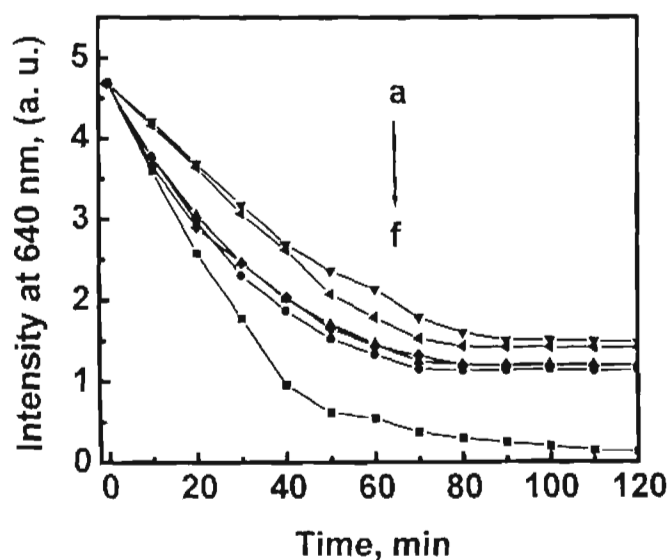
Figure 3.7. Changes in fluorescence intensity of **Au-MC** at 640 nm in the presence of (a) L-tyrosine (14.2 mM), (b) methyl DOPA (30 mM), (c) DL-DOPA (33 mM), (d) L-DOPA (42 mM), (e) L-tryptophan (16.7 mM), (f) in the absence of amino acid derivatives.

In the case of **Au-MC**, the emission intensity decreased gradually with time and the solution became practically non-fluorescent after 120 min. Interestingly, in the presence of various amino acids, an initial decrease in emission intensity was observed and then the fluorescence persisted (traces 'a-e' in Figure 3.5) for a long time. For the different systems we investigated, no appreciable changes in emission

intensities were observed for one hour. Based on the changes in emission intensity, it is concluded that a fraction of the merocyanines capped on Au nanoparticle gets complexed with amino acid derivatives (shown in Scheme 3.3) by means of the electrostatic interaction between the zwitterionic **MC** and amino acids, making it a versatile system for the controlled release of amino acid derivatives, in high concentration. The concentrations of the amino acid derivatives complexed as a
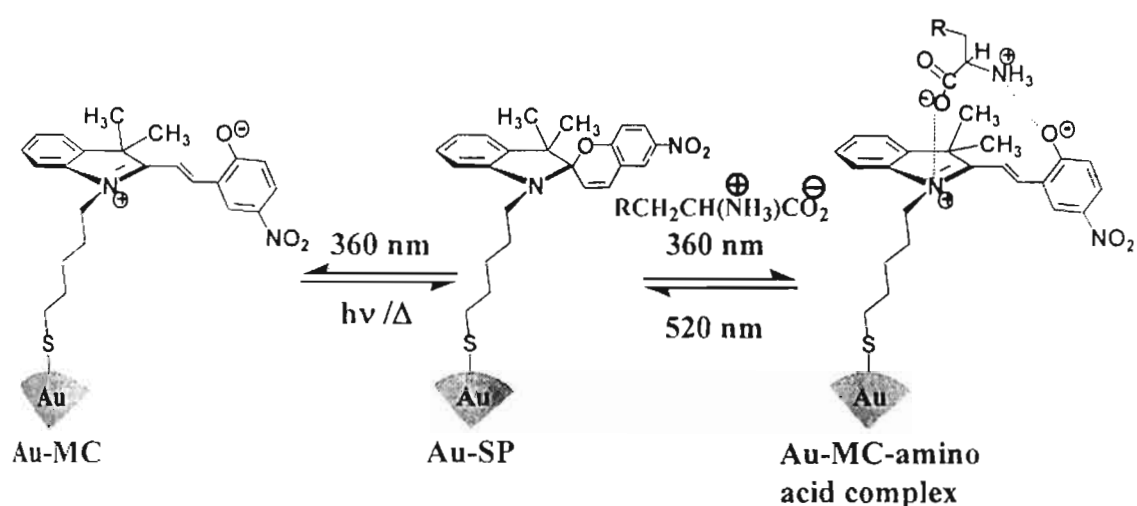
Scheme 3.3. Schematic representations of the photochemical ring opening and closing of **Au-SP** in the absence and presence of amino acids.

second layer on **Au-MC** in its photostationary state were estimated using ^{1}H NMR and fluorescence spectroscopic measurements.

3.3.4.1. Estimation of the concentration of MC1::::amino acid complexes

The isomer equilibrium constants in the photostationary states and the concentrations of different **MC1**::::amino acid complexes could be estimated using ^{1}H NMR spectroscopic methods from the signals corresponding to the

various characteristic groups of **SP1** and **MC1** (Scheme 3.4). It is difficult to adopt ^{1}H NMR spectroscopic methods for estimating the concentrations of merocyanine::::amino acid complexes bound on gold nanoparticles (Au-MC::::amino acid complex) since the signals of the alkyl protons of the thiol functionalized spiropyran (SP) overlaps with the *gem*-dimethyl protons. Therefore emission spectroscopic methods were resorted to. A calibration curve of the emission peak areas at different concentrations of the merocyanine::::amino acid complex (estimated using NMR studies, see proceeding paragraphs) was obtained by using the model compound (**SP1**), for various amino acids. This calibration curve was further used for estimating the concentration of the merocyanine::::amino acid complex bound to gold nanoparticle.
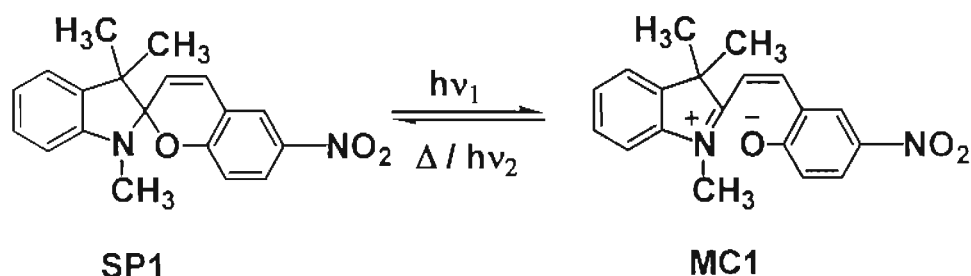

Scheme 3.4. Isomerization of model compound.

The ^{1}H NMR spectroscopic signals corresponding to the various characteristic groups of spiropyran and merocyanine forms are well established.[21a,33,34] The *gem*-dimethyl protons of the model spiropyran (**SP1**) appear at 1.07 and 1.18 ppm, respectively. The corresponding protons of the open merocyanine (**MC1**) are observed as a singlet at low field ($\delta = 1.72$ ppm) in methanol-d_4. The contributions

of **SP1** and **MC1** in the photostationary state were estimated on the basis of the integration values of the *gem*-dimethyl proton peaks. The **SP1**↔**MC1** isomerization equilibrium (K) was estimated as 0.25 and the extinction coefficient of **MC1** as 3.01 x 10^4 M^{-1} cm^{-1} (error limit ± 5 %). Similar isomer equilibrium constants are reported earlier for other spiropyran derivatives.[35]

The concentrations of the various merocyanine::::amino acid complexes formed were estimated as follows. The ^{1}H NMR spectrum of **SP1** was recorded under dark, in methanol-d_4, containing a known volume of toluene as internal standard and calibrated using the peak corresponding to the methyl protons. Methanolic solutions of **SP1** were irradiated for 60 min in the absence and in the presence of different amino acid derivatives in a Rayonet Photochemical Reactor (irradiated using 360 nm lamp in a 2 mm quartz cell) and their ^{1}H NMR spectra were recorded immediately (in less than 5 min). Absorption and emission studies have shown that the uncomplexed form of the merocyanine completely reverts back in around 90 min, whereas the merocyanine::::amino acid complexes are reasonably stable under these conditions. The irradiated **SP1** solutions containing different amino acid derivatives were kept under dark for 90 min and the ^{1}H NMR spectra were recorded again. The concentrations of merocyanine::::amino acid complex were estimated by comparing the integrations. By this procedure it was estimated that in the photostationary state a solution containing **SP1** (3 mM) and L-DOPA (4 mM) yielded 0.312 mM of merocyanine::::L-DOPA complex (~42 % yield based on **MC1** concentration).

For generating the calibration curve of the emission peak areas at different concentrations of the complex, solutions of **MC1::::**amino acid complexes were prepared in methanol under conditions identical to those employed for the ^{1}H NMR spectral studies. Emission peak areas of the complexes were recorded after
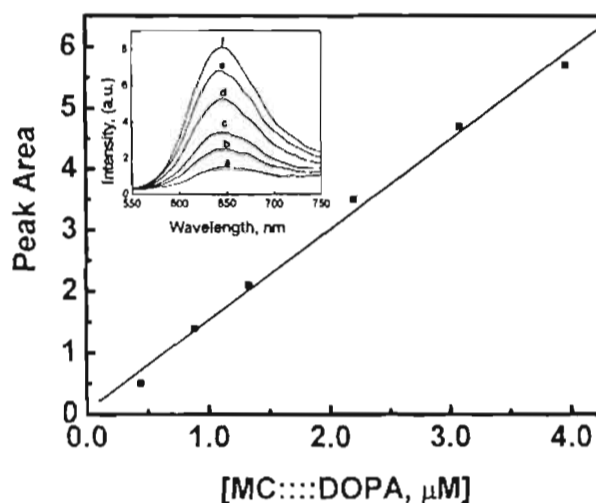

Figure 3.8. Calibration graph of emission peak areas obtained at different concentrations of **MC::::DOPA** complex. Inset shows the emission spectra obtained for different concentrations of **MC::::DOPA**. [**MC::::DOPA**]: a) 0.44 μM, b) 0.88 μM, c) 1.33 μM, d) 2.2 μM, e) 3.08 μM, f) 3.96 μM.

diluting with methanol. The merocyanine::::amino acid complex is found to be more or less stable on dilution. The possibility of quick dissociation on dilution was ruled out by keeping the resultant solution for 60 min (any dissociation will lead to the formation of unbound merocyanine). No appreciable decrease in the emission intensity due to the thermal ring closure of decomplexed merocyanine was observed. A calibration curve was obtained by plotting the emission peak areas obtained for different concentrations (for example Figure 3.8) of the

complex versus the concentration of **MC::::amino acid** (determined by means of ^{1}H NMR spectral studies).

3.3.4.2. Estimation of the concentration of Au-MC::::amino acid complexes

Calibration curves presented in Section 3.3.4.1. (for e.g., Figure 3.8) were used to determine the concentrations of amino acids complexed as a second layer on Au core-shell structures. Emission measurements in Sections 3.3.4.1. and 3.3.4.2. were carried out in one stretch and instrumental parameters (slit width etc) were kept identical for emission studies. In a typical example, **Au-SP** (6.9 µM) in methanol was irradiated in a 2 mm quartz cell in the presence of varying concentrations of L-DOPA for 60 min using a Rayonet Photochemical Reactor (360 nm). Irradiation conditions were kept identical to those employed for ^{1}H NMR
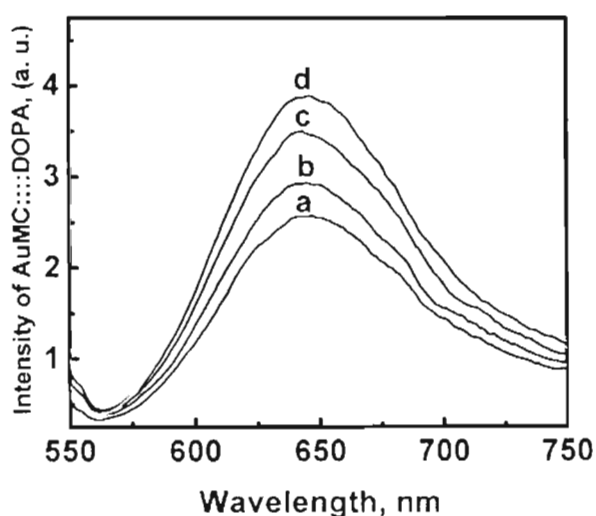
Figure 3.9. Fluorescence spectra of **Au-MC::::DOPA** formed at different concentrations of L-DOPA; [L-DOPA]: a) 0.11 mM, b) 0.23 mM, c) 0.34 mM, d) 0.46 mM.

spectral studies (Section 3.3.4). Solutions were kept under dark for 90 min, allowing the thermal ring closure of unbound merocyanine on Au nanoparticles.

The emission spectrum of the resultant **MC::::L-DOPA** complex bound to Au nanoparticle was recorded (Figure 3.9) and the concentrations of the complex formed were estimated from the calibration curve (Figure 3.8) and are presented in Table 3.1. Similar procedure was adopted for estimating the concentrations of various **Au-MC::::**amino acid complexes and the concentrations are represented in Tables 3.2 and 3.3.

Table 3.1. Au-MC::::L-DOPA complex formed on photoirradiating a solution of **Au-SP** (6.9 µM) in the presence of L-DOPA.

[L-DOPA] mM	[Au-MC::::L-DOPA], µM	Yield of [Au-MC::::L-DOPA]*
0.23	0.24	3.4
0.34	0.42	6.0
0.46	0.57	8.2
0.68	1.00	14.4

*based on **SP** concentration.

Table 3.2. Au-MC::::L-Tyrosin complex formed on photoirradiating a solution of **Au-SP** (28 µM) in the presence of L-Tyrosin.

| [L-Tyrosin] mM	[Au-MC::::L-Tyrosin], µM	Yield of [Au-MC::::L-Tyrosin]*
0.013	3.7	13
0.026	4.4	16
0.040	5.4	19
0.054	6.4	23

*based on **SP** concentration.

Table 3.3. Au-MC::::L-Tryptophan complex formed on photoirradiating a solution of **Au-SP** (28 µM) in the presence of L-Tryptophan.

[L-Tryptophan] mM	[Au-MC::::L-Tryptophan]. µM	Yield of [Au-MC::::L-Tryptophan]*
0.022	3.1	11
0.044	4.3	15
0.066	5.0	18
0.089	6.1	22

*based on **SP** concentration.*

3.3.4.3. Thermal stability of Au-MC::::amino acid complexes

In dark, **Au-MC**::::amino acid complexes dissociate very slowly and the dissociation/ring closure followed first order kinetics in all the three cases. The thermal dissociation rate constants were obtained by monitoring the changes in the emission intensity as a function of time at 640 nm (Figure 3.10).
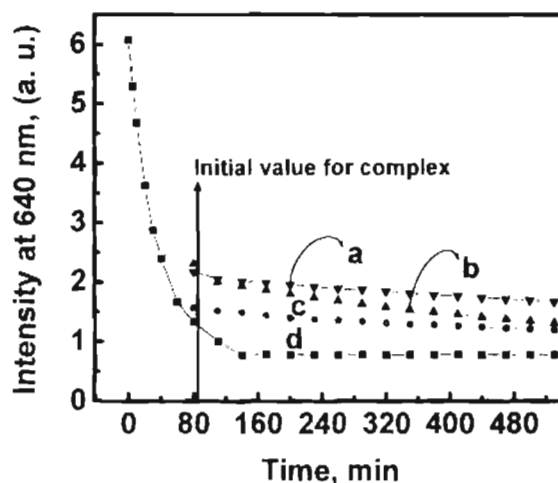
Figure 3.10. Changes in fluorescence intensity of **Au-MC** at 640 nm in the presence of (a) L-tyrosine (14.2 mM). (b) L-DOPA (42 mM), (c) L-tryptophan (16.7 mM) and (d) in the absence of amino acid derivatives. (Initial value was taken after 90 min for the complexes.)

The half-life for the thermal ring closure of merocyanine to spiropyran on the surface of gold, in the absence of amino acid derivatives, is estimated as 23 min. Spiropyran capped gold nanoparticles containing various amino acid derivatives were irradiated for 30 min. The solutions were kept under dark for 90 min, so that majority of the uncomplexed merocyanine on Au nanoparticles isomerizes back to the spiropyran. Emission intensity at 90 min was taken as the initial intensity (I_0). Emission intensity (I_t) was measured at different time intervals (t) for several hours (~10 h).

The rate constants for the thermal ring closure of the merocyanines were calculated using equation (3.5). Blank experiments carried out in the absence of amino acids indicate that the emission intensity of **Au-MC** decreases to a minimum value (I_α), which remains constant. The corresponding background values were taken into account, while calculating the rate constants for the thermal dissociation of Au-MC::::amino acid complexes

$$k = \frac{2.303}{t} \log \frac{I_0 - I_\alpha}{I_t - I_\alpha} \qquad\qquad 3.5$$

The dissociation rate constants at 25 ^{0}C were estimated as 1.4×10^{-5} s^{-1} for **Au-MC::::tyrosine** complex, 2.2×10^{-5} s^{-1} for **Au-MC::::L-DOPA** complex and 3.3×10^{-5} s^{-1} for **Au-MC::::tryptophan** complex. It may be noted that the half-life ($t_{1/2}$) for thermal dissociation/ring closure of **Au-MC::::tyrosine** complex· is ~14 h, whereas the $t_{1/2}$ of **Au-MC→Au-SP** is 23 min. The lower values of thermal dissociation rate constants obtained for these complexes indicate that the

amino acid derivatives are tightly bound to the photochemically generated **Au-MC** and are reasonably stable for any practical application.

The relative emission intensities of the **Au-MC::::**amino acid complexes formed depend on the concentrations of the amino acid derivatives. Emission spectra of **Au-MC** at different concentrations of amino acid derivatives (L-DOPA. L-tryptophan and L-tyrosine), observed 90 min after irradiation, are presented as Figures 3.11-3.13. Emission measurements were carried out in one stretch and instrumental parameters (slit width etc) were kept identical. It is observed that the emission intensity is greater for solutions containing higher concentrations of amino acids. But the low solubility of amino acids is the bottle neck for improving the yield of **Au-MC::::**amino acid complex formation. Attempts were made to remove unbound amino acid derivatives present along with **Au-MC::::**amino acid complexes. From a concentrated solution, it was found that unbound amino acids precipitate out first, leaving **Au-MC::::**amino acid complexes in solution.
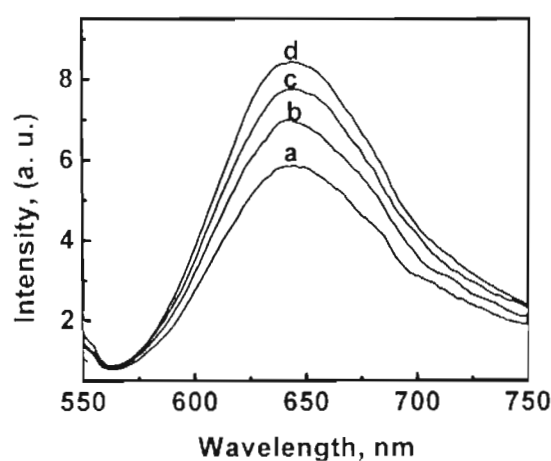
Figure 3.11. Emission spectra of **Au-MC** at different concentrations of L-DOPA observed 90 min after irradiation. [L-DOPA]: a) 14.2 μM. b) 28.5 μM. c) 42.8 μM, d) 57.14 μM.
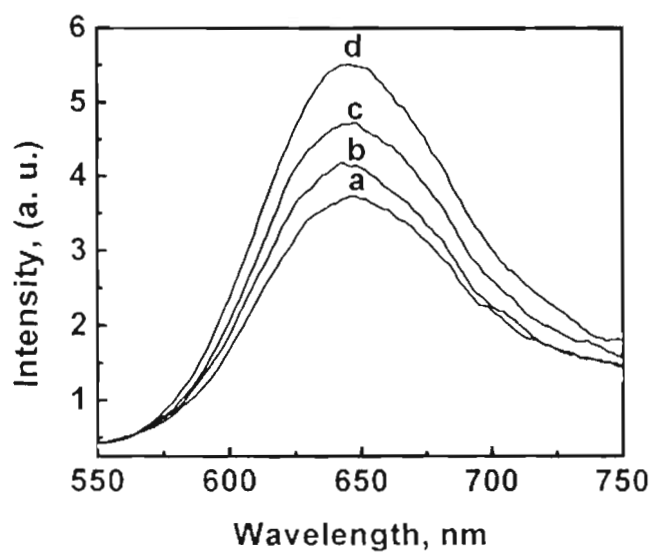
Figure 3.12. Emission spectra of **Au-MC** formed at different concentrations of L-tryptophan observed 90 min after irradiation. [L-tryptophan]: a) 22.2 μM, b) 44.5 μM, c) 66.8 μM, d) 89.14 μM.
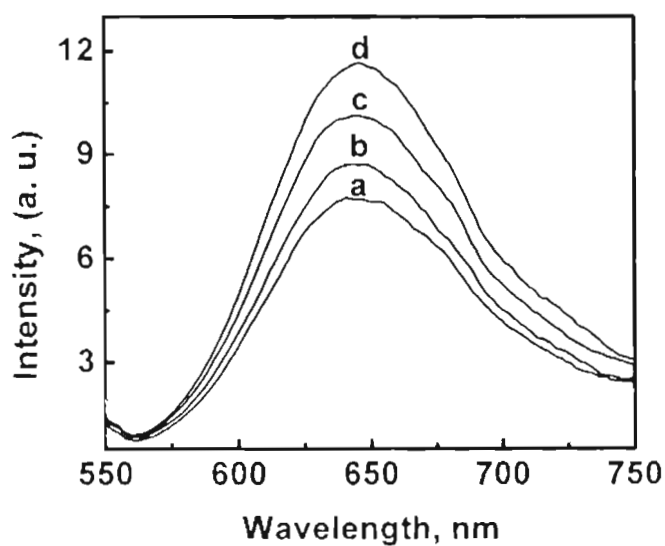
Figure 3.13. Emission spectra of **Au-MC** formed at different concentrations of L-tyrosin observed 90 min after irradiation. [L-tyrosin]: a) 13.4 μM, b) 26.8 μM, c) 40.2 μM, d) 53.7 μM.

3.3.5. Time resolved fluorescence studies

The formation of **Au-MC**::::amino acid complex was further confirmed by time resolved fluorescence studies. As a representative example, the singlet-excited state of **Au-MC**::::tryptophan complex was investigated. The solutions, in each

case were irradiated for 3 minutes using UV pencil lamp (360 nm) and the lamp was turned off for time resolved fluorescence measurements (in all the cases, we were able to acquire 10,000 counts in less than two minutes). The unbound merocyanine, **MC** followed a biexponential decay in methanol, with two short-lived species (100 ps and 266 ps). Lifetimes and relative abundance of both these species remain more or less unaffected after linking to Au nanoparticles (Au-MC)(Table 3.4). Interestingly, an additional component, with a longer lifetime (3 ns) was observed in the presence of tryptophan. The long-lived species is assigned to the Au-MC::::tryptophan complex and its relative abundance increased with increasing

Table 3.4. Time resolved fluorescence lifetime data[a-c] and fractional contributions[d].

System	Conc. of tryptophan, [mM]	τ_1, ns $|\chi_1 \%|$	τ_2, ns $|\chi_2 \%|$	τ_3, ns $|\chi_3 \%|$
MC	0	0.100 (52)	0.266 (48)	-
Au-MC	0	0.095 (45)	0.225 (55)	-
Au-MC::::tryptophan	8	0.112 (49)	0.278 (43)	3.3 (8)
Au-MC::::tryptophan	16.7	0.107 (49)	0.291 (37)	2.8 (14)

[a] τ_1, τ_2 and τ_3. [b] The quality of the fit is judged by means of the usual statistical parameter χ^2 (0.98 – 1.4); error limit $\pm$ 5%. [c] excited at 467 nm and emission followed at 640 nm. [d] χ_1, χ_2 and χ_3.

tryptophan concentration. The two point electrostatic interaction between **Au-MC** and tryptophan may restrict the torsional dynamics of merocyanine, leading to longer lifetimes.

3.4. Conclusions

In conclusion, we have demonstrated the photoswitchable self-assembly of different amino acid derivatives by anchoring spiropyrans on to the 3-dimensional surface of Au nanoparticles. It is possible to control the local concentration of amino acids on Au-nanoparticle scaffolds by suitably regulating the number of spiropyrans capped on the surface. The ability of these systems for light mediated binding and release of molecules by making use of the electrostatic interaction between the zwitterionic molecules offer intriguing possibilities for designing drug delivery systems with controlled release abilities. A cartoonic representation of the light driven 3-D self-assembly and release of amino acid derivatives is represented in Scheme 3.5. The site-specific binding properties of Au nanoparticles observed
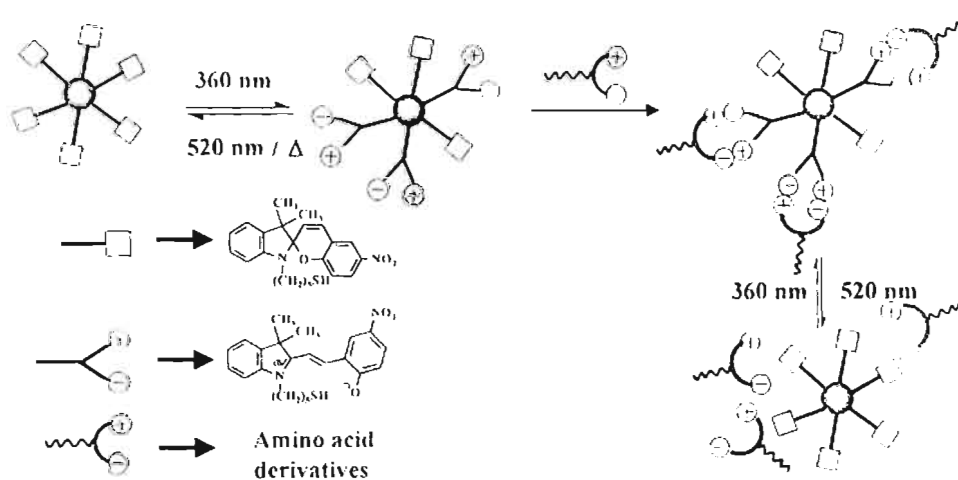
Scheme 3.5. Representation of the controlled-release of amino acid derivatives using **Au-SP**.

in biological systems make them more attractive for such applications. The low solubility of amino acids in methanol is a bottleneck for achieving higher concentrations of **MC::::**amino acid complex on the surface of gold nanoparticles.

3.5. Experimental Section
3.5.1. General

Solvents and reagents used were purified and dried by standard methods. All starting materials and reagents were purchased from Sigma-Aldrich and were used as such. The amino acid derivatives were purchased either from Sigma-Aldrich or from S. D. fine chemicals, India and were recrystallized before use. All melting points were determined with a Mel-Temp-II melting point apparatus and are uncorrected. ^{1}H and ^{13}C NMR spectra were measured on a 300 MHz Bruker Advance DPX spectrometer. IR spectra were recorded on a Nicolet Impact 400D infrared spectrophotometer. The electronic absorption spectra were recorded on an Agilent 8453-UV-visible (diode array) spectrophotometer. Emission spectra were recorded on a SPECTRACQ spectrofluorimeter and corrected using the program supplied by the manufacturer.

3.5.2. Instrumentation
3.5.2.1. Steady state experiments

Irradiations were carried out using band pass filters (360 nm and 520 nm) on an Oriel Optical Bench equipped with a 200 W high pressure mercury lamp. In the time dependent emission spectra, each spectrum was recorded with minimum

excitation slit width and maximum scan rate in order to avoid ring closure (**MC** to **SP**) by the excitation light source.

3.5.2.2. Singlet lifetime studies

For the characterization of the singlet-excited state of **MC**, **Au-MC**, **Au-MC::::tryptophan** complex, the solutions, in each case were irradiated for 3 min using spectroline pencil lamp model 36-380 longwave UV (365 nm) and the pencil lamp was turned off for time resolved fluorescence measurements (in all the cases, 10,000 counts were acquired in less than two min). Fluorescence lifetimes were measured using a Tsunami Spectra Physics single photon counting system. Ti Sapphire laser, having a fundamental wavelength of 934 nm, was used as the excitation source. The average output power is 680 mW with a pump power of 4.5W. The pulsewidth of the laser is <2 ps. The flexible harmonic generator (FHG) gives the second harmonic (467 nm) output from the Tsunami laser system. The fluorescence was detected using a two-stage microchannel plate photomultiplier (MCP-PMT R38094). The fluorescence decay measurements were further analyzed using the IBH software library, which includes an iterative shift of the fitted function as part of χ^2 goodness of the fit criterion.

3.5.3. Synthesis

3.5.3.1. Synthesis of the methylene derivative 3.2

Refluxing a mixture of 2,3,3-trimethylindolinine and excess 1,5-dibromopentane in acetonitrile for 24 h yielded the quarternary salt as a viscous

residue, which when treated with NaOH without purification yielded (75 %) the methylene derivative **3.2**.

3.5.3.2. Synthesis of Compound 3.3

Compound **3.2** (720 mg, 2.06 mmol) and 5-nitro-2-hydroxybenzaldehyde (410 mg, 2.47 mmol) were refluxed in dry ethanol (8 mL) for 8 h. On cooling, a precipitate was formed which was washed with cold ethanol. Recrystallisation of the precipitate from ethanol gave **3.3** (570 mg, 60%) as a white powder. mp 101 °C. FTIR (KBr) v_{max}; 3730, 2921, 2901, 2362, 1546, 1499, 1182, 872 cm^{-1}; ^{1}H NMR (300 MHz, CDCl$_3$, TMS) δ 1.28-1.86 (m, 12H, alkyl) 3.13-3.19 (m, 2H, NCH$_2$) 3.35-3.39 (t, 2H, J = 6.6 Hz, CH$_2$Br) 5.85-5.88 (d, 1H, J = 10.36 Hz, vinylic) 6.54-6.57 (d, 1H, J = 7.73 Hz, aromatic) 6.72-6.75 (d, 1H, J = 8.42 Hz, aromatic) 6.85-6.89 (t, 1H, J = 6.94 Hz, aromatic) 6.89-6.92 (d, 1H, J = 9.99 Hz, vinylic) 7.07-7.09 (d, 1H, J = 6.78 Hz, aromatic) 7.16-7.20 (t, 1H, J = 7.15 Hz, aromatic) 7.99 (s, 1H, aromatic) 7.99-8.02 (d, 1H, J = 11.22 Hz, aromatic)ppm; ^{13}C NMR (75 MHz, CDCl$_3$)δ 19.8, 20.6, 24.8, 25.9, 25.8, 28.0, 32.3, 33.6, 43.5, 52.6, 106.6, 108.5, 115.5, 118.4, 119.4, 121.7, 121.9, 122.7, 125.8, 127.7, 128.1, 128.6 ppm. exact mass calcd. for C$_{23}$H$_{25}$N$_2$O$_3$Br [MH$^+$]: 457.1127, found 457.1117 (FAB, high resolution mass spectroscopy).

3.5.3.3. Synthesis of Compound SP

A mixture of tetrabutylammonium fluoride (62.9 mg, 0.24 mmol) and hexamethyldisilathiane (46.8 mg, 0.262 mmol) in THF (2 mL) was added to

compound **3.3** (100 mg, 0.22 mmol) in THF (2 mL) kept at -10 °C. The mixture was allowed to warm to room temperature, while being stirred and was further stirred at room temperature for 12 h. The reaction mixture was diluted with dichloromethane and then washed with saturated ammonium chloride solution. The organic layer was concentrated and the product **SP** (40 mg, 60 %) was obtained by precipitation and recrystallisation from a mixture of ethyl acetate and hexane (1:5) as a yellow powder. mp 92 °C. FTIR (KBr) v_{max}; 3434, 2962, 2621, 2854, 2355, 1600, 1506, 1472, 1337, 1263 cm $^{-1}$; ^{1}H NMR (300 MHz, CDCl$_3$, TMS)δ 1.17-1.56 (m, 12H, alkyl) 2.57-2.62 (t, 2H, J = 7.28 Hz, CH$_2$SH) 3.13-3.19 (m, 2H, NCH$_2$) 5.83-5.87 (d, 1H, J = 10.56 Hz, vinylic) 6.54-6.56 (d, 1H, J = 7.72 Hz, aromatic) 6.72-6.74 (d, 1H, J = 8.74 Hz, aromatic) 6.83-6.88 (t, 1H, J = 7.51 Hz, aromatic) 6.88-6.91 (d, 1H, J = 8.93, vinylic) 7.07-7.09 (d, 1H, J = 7.28, aromatic) 7.15-7.20 (t, 1H, J = 7.06 Hz, aromatic) 7.99 (s, 1H, aromatic) 8.01-8.02 (d, 1H, J = 8.36 Hz, aromatic)ppm; ^{13}C NMR (75 MHz, CDCl$_3$) δ 19.8, 26.0, 28.4, 28.7, 38.4, 38.6, 43.5, 52.6, 106.6, 108.5, 115.5, 118.4, 119.4, 121.7, 121.9, 122.7, 125.8, 127.7, 128.1, 127.6 ppm. exact mass calcd. for C$_{23}$H$_{26}$N$_2$O$_3$S [MH$^+$]: 411.1742, found 411.1745 (FAB, high resolution mass spectroscopy).

3.5.3.4. Synthesis of Compound SP1

Synthesis of **SP1** was carried out similar to that of **SP**. The quarternization involved the stirring of 2.3.3-trimethylindolinine and iodomethane in acetonitrile

with ice-water circulation. Compound **3.4** precipitated out which on condensation with 5-nitro-2-hydroxybenzaldehyde afforded **SP1** in very high yields (90 %).

3.5.3.5. Synthesis of gold nanoparticles Au-SP

To a stirred solution of tetraoctylammonium bromide (0.056 g, 0.102 mmol) in 5 mL toluene, an aqueous solution of hydrogen-tetrachloroaurate(III)trihydrate (9 mg, 0.0228 mmol) was added dropwise. Compound **SP** (10 mg, 0.0248 mmol) in 2 mL toluene was added to the above solution. After 30 min, an aqueous solution of sodium borohydride (9 mg, 0.23 mmol) was added dropwise and stirred for a further 3 h. The organic layer was collected and suspended in ethanol (75 mL). It was kept in ice and the precipitate obtained was suspended in a mixture of toluene (1 mL) and methanol (4 mL). This was centrifuged at 6000 rpm for 40 min and the precipitate obtained was again suspended in toluene-methanol mixture and the process was repeated thrice to remove any unbound thiol from the suspension.

3.6. References

(1)   *Nanotechnology Research Directions*; Roco, M. C.; Williams, R. S.; Alivisatos, P., Eds.; Kluwer Academic Publishers: Dordrecht, The Netherlands, 2001.

(2)   Shipway, A. N.; Katz, E.; Willner, I. *ChemPhysChem* **2000**, *1*, 18.

(3)   Templeton, A. C.; Wuelfing, W. P.; Murry, R. W. *Acc. Chem. Res.* **2000**, *33*, 27.

(4)   (a) Imahori, H.; Fukuzumi, S. *Adv. Mater.* **2001**, *13*, 1197. (b) Kamat, P. V. *J. Phys. Chem. B* **2002**, *106*, 7729.

(5)   Thomas, K. G.; Ipe, B. I.; Sudeep, P. K. *Pure & Appl. Chem.* **2002**, *74*, 1731.

(6)   Makarova, O. V.; Ostafin, A. E.; Miyoshi, H.; Norris, J. R.; Meisel, D. *J. Phys. Chem. B* **1999**, *103*, 9080.

(7)   Aguila, A.; Murray, R. W. *Langmuir* **2000**, *16*, 5949.

(8)   Thomas, K. G.; Kamat, P. V. *J. Am. Chem. Soc.* **2000**, *122*, 2655.

(9)   Hu, J.; Zhang, J.; Liu, F.; Kittredge, K.; Whitesell, J. K.; Fox, M. A. *J. Am. Chem. Soc.* **2001**, *123*, 1470.

(10)   Alivisatos, P. *J. Phys. Chem. B* **1996**, *106*, 13226.

(11)   Link S.; El-Sayed, M. A. *J. Phys. Chem. B* **1999**, *103*, 4312.

(12)   Henglein, A.; Meisel, D. *Langmuir* **1998**, *14*, 7392.

(13)   Hainfeld, J. M.; Powell, R. D. *J. Histochem. Cytochem.* **2000**, *48*, 471.

(14)   Nam, J.-M.; Park, S.-J.; Mirkin, C. A. *J. Am. Chem. Soc.* **2002**, *124*, 3820.

(15)   Shipway, A. N.; Lahav, M.; Willner, I. *Adv. Mater.* **2000**, *12*, 993.

(16)   Han, S.; Lin, J.; Satjapipat, M.; Baca, A. J.; Zhou, F. *Chem. Commun.* **2001**, 609.

(17)   Su, X.; Li, S. F. Y.; O'Shea, S. J. *Chem. Commun.* **2001**, 755.

(18)   Shenhar, R.; Rotello, V. M. *Acc. Chem. Res.* **2003**, *36*, 549.

(19)   Boal, A. K.; Rotello, V. M. *J. Am. Chem. Soc.* **1999**, *121*, 4914.

(20)   Boal, A. K.; Rotello, V. M. *J. Am. Chem. Soc.* **2000**, *122*, 734.

(21) (a) Guglielmetti, R. "4n+2 System: Spriopyran" in *Photochromism: Molecules and Systems* (Eds: H. Durr, H. Bouas-Laurent). Elsevier. Amsterdam. 1990. p314; (b) Merocyanine exists in two extreme resonance structures, the highy polar zwitterionic and the less polar quinonoid forms. in which the former structure contributes more, due to its aromaticity.

(22) Willner, I.; Willner, B.; "Photochemical Biomolecular Switches: The Route to Optobioelectronics" in *Molecular Switches* (Ed. B. L. Feringa), Wiley-VCH, Weinheim, 2001, p165.

(23) Angelini, N.; Corrias, B.; Fissi, A.; Pieroni,O.; Lenci, F. *Biophys. J.* **1998**, *74*, 2601.

(24) Menju, A.; Hayashi, K.; Irie, M. *Macromolecules* **1981**, *14*, 755.

(25) Rosario, R.; Gust, D.; Hayes, M.; Jahnke, F.; Springer, J.; Garcia, A. A. *Langmuir* **2002**, *18*, 8062.

(26) (a) Garcia, A. A.; Cherian, S.; Park, J.; Gust, D.; Jhanke, F.; Rosario, R. *J. Phys. Chem. A* **2000**, *104*, 6103. (b) Kimura, K.; Kaneshige, M.; Yamashita, T.; Yokoyama, M. *J. Org. Chem.* **1994**, *59*, 1251. (c) Sunamoto, J.; Iwamoto, K.; Mohri, Y.; Kominato, T. *J. Am. Chem. Soc.* **1982**, *104*, 5502.

(27) (a) Raymo, F. M.; Giordani, S. *J. Am. Chem. Soc.* **2002**, *124*, 2002. (b) Raymo, F. M.; Giordani, S. *J. Am. Chem. Soc.* **2001**, *123*, 4651.

(28) Doron, A.; Katz, E.; Tao, G.; Willner, I. *Langmuir* **1997**, *13*, 1783.

(29)   Brust, M.; Walker, M.; Bethell, D.; Schiffrin, D. J.; Whyman, R. *J. Chem. Soc., Chem. Commun.* **1994**, 801.

(30)   Chen, S.; Murray, R. W. *Langmuir* **1999**, *15*, 682.

(31)   Evans, S. D.; Johnson, S. R.; Ringsdorf, H.; Williams, L. M.; Wolf, H. *Langmuir* **1998**, *14*, 6436.

(32)   Bahr, J. L.; Kodis, G.; de la Garza, L.; Lin. S.; Moore, A. L.; Moore, T. A.; Gust, D. *J. Am. Chem. Soc.* **2001**, *123*, 7125.

(33)   Inouye, M.; Ueno, M.; Tsuchiya, K.; Nakayama, N.; Konishi, T.; Kitao, T. *J. Org. Chem.* **1992**, *57*, 5377.

(34)   Pozzo, J-L.; Samat, A.; Guglielmetti, R.; Keukeleire, D. D. *J. Chem. Soc. Perkin Trans. 2* **1993**, 1327.

(35)   Khairutdinov, R. F.; Giertz, K.; Hurst, J. K.; Voloshina, E. N.; Voloshin. N. A.; Minkin, V. I. *J. Am. Chem. Soc.* **1998**, *120*, 12707.

CHAPTER 4

Nanophosphors, Nanosensors and Superstructures from Bipyridine Functionalized Gold Nanoparticles

4.1. Abstract

Synthesis and photophysical studies of a thiol derivative of 2.2'-bipyridyl, **BT** and its three dimensional assembly on gold nanoparticles (**Au-BT**) are reported. Metal ion binding properties of these bipyridine functionalized gold nanoparticles were investigated in detail. The strong coordination ability of Cu^{II} ions brings **BT**s on adjacent gold nanoparticles closer, leading to the formation of three dimensional superstructures through metal induced self-assembly of ligands. Superstructures were characterized using TEM studies and a red shifted absorption band was observed as a result of interparticle plasmon coupling. The luminescence of Eu^{III} was found to increase manifold upon complexation with bipyridine capped Au nanoparticle. Based on Job's continuous variation method, it is concluded that a 1:1 complexation stoichiometry exists between **BT** on the surface of gold nanoparticles and Eu^{III}/Tb^{III}. High stability constant ($\sim 10^4$ M^{-1}) for the complex formation of **Au-BT** with Eu^{III}/Tb^{III} indicates that such systems may have potential application as nanophosphors. The luminescence lifetimes of Eu^{III} and Tb^{III} in the presence of **BT** were estimated as 0.4 ms and 0.56 ms, respectively. The lifetimes

of lanthanide complexes remain unquenched when functionalized on Au nanoparticles. Allosteric effects of Ca^{II} and Mg^{II} on **Au-BT:Eu^{III}** complex in acetonitrile were also investigated. The dramatic quenching of emission observed in the present case revealed that Ca^{II}/Mg^{II} ions replace Eu^{III} from **Au-BT:Eu^{III}**.

4.2. Introduction

Manipulation of metal nanoparticles with organic ligands is gaining considerable attention due to their processibility, ease of tunability of their physicochemical properties, and biocompatibility.[1-11] In addition, the fascinating size as well as shape dependent optoelectronic properties of metal and semiconductor quantum dots bestows them with immense potential in nanophotonics (e.g. plasmonics) and nanoelectronics.[12-18] Plasmonics is a fast growing technology;[19] by means of near-field coupling it has been recently demonstrated that closely spaced arrays of metal nanoparticles can act as guides for electromagnetic radiations.[20] Such waveguides are usually prepared by means of electron beam lithography. Several approaches have been suggested for tailoring supramolecular-assemblies of nanoparticles for nanophotonic devices. A summary on various possibilities of nanophotonic materials and their applications was reviewed recently by Prasad and coworkers.[21]

Another approach of designing nanophotonic materials is by linking photoresponsive molecules around metal nanoparticles. In this Chapter, a novel strategy for the design of well ordered supramolecular-assemblies of nanometer

dimension by functionalizing chelating groups on metal nanoparticles by using chemical methods and further organizing rare earth metal ions around gold nanoparticle core by ligand induced complexation is reported. Incorporation of rare earth complexes around gold nanoparticles could yield interesting phosphorescent materials. The multifaceted characters of phosphorescent materials offer a wide range of research and development possibilities in diverse areas of photonics, electronics, material science, and biology (see, for example, refs. 22-25 on the design, properties and applications of phosphorescent materials). A brief introduction on the photophysical properties and applications of rare earth based phosphorescent materials is presented below.

4.2.1. Photophysical properties of lanthanide complexes

The photophysical properties of lanthanide complexes are extensively investigated in the literature[24] and a brief outline of their basic features are summarized below.

(1) The emission of lanthanides results from transitions involving *4f* orbitals, which are forbidden transitions. As a result, the absorption coefficient of lanthanides is low ($\sim$10 M^{-1}cm^{-1}) and possess long lifetimes (ranges from 0.4 - 0.8 ms) due to the forbidden nature of the transition.

(2) Lanthanides display line like emission spectra unlike organic chromophores. The emission observed in the red as well as near-infrared region depends on the nature of lanthanide metal ion.

(3) Due to their weak absorption, lanthanides are usually not directly excited, but are rather excited through chelated organic ligands.

(4) Lanthanide complexes possess high absorption coefficient in the UV region and very high quantum yield of emission in the visible and near-infrared region. The main route of non-radiative decay in these systems is by coupling to the vibrations of water.

Complexes of rare earth metals like Eu^{3+} and Tb^{3+} with organic ligands like bipyridine, phenanthroline,[26] are found to show strong emission due to an energy transfer from the complexed ligands to the rare earth ions (antenna effect).[27,28] The mechanism involves the sensitization of the ^5D_J - ^7F_J emission of the metal ion by the triplet excited state of the heterocyclic ligand. An abbreviated scheme of this absorption-energy transfer-emission (A-ET-E) process is shown in Figure 4.1.[29]
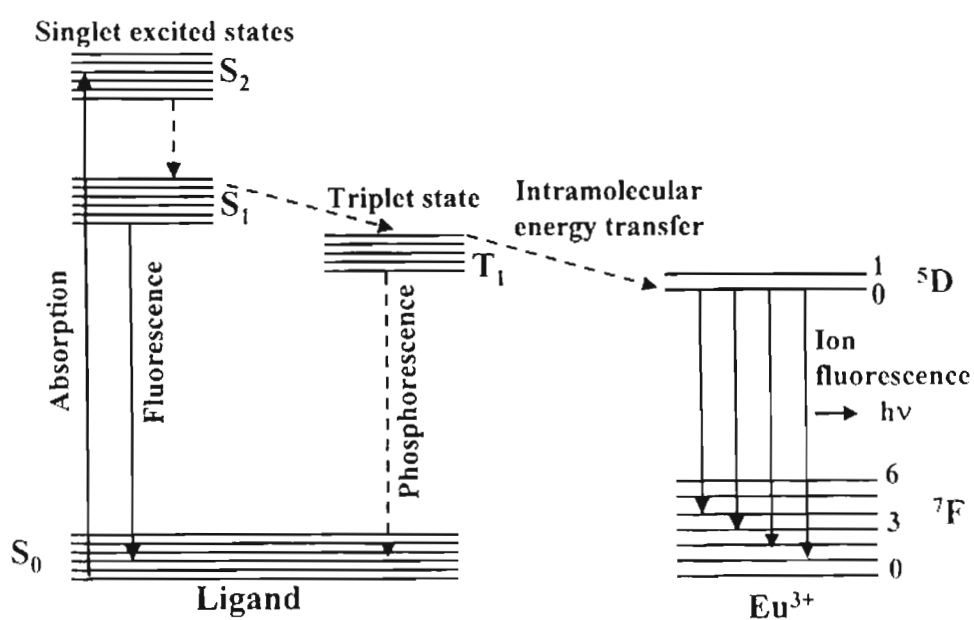
Figure 4.1. Mechanism of luminescence from lanthanide complexes by means of fluorescence resonance energy transfer from ligands.[29]

The π-system of the heterocyclic ligand encapsulating the metal cation is electronically excited to its singlet state by irradiation with UV light. The energy from the S_1 level is transferred in a radiationless way to the triplet state of the ligand by a process known as intersystem crossing. The chelating ligands act as energy donors by transferring the excitation energy to the complexed lanthanide cation by an intramolecular energy transfer process (review of antenna effect and resonance energy transfer in lanthanides is given in reference 24). The chelated lanthanide metal cations in turn emit at longer wavelengths while an undesirable loss of energy may occur by fast emission from the singlet excited state of the ligand.

Lanthanides as well as their chelate complexes are widely used in luminescent devices and as biological probes owing to their unusual photophysical properties which include millisecond lifetimes, large stokes shift, high quantum yields and excellent solubility. A few of the present day applications of lanthanide complexes are briefly described below.

4.2.2. Lanthanide complexes as biological probes

Lanthanide complexes are much superior probes for biological applications compared to organic fluorophores. Organic fluorophores display fluorescence lifetimes between 1-10 ns. All biological samples display autofluorescence (from the aromatic residues), which usually decays in nanosecond timescale, as does the fluorescence of most fluorophores. Similarity in their lifetimes is one of the major limiting factors in high sensitive detection of biological samples. Lanthanide

complexes are uniquely fluorescent, which display long lived emission with decay times of 0.5-3 ms and continue to emit following the disappearance of autofluorescence from biological samples. Hence lanthanide complexes have widespread use in high-sensitive detection, particularly for immunoassays. For example, antigen-antibody interactions are investigated by using photoactive lanthanide complexes possessing long luminescence lifetime, compared to emission lifetime of aromatic residues in proteins.[29]

In biological and artificial systems, allosteric regulation is effective in controlling molecular functions (for example, molecular recognition and catalytic activity).[30] Allosteric effects occur when the binding properties of a macromolecule change as a consequence of binding of a second ligand (or metal ion) to the macromolecule, altering its affinity towards the first ligand (or metal ion). If both the ligands are the same then the phenomenon is termed as "homotropic allosteric effect" and if different, termed as "heterotropic allosteric effect." For example, lanthanide ions were reported to substitute biologically important ions such as calcium in many calcium dependent proteins.[30]

## 4.2.3. Lanthanide based phosphorescent materials

Synthesis of phosphorescent materials, with high emission yield, is a field of considerable importance due to their industrial as well as technological applications. For example, the oxides of europium, terbium, yttrium and cerium are widely used in the manufacture of fluorescent lamps. Also, rare earth compounds are used

extensively as phosphors in a wide variety of products, including electroluminescent devices and display screens in cathode ray tubes. Conventionally, the size of phosphors used in such devices is in micrometer range and they are synthesized by a "top-down" approach such as ball milling (Scheme 4.1). The phosphorescence quantum yield of such materials is critical for technological applications and could be enhanced by increasing the surface area by designing phosphors of nanometric dimension.
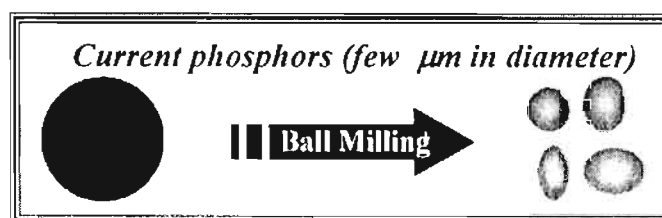
Scheme 4.1. Top down approach currently used for preparing phosphors.

Design of nanostructured phosphors (nanophoshors), adopting the "bottom up approach" and thereby increasing the surface area may be a convenient way to enhance the phosphorescence efficiency of these systems (Scheme 4.2). Linking phosphorescent molecules on the surface of Au nanoparticles could give rise to phosphors in the nanometric size regime.
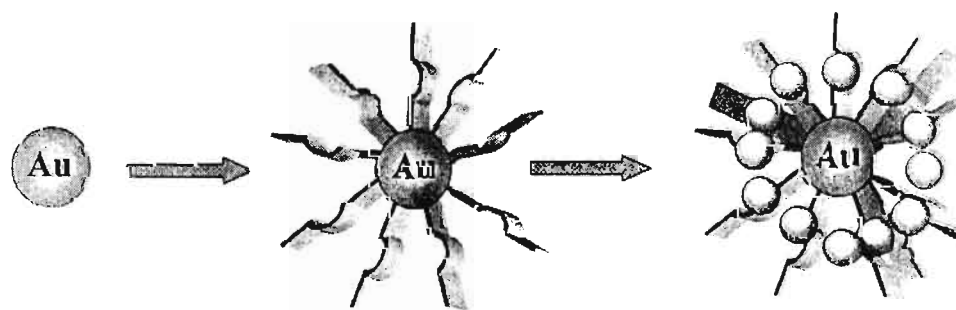
Scheme 4.2. "Bottom-up approach" adopted in this chapter for the synthesis of nanophosphors.

In the present study, a thiol functionalized chelating molecule, namely bipyridine, was anchored to gold nanoparticles. Bipyridine ligands have been extensively used as a chelating group for metal ions. Among these the 2,2'-bipyridine ligands are excellent due to their robust redox stability and ease of functionalization.[31] Chelates of metal ions containing two or more 2,2'-bipyridine ligands possess well-defined spatial arrangement and a representative example is shown in Chart 4.1.[31] Such lanthanide complexes with well-defined geometry find potential applications in luminescent devices as well as in nanophotonics and optoelectronics. In the present study, a thiol derivative of 2,2'-bipyridine (BT)(Chart 4.2) was synthesized and functionalized on the surface of gold
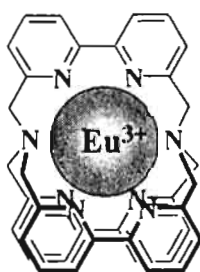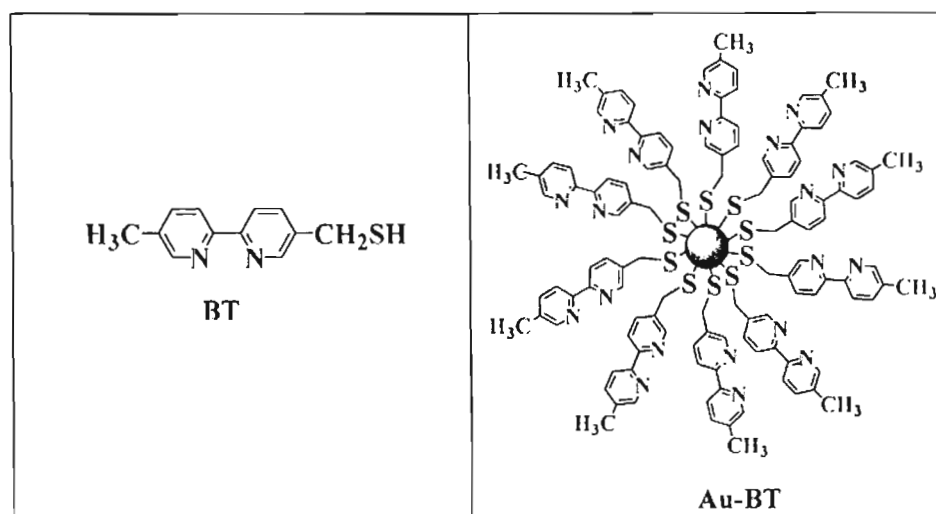

Chart 4.1.

Chart 4.2.

nanoparticles along with dodecanethiol (dodecanethiol is omitted in the representation of **Au-BT** for clarity). Bipyridines which possess co-ordination sites for complexation with metal ions, arranged on the three dimensional surface of gold nanoparticles, can be visualized as an antenna system.

A detailed investigation on the photophysical properties of bipyridine capped gold nanoparticles was carried out with the following objectives.

(i)   Exploring the self-assembly of **Au-BT** in the presence of transition metals like Cu^{II} which could give rise to a high density 'ion-sponge' (Au-BT)(Chart 4.2) having potential application in medical diagnostics.[33]

(ii)   Fabricating nanophosphors of Eu^{III}/Tb^{III} by taking advantage of FRET (fluorescence resonance energy transfer) from **BT** to the lanthanide ions which can have potential applications in display devices.

(iii)   Exploiting such phosphorescent complexes for sensing biologically important metal cations (for example Ca^{2+}/Mg^{2+} ions) by making use of allosteric effect[34,35] (high local concentration of lanthanide complexes around Au nanoparticle and site specific binding of Au nanoparticle make these systems attractive for biological application).

4.3. Results and Discussion

4.3.1. Synthesis and characterization

Synthesis of the thiol derivative of 2,2'-bipyridine (**BT**) was carried out in two steps as shown in Scheme 4.3. The mono bromo derivative (**4.2**) of 5,5'-

dimethyl-2,2'-bipyridine (**4.1**) was prepared by its treatment with N-bromosuccinimide. It was then converted to the corresponding thiol derivative using a procedure reported by Fox and coworkers.[36] The details of the synthetic procedure, spectral characterization of **BT** and intermediates are given in the Experimental Section 4.5.
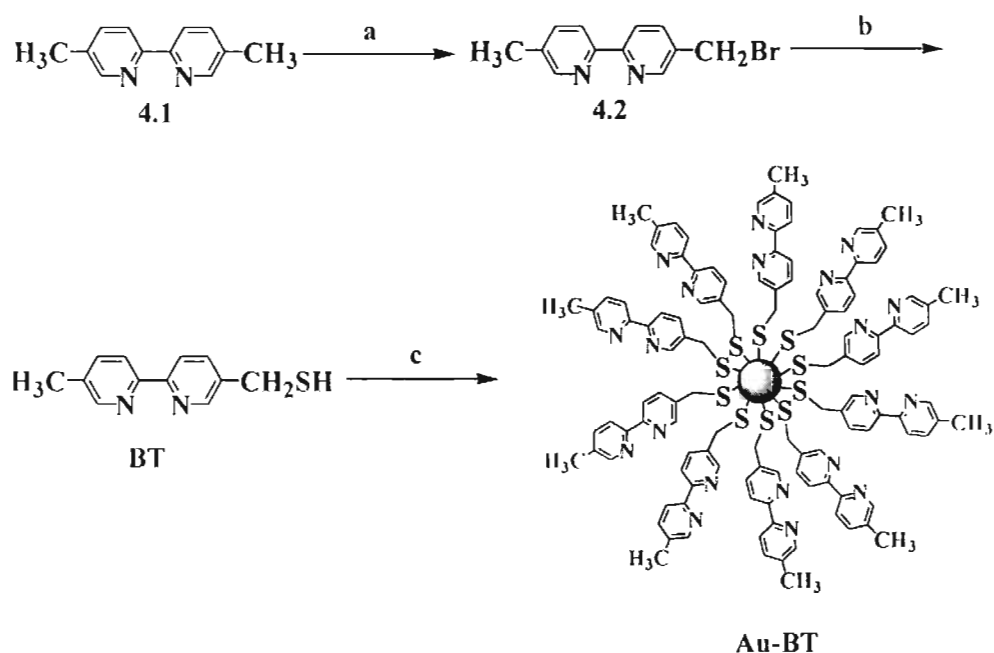

Scheme 4.3. Reaction scheme for the preparation of **BT** and **Au-BT**. a) NBS, CHCl$_3$ b) HMDST, TBAF c) dodecanethiol, HAuCl$_4$, TOAB, NaBH$_4$.

BT was attached to gold nanoparticles (**Au-BT**) by adopting a modification of Brust's method.[1] The gold nanoparticles were co-binded with dodecanethiol in order to impart better stability for **Au-BT**. Removal of any unbound **BT** and dodecanethiol from the suspension was ensured by repeated centrifugation using ethanol and the details are presented in the Experimental Section (Section 4.5). Bipyridine functionalized gold nanoparticles (**Au-BT**) were characterized by means of electronic absorption and transmission electron microscopic studies.

4.3.2. Absorption studies

Theoretical calculations suggest that, 2,2'-bipyridine exists in a *trans* conformation in the solid state and also when dissolved in organic solvents and basic media.[37] The absorption spectrum of **BT** was recorded in solvents of varying polarity, from cyclohexane to methanol. Representative examples are shown in Figure 4.2.

The thiol derivative of bipyridine (**BT**) in acetonitrile possesses two absorption maxima; one at 249 nm and other at 295 nm. It has been reported that the latter band orginates from a π-π^* transition.[38] The monoprotonated form of 2,2'-bipyridines has a *cis* conformation, stabilized by a cationic hydrogen bond.[39] As a result of the *cis*-conformation, the π-π^* transitions are shifted by about 20 nm towards longer wavelength regions and possess higher intensities. Further addition
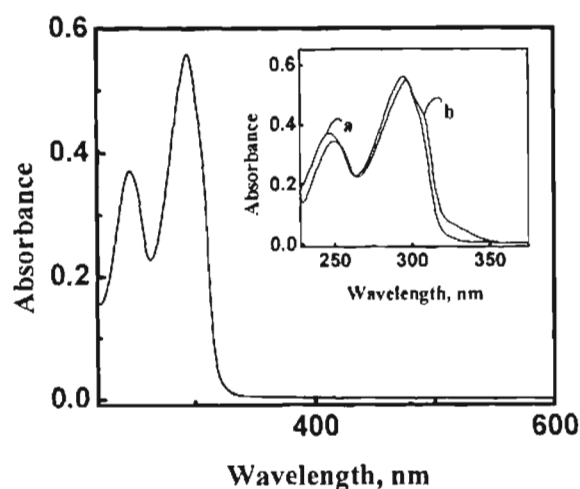
Figure 4.2. Absorption spectrum of **BT** in acetonitrile. Inset shows the absorption of **BT** (a) in methanol and (b) in dichloromethane.

of acid results in the formation of the diprotonated forms of 2,2'- bipyridines. In order to reduce both steric hindrance and electrostatic repulsions, the *cis*

conformation of the monoprotonated 2,2'-bipyridine usually transforms to a *trans* conformation in the diprotonated form, resulting in a shift of 12 nm towards shorter wavelengths.[39] We have investigated the effect of trifluoroacetic acid on the absorption properties of **BT** and spectral changes were different from the previous observations. The spectral changes are represented in Figure 4.3.
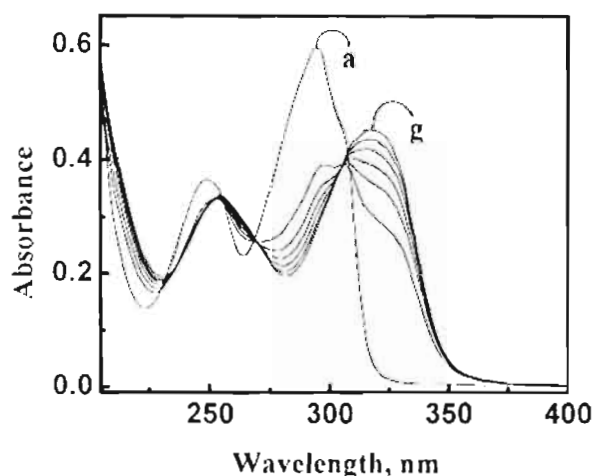
Figure 4.3. Effect of trifluoroacetic acid on the absorption properties of **BT**. [TFA]: (a) 0 μM, (b) 37 μM, (c) 74.2 μM, (d) 111.2 μM, (e) 148.3 μM, (f) 185.4 μM, (g) 222.5 μM.

On addition of various concentrations of trifluoroacetic acid to **BT**, no significant change in the absorbance was observed for the short wave length band. The intensity of 295 nm band decreased considerably with the concomitant emergence of a new band (λ_{max} at 318 nm). On further addition of acid, no significant spectral change was observed for **BT**, indicating that the *cis* conformation is maintained both in the folded monoprotonated as well as the diprotonated species. The two isosbestic points observed at 270 nm and 306 nm represent the existence of the protonated as well as the non-protonated forms of

BT. A diprotonated form of bipyridine derivative with *cis* conformation was earlier reported by Albrecht-Gary and coworkers.[40] It is observed that the solvent polarity has little influence on the absorption properties of BT. The inset in Figure 4.2 represents the absorption of BT in solvents of extreme polarities: dichloromethane and methanol. Molar extinction coefficients of the compound BT for both the bands, in solvents of varying polarity were evaluated and are summarized in Table 4.1.

**Table 4.1.** Absorption characteristics of BT in different solvents

Solvent	Molar absorptivity (ε), $M^{-1}cm^{-1}$	
	λ_1 (249 nm)	λ_2 (295 nm)
Cyclohexane	1.37×10^4	2.24×10^4
Dichloromethane	1.29×10^4	2.07×10^4
Tetrahydrofuran	1.41×10^4	2.30×10^4
Acetonitrile	1.33×10^4	2.17×10^4
Methanol	1.40×10^4	2.12×10^4

4.3.2.1. Absorption properties of Au-BT

The absorption spectrum of gold nanoparticles functionalized with bipyridine thiol (**Au-BT**) was recorded in acetonitrile (Figure 4.4). The solution of **Au-BT**
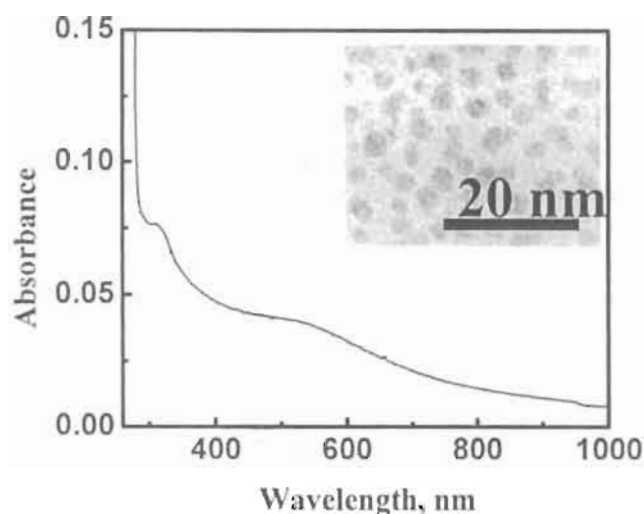
Figure 4.4. Absorption spectrum of **Au-BT** recorded in acetonitrile. Inset shows the TEM image of **Au-BT** placed on a carbon coated Cu grid.

in toluene was diluted using acetonitrile and the toluene content in the resultant solution was <3 %. The concentration of **BT** per Au nanoparticle was estimated based on absorption and transmission electron microscopic studies. The functionalization of bipyridine ligands on nanoparticles is not quantitative and the concentration of the unreacted ligands was estimated from the absorption intensity of the filtrate. Also it is assumed that the reacted chromophores are evenly distributed on each nanoparticle.

TEM image shown in the inset of Figure 4.4 exhibits particles of approximately 4 nm size. The TEM image of **Au-BT** was recorded by placing a drop of the dilute solution of nanoparticles in toluene on a carbon coated Cu grid and the solvent was allowed to evaporate. From the mean diameter of gold core in **Au-BT** (~4 nm), an average formula of $Au_{820}BT_{343}$ was estimated. The above

calculation is based on the tight-packed spherical model, according to which gold nanoparticles have a densely packed core of density 58.01 atoms/nm^3 covered with a skin of hexagonally closed-packed gold atoms.[41] Assuming uniform surface coverage, the number of **BT** per nanoparticle is calculated as ~340 based on the amount of **BT** reacted (absorption spectral studies) and size of metal core (TEM studies).

The absorption spectrum of **Au-BT** (Figure 4.4) consists of two bands in the UV-Vis region. It represents an additive absorption spectrum corresponding to the absorption of **BT** and that of gold nanoparticles. The band at 300 nm corresponds to the characteristic absorption of **BT** while the broad band centered around 520 nm corresponds to the plasmon absorption of gold nanoparticles. For **Au-BT**, the short wavelength band of **BT** is merged with the absorption of gold nanoparticles. The $\pi - \pi^*$ transition of **BT** at 295 nm is observed as a shoulder when functionalized on to the surface of gold nanoparticle. Murray and coworkers have investigated the surface plasmon characteristics and the average size of gold nanoparticles, stabilized with arenethiolate ligands.[42] In the present case, bipyridine chromophore is linked to the gold nanocore by a single methylene spacer. The strong interaction of the bipyridine chromophore and plasmon electrons of the nanoparticles results in the perturbation of the electronic properties of both bipyridine and gold nanoparticles. Thus, as in the case of arenethiolate stabilized gold nanoparticles, the plasmon absorption band of **Au-BT** is broader.[42]

4.3.2.2. Absorption properties of BT and Au-BT in the presence of cations

As mentioned in Section 4.2, bipyridine ligands form strong complexes with inner-transition metal ions, which could yield highly phosphorescent materials by means of FRET. We have investigated the complexation of **Au-BT** in the presence of lanthanide ions namely Eu^{III} and Tb^{III} by following their absorption properties (Figures 4.5-4.6).

On addition of increasing concentrations of Eu^{III} to **BT**, there is a decrease in the intensity of the π-π^* absorption band (295 nm) corresponding to that of **BT**, along with the concomitant emergence of a new band around 320 nm (Figure 4.5A). Similar absorption changes were observed for **BT** on addition of various
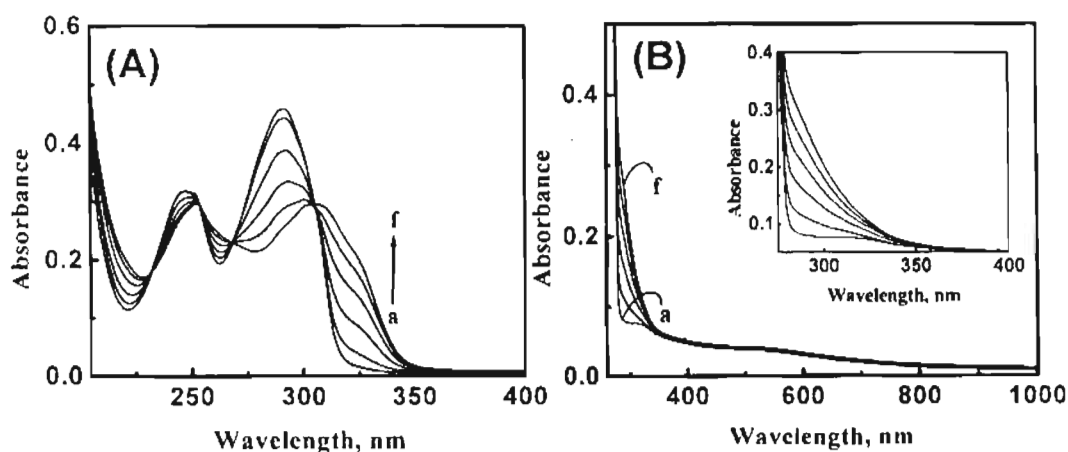
Figure 4.5. Absorption spectral changes of A) **BT** and B) **Au-BT** in the presence of different concentrations of Eu^{III};[Eu^{III}]: (a) 0 μM, (b) 12 μM, (c) 24 μM, (d) 36 μM, (e) 48 μM, (f) 60 μM.

concentrations of acid. The emergence of a new ligand to metal charge transfer (LMCT) band at 320 nm indicates the strong interaction between the ligand and metal ions (Eu^{III}) as well as the change in the conformation of the ligand, on metal

coordination. Similarly, the effect of increasing concentrations of Eu[III] on the absorption properties of **Au-BT** is represented in Figure 4.5B. The emergence of an LMCT band at 320 nm for **Au-BT** clearly indicates the effective coordination of Eu[III] with **BT** functionalized to gold nanoparticles and also the change in the conformation of **BT** brought about by metal coordination. The inset of Figure 4.5B represents an expanded view of the LMCT band in the case of **Au-BT**. Similar changes in the absorption characteristics of **Au-BT** were observed in the presence of Tb[III], and are presented in Figure 4.6.
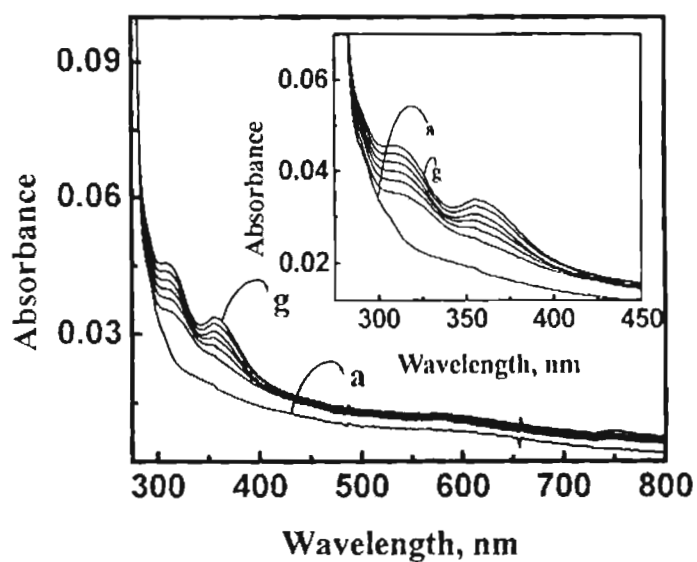
Figure 4.6. Absorption spectral changes of **Au-BT** in the presence of different concentrations of Tb[III];[Tb[III]]: (a) 0 μM, (b) 33.2 μM, (c) 66.4 μM, (d) 99.7 μM, (e) 132.9 μM, (f) 166 μM, (g) 199.3 μM.

Transition metal ions are known to coordinate strongly with bipyridine ligands.[24] The absorption spectral changes for **Au-BT** associated with the addition of various concentrations of copper(II)perchlorate (Figure 4.7A) indicate the emergence of a new band at 780 nm, in addition to the LMCT band observed at
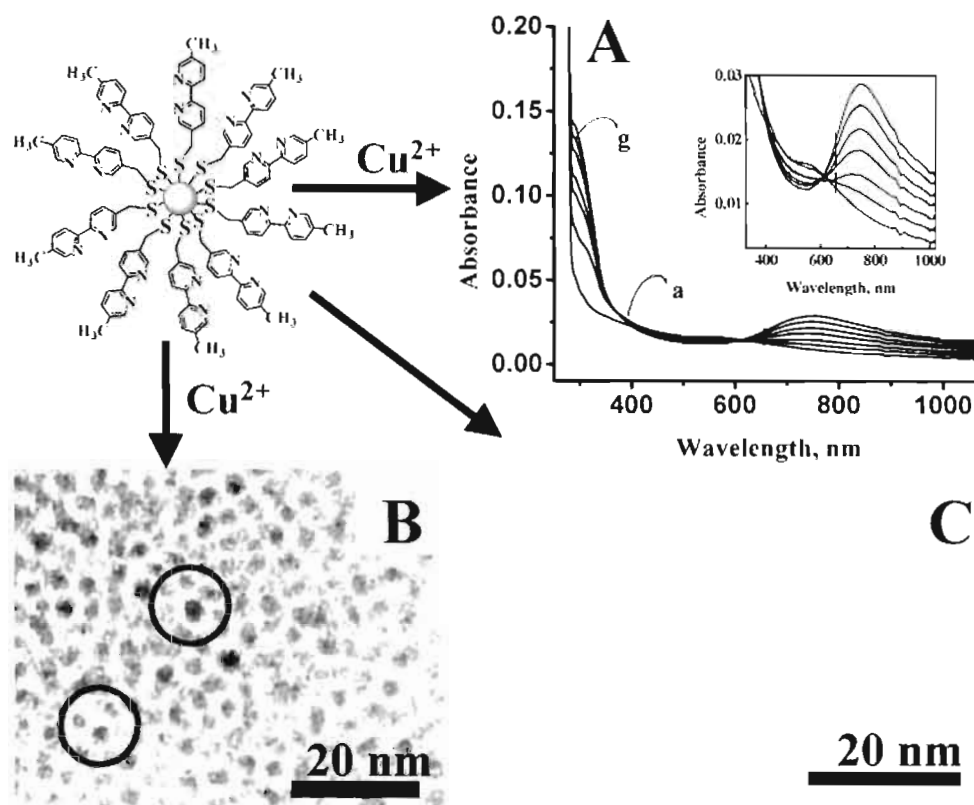
Figure 4.7. A) Effect of Cu^{II} on the absorption properties of **Au-BT**. |Cu^{II}|: (a) 0 μM, (b) 31.6 μM, (c) 63.2 μM, (d) 94.8 μM, (e) 126.5 μM, (f) 158 μM, (g) 189.6 μM, B) TEM image of **Au-BT** in the presence of Cu^{II}, C) TEM image of **Au-BT**.

320 nm. With the emergence of the new band at 780 nm, one could also observe a concomitant decrease in the plasmon absorption band of **Au-BT** at 520 nm (inset of Figure 4.7A). The strong coordinating ability of Cu^{II} ions can bring the **BT**s on adjacent gold nanoparticles together, leading to the formation of superstructures through metal induced three dimensional self-assembly of ligands. The concomitant emergence of the absorption band at 780 nm originates from interparticle plasmon coupling resulting from the close interaction of metal particles in the superstructures. In the absence of Cu^{II} ions, plasmon absorption band was observed for **Au-BT** only at 520 nm. Willner and coworkers have

demonstrated the appearance of an additional red shifted absorption band in gold nanoparticle superstructures.[43] Metals can be considered to be in a plasma state composed of positively charged nuclei and negatively charged electrons. In the presence of an electromagnetic radiation, these electrons are perturbed so as to screen the nuclei from the external radiation. The motion of electrons with respect to the nuclei is governed mainly by the coulombic attraction between the nuclei and electrons. Hence the electrons oscillate with a particular frequency referred to as "plasmon frequency." This collective oscillation of electrons in metal nanoparticles is called dipole plasmon resonance.[44]

The red shifted absorption observed in the present case is attributed to interparticle plasmon coupling, facilitated by the formation of superstructures. When two metal nanoparticles are placed close (at nanometric distance) to each other, an additional force (either attractive or repulsive) act on the electron charge cloud of both particles.[45] As a result the repulsive force within a single particle weakens, leading to a correspondingly lower resonance frequency for the oscillation of the electron cloud. This reduction in the frequency of oscillation is reflected as a red shift in the absorption.

Copper ion induced self-assembly of **Au-BT** was conclusively proved from the TEM image of **Au-BT** in the presence of Cu^{II} ions. The images are presented in Figure 4.7B (see the highlighted portion). Ring structures in the present case are common for bilayer agglomerates.[46] In the present case, ring structures with external diameter of about 10 nm are observed. Thus, based on TEM studies, the

absorption at 780 nm is attributed to an interparticle plasmon band (originating from the overlaping of electronic levels of gold nanoparticles) in the superstructure. Similarly some sort of self-assembly was observed for **Au-BT** in the presence of Eu^{III} and the TEM images are shown in Figure 4.8. However, in this case no interparticle plasmon absorption was observed.
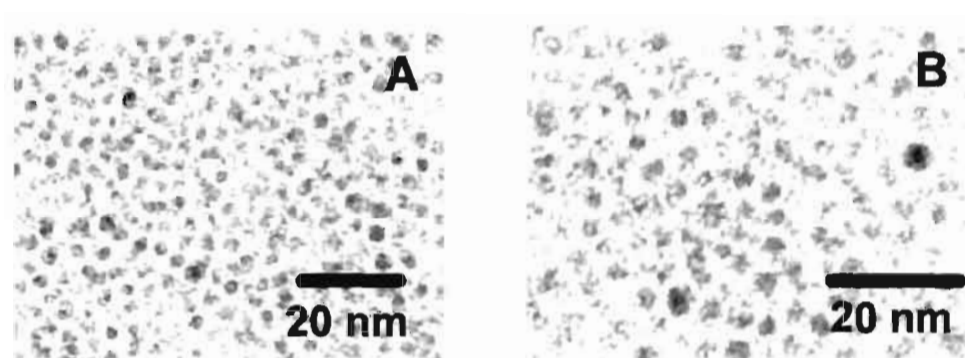
Figure 4.8. TEM image of **Au-BT** in the presence of Eu^{III} at two different magnifications.

The stoichiometry for the complexation of inner transition metal ions with **BT** on the surface of gold nanoparticles was investigated by means of the continuous variation method.[47] In the present case, the concentration of Ln^{III} was varied to that of **BT** on the surface of gold (mole ratio) and the absorbance of LMCT band at 320 nm, was monitored. After successive addition of metal ions, solutions were kept for ~5 min for equilibration. The metal to ligand stoichiometry was estimated from Job's plot presented in Figure 4.9A. In the present case, the absorbance of LMCT band at 320 nm increases on successive addition of metal ions until the concentration of the ligands on the surface of gold becomes equal to that of Ln^{III} ions. On further addition of Ln^{III} ions, the LMCT band remains

unaffected indicating that all the ligands have been used up. Based on these studies, it is concluded that a 1:1 complexation stoichiometry exists between BT on the surface of gold nanoparticles and Ln^{III}.
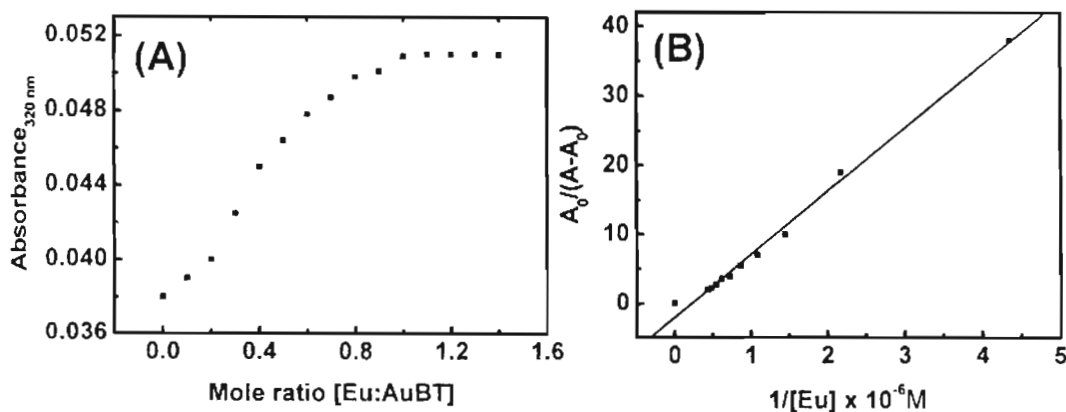
Figure 4.9. Plot of A) absorbance at 320 nm for **Au-BT** in the presence of increasing concentrations of Eu^{III}, **B)** $A_0/(A-A_0)$ versus reciprocal concentration of Eu^{III} for the complexation of **Au-BT** with Eu^{III} in acetonitrile.

The stability constant for the complex formation of **Au-BT** with Ln^{III} was estimated using the Benesi-Hildebrand equation (Equation 4.1) for a 1:1 metal to ligand stoichiometry. The equilibrium constant for the formation of **Au-BT:::Eu** complex was determined from the relationship (Equation 4.1),

$$A_0/(A - A_0) = (\varepsilon/\varepsilon - \varepsilon')\{1/K[Eu] + 1\} \qquad (4.1)$$

where A and A_0 are the absorption of the complexed and uncomplexed **Au-BT** at 320 nm, K is the equilibrium constant for complex formation, ε and ε' are the molar absorptivities of free **Au-BT** and complexed **Au-BT**. A plot of $A_0/A-A_0$ vs $1/[Eu]$ gave a straight line (Figure 4.9B) further confirming the 1:1 complex formation between Eu^{III} and **BT** on gold surface. The equilibrium constant (K) was

estimated from the slope and Y-intercept, and was found to be 2.3 x 10^4 M^{-1}. Significantly high association constant indicates the credibility of this system for potential applications as nanophosphors.

4.3.3. Steady state emission studies

The emission spectra of **BT** and **Au-BT** measured in acetonitrile are presented in Figure 4.10A and 4.10B. The broad unstructured emission band, observed for **BT** between 320 nm to 450 nm, (excitation at 300 nm) is characteristic of bipyridine fluorescence.[40] The fluorescence quantum yields of bipyridines are very low due to their high intersystem crossing efficiency to the triplet excited states.[40] The emission spectrum of **Au-BT** in acetonitrile is presented in Figure 4.10B.
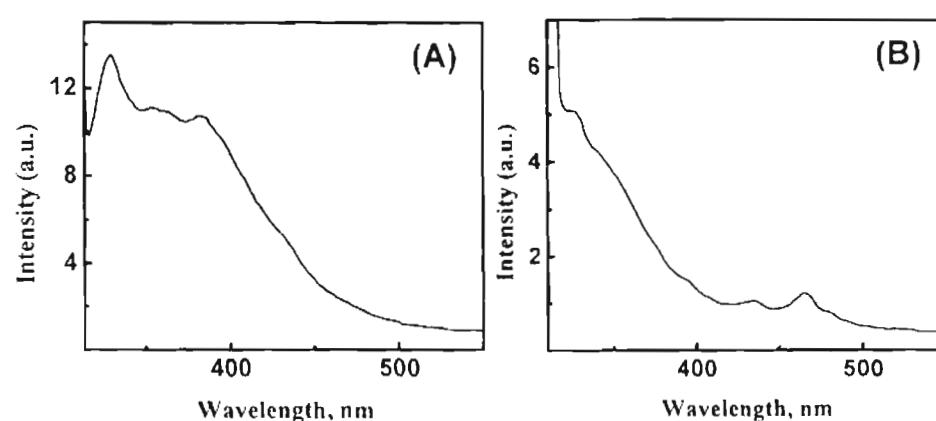
Figure 4.10. Emission spectra of A) **BT** and B) **Au-BT**, in acetonitrile after exciting at 300 nm.

Investigation of the luminescence behavior of **Au-BT** in the presence of varying concentrations of lanthanide ions (Eu^{III}, Tb^{III}) has indicated a dramatic enhancement of luminescence on excitation of **BT** capped on the surface of gold

nanoparticles. All luminescence measurements were recorded after exciting the charge transfer band at 320 nm. The emission spectral changes of **Au-BT** in acetonitrile containing varying concentrations of Eu^{III} and Tb^{III} are represented in Figure 4.11. The dramatic enhancement of emission observed in the present case is attributed to the efficient fluorescence resonance energy transfer (FRET) from **BT** to the coordinated Ln^{III} ions on the surface of Au nanoparticles.
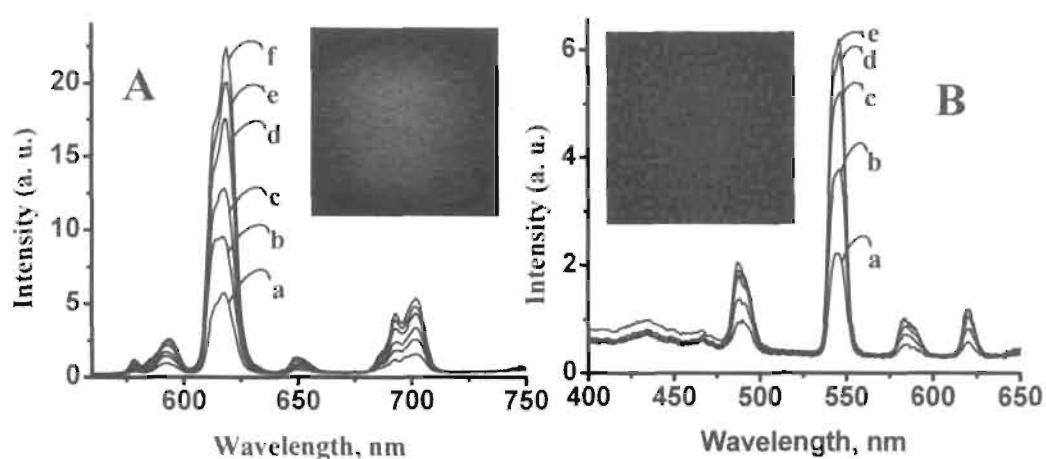
Figure 4.11. Luminescence spectrum of **Au-BT** in acetonitrile. A) on addition of various concentrations of Eu^{III}. [Eu]: (a) 2.4 µM. (b) 4.8 µM. (c) 7.2 µM. (d) 9.7 µM, (e) 12 µM. (f) 14.5 µM and B) on addition of various concentrations of Tb^{III}. [Tb^{III}]: (a) 5.5 µM. (b) 11 µM. (c) 16.6 µM. (d) 22 µM. (e) 27.7 µM after exciting at 320 nm.

Europium (III) ion is known to have a prominent emission at 615 nm ($^5D_0$-$^7F_1$) by fluorescence resonance energy transfer from bipyridine.[39] Varying concentrations of Eu^{III} were added to a solution of **Au-BT** in acetonitrile and emission properties were investigated (Figure 4.11A). An enhancement in the fluorescence intensity at 615 nm was observed with increasing Eu^{III} concentration and the luminescence levels

off on addition of Eu^{III} above 15 µM. Absolute quantum yields of **Au-BT: Eu^{III}** and **Au-BT: Tb^{III}** systems are reported in the following section.

Similar complexation studies were carried out with Tb^{III} ions. The enhancement of luminescence from Tb^{III} on complexation with bipyridines capped on Au is presented in Figure 4.11B (excitation wavelength 320 nm). It is reported that complexes of Tb^{III} possess a prominent emission at 545 nm ($^5D_4$-$^7F_1$) by fluorescence resonance energy transfer (FRET) from bipyridine.[39] Saturation in luminescence intensity was observed at higher concentrations of Tb^{III} ions.

The excitation spectra of **Au-BT** in the presence of Eu^{III} ions and Tb^{III} ions, following the emission at 545 nm, are shown in Figure 4.12. The excitation spectrum at 320 nm matches with the charge transfer band of the lanthanide ion complex of **Au-BT** (**Au-BT: Ln^{III}**). These studies indicate that the luminescence originates from the excitation of the charge transfer band (CT of lanthanide ion complex of **Au-BT** at 320 nm). This is followed by fluorescence resonance energy transfer (FRET) from the bipyridine ligand to the D levels of the lanthanide ions, which further relaxes to different F levels through radiative emission. The phosphorescence of **Au-BT: Eu^{III}** and **Au-BT: Tb^{III}** complexes, (illuminated using a 320 nm UV light source) are shown in the inset of Figure 4.11. A luminescence enhancement of 10^4-10^5 fold was observed for Eu^{III}/Tb^{III} ions when complexed on **Au-BT**. The luminescence quantum yields of **Au-BT: Eu^{III}** and **Au-BT: Tb^{III}** complexes were obtained by the method described by Haas and Stein[48] using $Ru(bpy)_3]^{2+}$ (Φ = 0.028 in aerated water)[49] as a standard for the Eu^{3+}

complex, and quinine sulphate (Φ = 0.546 in 1 N H_2SO_4)[50] as a standard for the Tb^{3+} complex. The luminescence quantum yields were found to be 0.0096 and 0.038 for the **Au-BT: Eu**[III] and **Au-BT: Tb**[III] complexes respectively. It may be noted that there are ~340 **BT** molecules attached on each nanoparticle surface (~4 nm diameter). A novel "bottom-up" strategy is reported here for the design of nanophosphors by functionalizing bipyridine groups on metal nanoparticles and further organizing rare earth metal ions around gold nanoparticle core by ligand induced complexation. Such supramolecular complexes may have potential application in display devices.
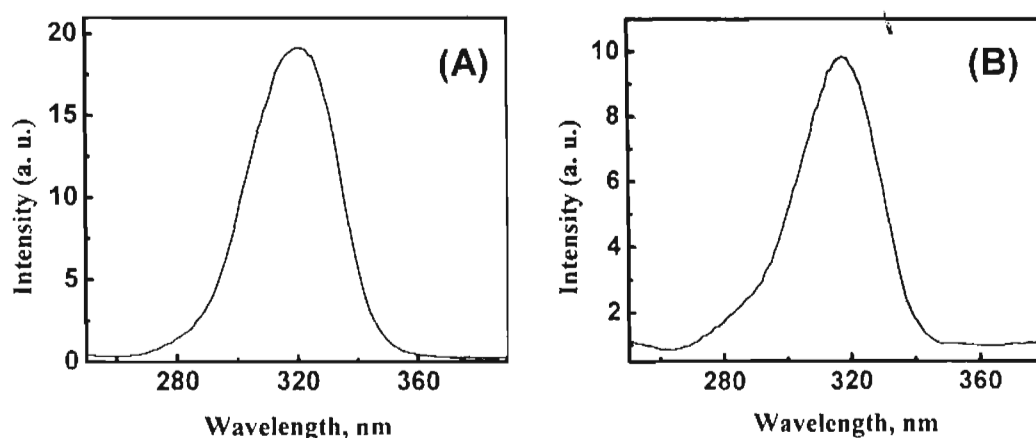
Figure 4.12. Excitation spectrum of **Au-BT**, A) at maximum concentration of europium [Eu]: 14.5 μM (emission followed at 616 nm) and B) at maximum concentration of Terbium [Tb[III]]: 27.7 μM (emission followed at 545 nm) in acetonitrile.

4.3.4. Time resolved luminescence studies

Phosphorescence lifetimes of the complexes of **Au-BT** with Ln[III] were measured in a SPEX model 1934D phosphorimeter equipped with a flash lamp. The signals from the sample falling on the photomultiplier are collected by a

control module for a preset length of time. The solutions were thoroughly degassed before carrying out lifetime studies. Plots of the luminescence decay for Eu^{III}/Tb^{III} ions, in the presence of **BT** and **Au-BT** are presented in Figures 4.13 and 4.14.
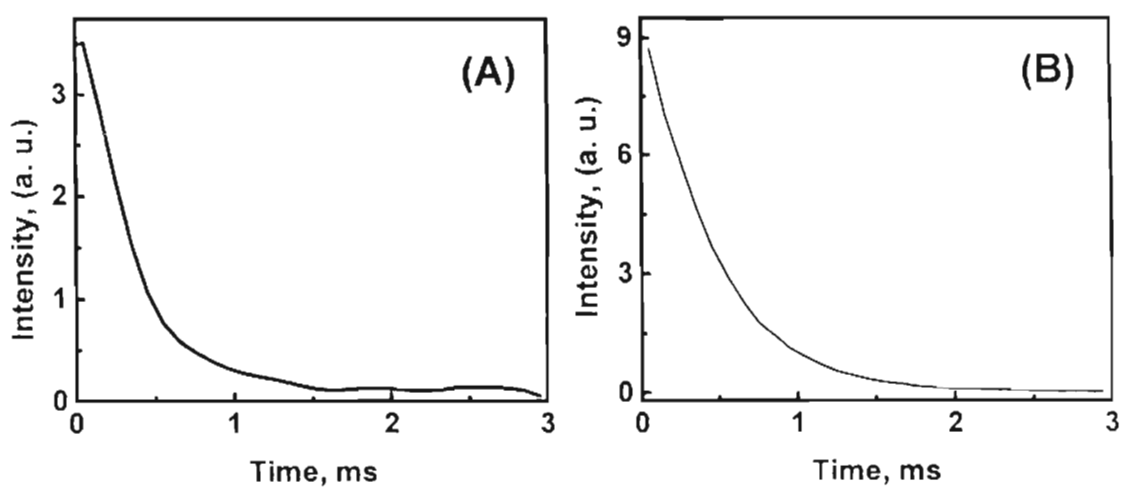
Figure 4.13. Phosphorescence decay profile of Eu^{III}, A) in the presence of **Au-BT**, B) in the presence of **BT**.
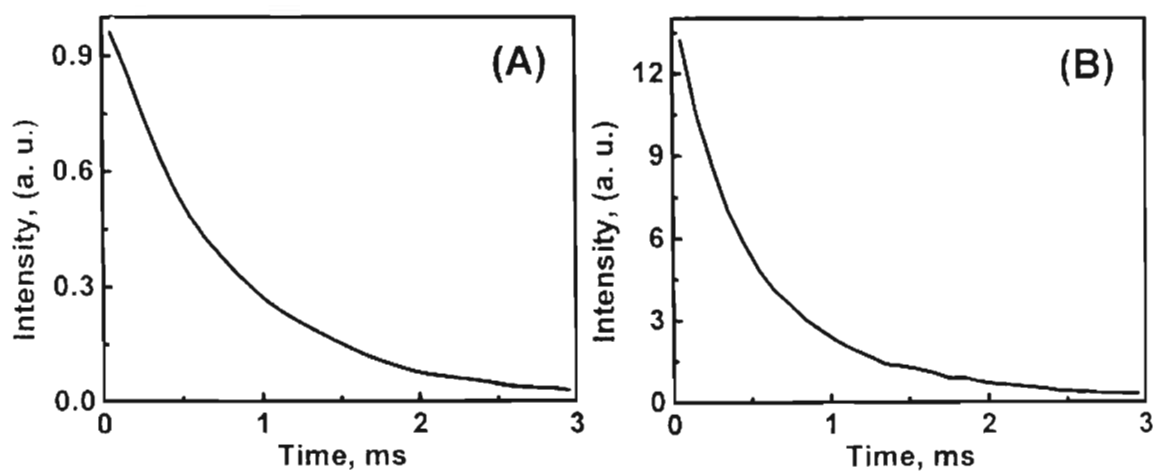
Figure 4.14. Phosphorescence decay profile of Tb^{III}, A) in the presence of **Au-BT**, B) in the presence of **BT**.

The fluorescence intensities decay exponentially with first order kinetics over time t, obeying equation (4.2),

$$I_t = I_0 \exp(-t/\tau) \tag{4.2}$$

where I_0 and I_t are the fluorescence intensities at zero time and at time t, respectively. The emission lifetime of fluorescence, τ, was obtained by fitting the fluorescence decay curve into equation (4.2). At room temperature, the luminescence lifetimes of Eu^{III} and Tb^{III} in the presence of **BT** are 0.4 ms and 0.56 ms, respectively. Interestingly, linking on to gold nanoparticles does not influence the luminescence lifetimes of the bipyridine complex of Eu^{III} and Tb^{III} ions. The luminescence lifetimes of **Au-BT:Eu^{III}** and **Au-BT:Tb^{III}** complexes were estimated as 0.36 ms and 0.7 ms, respectively.

4.3.5. Allosteric studies

The emissive supramolecular complex around Au nanoparticle was further used for sensing biologically important metal cations as well as transition metal ions. The influence of alkali metals (Na^+ K^+), alkaline earth metals (Ca^{2+} Mg^{2+}) and transition metals (Cu^{2+} Ni^{2+} Zn^{2+}) on the luminescence property of **Au-BT:Eu^{III}** complex in acetonitrile was investigated. A dramatic quenching of the luminescence was observed on addition of alkaline earth metals (Ca^{2+} Mg^{2+}) and transition metals (Cu^{2+} Ni^{2+} Zn^{2+}) to an acetonitrile solution containing **Au-BT:Eu^{III}** complex while no influence on luminescence intensity was observed in the presence of alkali metals (Na^+ and K^+). The relative decrease in the

fluorescence of **Au-BT-Eu** with different metal ions is shown in Figure 4.15. In all these measurements. sufficient time to attain equilibrium was given (5 min) after each addition of metal ions.

The relative decrease is much larger for transition metal ions compared to alkaline earth metals. The better binding ability of the transition metal ions over Eu^{III} and their similar in size are responsible for the displacement of Eu^{III} from **Au-BT:Eu^{III}** complex compared to alkaline earth metals.
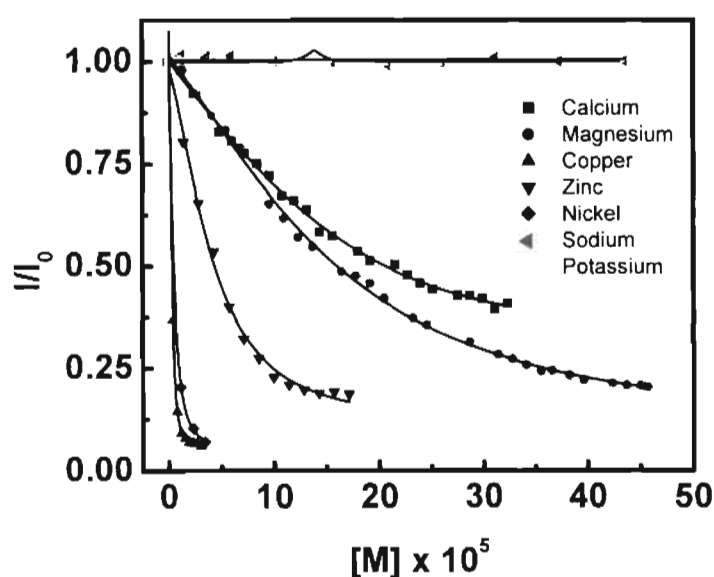
Figure 4.15. Relative decrease in the luminescence intensity of **Au-BT-Eu** in the presence of various concentrations of different metal ions.

Earlier studies indicate that biological activity is often retained, or at least partially by systems in which Ca^{2+} has been replaced by Ln^{3+} ions.[34,35] Hence their isomorphous substitution with Ln^{3+} is a promising way to exploit the rich and varied spectroscopic properties of Ln^{3+} ions for obtaining information on the structural aspects of the biochemistry of Ca^{2+} and Mg^{2+}. Since gold nanoparticles
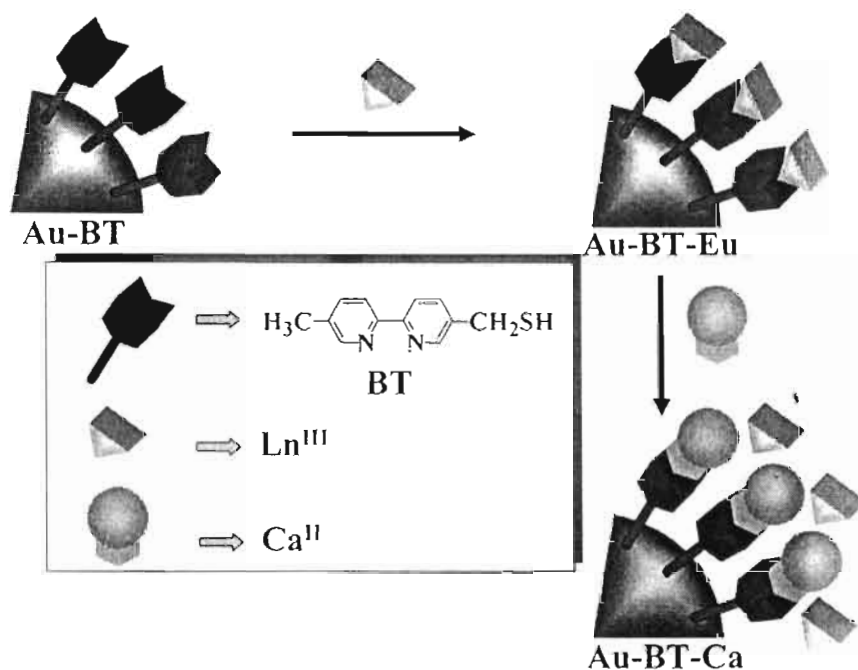
Scheme 4.4 Pictorial representation of the isomorphous substitution of lanthanide ions by calcium ions on bipyridine capped Au nanoparticles.

could be easily functionalized with probes which can selectively bind at specific sites. Ln^{III} doped **Au-BT** can be used to understand various processes in biological systems. Scheme 4.4 depicts a pictorial representation of the isomorphous substitution of Ln^{III} with Ca^{II} in **Au-BT:Ln^{III}** complexes. The allosteric effect of **Au-BT: Eu^{III}** complex as well as the site-specific binding of Au nanoparticle make these systems attractive for biological application.

4.4. Conclusions

Gold nanoparticles capped with bipyridyl ligands (**Au-BT**) were synthesized and their photophysical properties were investigated, in detail. **Au-BT** system behaves as an excellent ion sponge possessing nanometric dimensions due to the high local concentration of bipyridine units on Au nanoparticle (~340

bipyridine units per Au nanoparticle). Complexation ability of **Au-BT** nanohybrids with inner transition metal ions and Cu^{II} was investigated, in detail. A dramatic enhancement of luminescence (10^4-10^5 fold) was observed for Eu^{III}/Tb^{III} ions when complexed on **Au-BT** and such luminescent systems in nanosize domain may have potential application as nanophosphors. Luminescence studies also revealed that the isomorphous substitution of **Au-BT:Eu^{III}** with Ca^{II}/Mg^{II} ions is possible and such systems possess potential application as probes in biological systems.

4.5. Experimental Section

4.5.1. Materials and instrumental techniques

Solvents and reagents used were purified and dried as per standard procedures. All starting materials and reagents were purchased from Sigma-Aldrich and were used as such. Photophysical studies were carried out using spectroscopic grade solvents.

All melting points were determined with a Mel-Temp-II melting point apparatus and are uncorrected. ^1H and ^{13}C NMR spectra were measured on a 300 MHz Bruker Advance DPX spectrometer. IR spectra were recorded on a Nicolet Impact 400D infrared spectrophotometer. Fluorescence spectra were recorded on a SPEX fluorolog F-112 X spectrofluorimeter and corrected using the program supplied by the manufacturer. The electronic absorption spectra were recorded on a Shimadzu Model UV-3101 PC UV-Vis-NIR scanning spectrophotometer. For TEM studies, a drop of colloidal gold solution was placed on a carbon coated Cu

grid and the solvent was allowed to evaporate. Specimens were examined on a Hitachi H600 transmission electron microscope. Phosphorescence lifetimes of the complexes were measured using a 1934D phosphorimeter equipped with a flash lamp. The signals from the sample falling on photomultiplier were collected by the control module for a preset length of time.

4.5.2. Synthesis of compound 4.2.

To a solution of 5,5'-dimethyl-2,2'-bipyridine (**4.1**) (1.034 g, 5.62 mmol) and N-bromosuccinamide (1 g, 5.62 mmol) in dry carbon tetrachloride (50 mL), catalytic amount of AIBN was added and refluxed at 77 ^{0}C for 17 h under dry conditions. The solution was filtered while hot and kept for two days to precipitate out any dibromo derivative formed. The solution was filtered and the filtrate was concentrated under reduced pressure. The residue obtained was chromatographed over silica gel (100-200 mesh size) using a mixture (3:1) of hexane and ethyl acetate which gave compound **4.2** (1 g, 70 %) as a white powder which melted at 80 ^{0}C. IR (KBr) ν_{max} ; 2369, 1587, 1553, 1458, 1371, 1216, 1027, 879, 831, 744, 670, 616 cm^{-1}; ^{1}H NMR (CDCl$_3$, 300 MHz) δ 2.39 (s, 3H, -CH$_3$) 4.53 (s, 2H, -CH$_2$Br) 8.66 (s, 1H, ar) 8.49 (s, 1H, ar) 8.3-8.27 (d, 1H, J = 8.1 Hz, ar) 8.25-8.23 (d, 1H, J = 8.1 Hz, ar) 7.8-7.83 (d, 1H, J = 8.1 Hz, ar) 7.62-7.65 (d, 1H, J = 8.1 Hz, ar)ppm; ^{13}C NMR (CDCl$_3$, 75 MHz) δ 156.27, 153.07, 149.7, 137.44, 133.68, 120.7, 29.65, 25.14 ppm.

4.5.3. Synthesis of compound BT

To an ice cooled solution of compound **4.2** (200 mg, 0.76 mmol) in freshly distilled THF (3 mL), a mixture of tetrabutylammonium fluoride (221 mg, 0.84 mmol) and hexamethyldisilathiane (166.8 mg, 0.92 mmol) in freshly distilled THF (2 mL) was added and stirred. The reaction mixture was stirred for a further period of 12 h. The reaction mixture was diluted with dichloromethane, washed with saturated ammonium chloride (10 mL) and then with distilled water (20 mL x 2). The organic layer was separated, dried over anhydrous sodium sulphate and the solvent was removed under reduced pressure to give a residue which was recrystallized from a mixture (9:1) of hexane and ethyl acetate to give white crystals of **BT** (40 mg, 40 %), mp 106 ^{0}C. IR (KBr) v_{max} ; 2369, 1593, 1560, 1465. 1371, 1236, 1128, 1027, 838, 737, 663 cm^{-1} ; ^{1}H NMR (CDCl$_3$, 300 MHz) δ 2.39 (s, 3H, -CH$_3$) 3.66 (s, 2H, -CH$_2$SH) 8.51 (s, 1H, ar) 8.49 (s, 1H, ar) 8.34-8.31 (d, 1H, J 8.1 Hz, ar) 8.28-8.26 (d, 1H, J 8.1 Hz, ar)7.70-7.68 (d, 1H, J 8.1 Hz, ar),7.69-7.67 (d, 1H, J 8.1 Hz, ar)ppm; ^{13}C NMR (CDCl$_3$, 75 MHz) δ 32.57, 40.06, 120.6, 132.65, 137.5, 149.6, 153.16, 155.46 ppm. exact mass calcd. for C$_{12}$H$_{12}$N$_2$S [MH$^+$]: 217.0799, found 217.0805 (FAB, high resolution mass spectroscopy).

4.5.4. Synthesis of gold nanoparticles capped with BT

To a stirred solution of tetraoctylammonium bromide (0.068 g,) in toluene (5 mL), an aqueous solution of hydrogentetrachloroaurate (III)-hydrate (11 mg, 0.028 mmol) was added dropwise and stirred for 20 minutes. The reaction mixture

was washed with distilled water (10 mL) several times and the organic layer was separated. A mixture of compound **BT** (4.2 mg, 0.0196 mmol) and dodecanethiol (1.7 mg, 0.0084 mmol) in toluene (2 mL) was added to the above solution and stirred. After 30 min, an aqueous solution of sodium borohydride (11 mg, 0.28 mmol) was added dropwise and stirred for a further period of 3 h. The organic layer was washed with water and diluted with methanol (250 mL). It was kept in ice and the precipitate obtained was further purified by resuspending in toluene and then centrifuging after adding methanol (10 mL). This process was repeated twice to remove any unbound thiol. The residue obtained was redispersed in 5 mL toluene.

4.6. References

(1)   Brust, M.; Walker, M.; Bethell, D.; Schffrin, D. J.; Whyman, R. *J. Chem. Soc., Chem. Commun.* **1994**, 801.

(2)   Bethell, D.; Brust, M.; Schiffrin, D. J.; Kiely, C. *J. Electroanal. Chem.* **1996**, *409*, 137.

(3)   Amihood, D.; Katz, E.; Willner, I. *Langmuir* **1995**, *11*, 1313.

(4)   Han, W.; Li, S.; Lindsay, S. M.; Gust, D.; Moore, T. A.; Moore, A. L. *Langmuir* **1996**, *12*, 5742.

(5)   Fink, J.; Kiely, C.; Bethell, D.; Schiffrin, D. J. *Chem. Mater.* **1998**, *10*, 922.

(6)   Makarova, O. V.; Ostafin, A. E.; Miyoshi, H.; Norris, J. R.; Meisel, D. *J. Phys. Chem. B* **1999**, *103*, 9080.

(7) Fitzmaurice, D.; Rao, S. N.; Preece, J. A.; Stoddart, J. F.; Wenger, S.; Zaccheroni, N. *Angew. Chem. Int. Ed. Engl.* **1999**, *38*, 1147.

(8) Templeton, A. C.; Cliffel, D. E.; Murray, R. W. *J. Am. Chem. Soc.* **1999**, *121*, 7081.

(9) George, T. K.; Kamat, P. V. *J. Am. Chem. Soc.* **2000**, *122*, 2655.

(10) Imahori, H.; Norieda, H.; Yamada, H.; Nishimura, Y.; Yamazaki, I.; Sakata, Y.; Fukuzumi, S. *J. Am. Chem. Soc.* **2001**, *123*, 100.

(11) Hu, J.; Zhang, J.; Liu, F.; Kittredge, K.; Whitesell, J. K.; Fox, M. A. *J. Am. Chem. Soc.* **2001**, *123*, 1464.

(12) Brus, L. *New J. Chem.* **1987**, *11*, 123.

(13) Kamat, P. V. *Chem. Rev.* **1993**, *93*, 267.

(14) Alivisatos, P. *J. Phys. Chem.* **1996**, *100*, 13226.

(15) Alvarez, M. M.; Khoury, J. T.; Schaaff, T. G.; Shafigullin, M. N.; Vezmar, I.; Whetten, R. L. *J. Phys. Chem. B* **1997**, *101*, 3706.

(16) *Semiconductor Nanoclusters-Physical, Chemical and Catalytic Aspects*; Kamat, P. V.; Meisel, D., Eds.; Elsevier Science: Amsterdam, 1997, pp. 474.

(17) Chen, S.; Ingram, R. S.; Hostetler, M. J.; Pietron, J. J.; Murray, R. W.; Schaaff, T. G.; Khoury, J. T.; Alvarez, M. M.; Whetten, R. L. *Science* **1998**, *280*, 2098.

(18) Link, S.; El-Sayed, M. A. *J. Phys. Chem. B* **1999**, *103*, 4212.

(19) Maier, S. A.; Brongersma, M. L.; Kik, P. G.; Atwater, H. A. *Phy. Rev. B* **2003**, *65*, 193408.

(20) Maier, S. A.; Kik, P. G.; Atwater, H. A.; Meltzer, S.; Hare, E.; Koel, B. E.; Requicha, A. A. G. *Nature Materials* **2003**, *2*, 229.

(21) Shen, Y.; Friend, C. S.; Jiang,Y.; Jakubczyk, D.; Swiatkiewicz; J.; Prasad, P. N. *J. Phys. Chem. B* **2000**, *140*, 7577.

(22) Lis, S.; Hnatejko, Z.; Barczynski, P.; Elbanowski, M. *J. Alloys Comp.* **2002**, *344*, 70.

(23) Werts, M. H. V.; Jukes, R. T. F.; Verhoeven, J. W. *Phys. Chem. Chem. Phys.* **2002**, *4*, 1542.

(24) Sabbatini, N.; Guardigli, M.; Lehn, J-M. *Coord. Chem. Rev.* **1993**, *123*, 201.

(25) Klonkowski, A. M.; Lis, S.; Pietraszkiewicz, M.; Hnatejko, Z.; Czarnobaj. K.; Elbanowski, M. *Chem. Mater.* **2003**, *15*, 656.

(26) Rodrriguez-Ubis, J.-C.; Alpha, B.; Plancherel, B. D.; Lehn, J.-M. *Helv. Chim. Acta.* **1984**, *67*, 2264.

(27) Sabbatini, N.; Perathoner, S.; Balzani, V.; Alpha, B.; Lehn, J.-M. *'Supra molecular Photochemistry'*, V. Balzani, Reidel, Dordrecht, ed.; 1987, p. 187.

(28)   Alpha, B.; Ballrdini, R.; Balzani, V.; Lehn, J.-M.; Perathoner, S.; Sabbatini, N. *Photochem. Photobiol.* **1990**, *52*, 299.

(29)   Pietraszkiewicz, M. in *Comprehensive Supramolecular Chemistry;* Lehn, J.-M. Ed.;Elsevier Science Ltd. London, 1996, Chapter 10, p. 225.

(30)   (a) Perutz, M. F. *Mechanisms of Cooperativity and Allosteric Regulation in Proteins*; Cambridge University Press: Cambridge, 1989. (b) Rebek, J., Jr. *Acc. Chem. Res.* **1984**, *17*, 258. (c) Tabushi, I. *Pure Appl. Chem.* **1988**, *60*, 581. (d) Nabeshima, T. *Coord. Chem. Rev.* **1996**, *148*, 151.

(31)   Richardson, F. S. *Chem. Rev.* **1982**, *82*, 543.

(32)   Dominguez, O.; Echegoyen, L.; Cunha, K.; Nongijian, T. *Langmuir* **1998**, *14*, 821.

(33)   Soini, E.; Levgren, T. *Crit. Rev. Anal. Chem.* **1987**, *18*, 105.

(34)   Horrocks, Jr. W. D.; Sudnick, D. R. *Acc. Chem. Res.* **1981**, *14*, 384.

(35)   Martin, R. B.; Richardson, F. S. *Q. Rev. Biophy.* **1979**, *12*, 181.

(36)   Hu, J.; Fox, M. A. *J. Org. Chem.* **1999**, *64*, 4959.

(37)   Howard, S. T. *J. Am. Chem. Soc.* **1996**, *118*, 10269.

(38)   Mason, S. F. *Inorg. Chim. Acta* **1968**, *2*, 89.

(39)   Linnell, R. H.; Kaczmarczyk, A. *J. Phys. Chem.* **1961**, *65*, 1196.

(40) Fatin-Rouge, N.; Blanc, S.; Leize, E.; Dorsselaer, A. V.; Baret, P.; Pierre. J-L.; Albrecht-Gary, A-M. *Inorg. Chem.* **2000**, *39*, 5771.

(41) Terill, R. H.; Postlethwaite, T. A.; Chen, C.-H.; Poon, C.-D.; Terzis, A.; Hutchison, J. E.; Clark, M. R.; Wignall, G.; Londone, J. D.; Superfine. R.; Falvo, M.; Johnson, C. S. Jr.; Samulski, E. T.; Murray, R. W. *J. Am. Chem. Soc.* **1995**, *117*, 12537.

(42) Chen, S.; Murray, R. W. *Langmuir* **1999**, *15*, 682.

(43) Lahav, M.; Gabriel, T.; Shipway, A. N.; Willner, I. *J. Am. Chem. Soc.* **1999**, *121*, 258.

(44) Kelly, K. L.; Coronado, E.; Zhao, L. L.; Schatz, G. C. *J. Phys. Chem. B* **2003**, *107*, 668.

(45) Rechberger, W.; Hohenau, A.; Leitner, A.; Krenn, J. R.; Lamprecht, B.; Aussenegg, F.R. *Opt. Commun.* **2003**, *220*, 137.

(46) Fink, J.; Kiely, C. J.; Bethell, D.; Schiffrin, D. J. *Chem. Mater.* **1998**, *10*, 922.

(47) Gil, V. M. S.; Oliveira, N. C. *J. Chem. Educ.* **1990**, *67*, 473.

(48) Haas, Y.; Stein, G. *J. Phys. Chem.* **1971**, *75*, 3668.

(49) Nakamura, K. *Bull. Chem. Soc. Japan* **1982**, *55*, 2697.

(50) Meech, S. R.; Philips, D. *J. Photochem.* **1983**, *23*, 193.

List of publications derived from the thesis:

1) Photochemistry of chromophore functionalized gold nanoparticles,
   K.George Thomas, **B. I. Ipe** and P. K. Sudeep,
   Pure & Appl. Chem. 74, 1731 **(2002)**.

2) Photoinduced Charge Separation in a Fluorophore- Gold Nanoassemblies,
   B. I. Ipe, K.George Thomas, S. Barazzouk, S. Hotchandani and
   P. V. Kamat,
   J. Phys. Chem. B **105**, 18-21**(2002)**.

3) Light induced modulation of Self-Assembly on Spiropyran-capped Gold
   Nanoparticles: A Potential System for the Controlled Release of Amino Acid
   Derivatives
   B. I. Ipe, S. Mahima, K. George Thomas,
   J. Am. Chem. Soc. **125**, 7174-7175 **(2003)**.

4) Design of Nanophosphors, Nanosensors and Superstructures from Bipyridine
   Functionalized Gold Nanoparticles
   B. I. Ipe, K. Yoosuf, K. George Thomas,
   J. Am. Chem. Soc. **(2003)** (under submission).